This thesis was supervised by Prof. Raúl Toral at the Institute for Cross-Disciplinary Physics and Complex Systems (IFISC) and the University of the Balearic Islands (UIB).

It covers different aspects of scientific research. On one end there is an analysis of a specific model for intestinal absorption. A good theoretical understanding of the mathematics can be a guide to the experimentalist and help estimate the fitting of the model parameters to the measurements. On the other end there are abstract models whose relation to specific physical or biological systems seems far but the conclusions drawn from them tend to be quite general. We analyse 'magnetic' systems with diverse parameters that show transitions between disordered and ordered states. Within both ends of the scientific spectrum we investigate a system of coupled biochemical oscillators resembling a simplified version of the circadian pacemaker neurons and a more abstract oscillatory (excitable) system called "active rotators". We are interested in the effects of diversity in the parameters on the collective motion of the oscillators.

Aquesta tesi va ser dirigida pel professor Raúl Toral, a l'Institut de Física Interdisciplinària i Sistemes Complexos (IFISC) i la Universitat de les Illes Balears (UIB).

Cobreix diversos aspectes de la investigació científica. En un extrem es fa una anàlisi d'un model específic per a l'absorció intestinal. Un bon coneixement teòric de les matemàtiques pot ser una guia per a l'experimentador i ajuda a estimar els paràmetres dels models a partir dels mesuraments. A l'altre extrem hi ha models abstractes la relació dels quals amb els sistemes físics o biològics sembla llunyana, però les conclusions extretes d'ells tendeixen a ser bastant generals. Analitzem sistemes 'magnètics' amb paràmetres diversos que mostren transicions entre els estats desordenats i ordenats. En mig d'ambdós extrems de l'espectre s'investiguen oscil·ladors bioquímics diversos que són una versió simplificada de les neurones marcapassos dels ritmes circadians en els organismes i els efectes de la diversitat en un sistema oscil·latori (excitables) més abstracte, els "rotors actius". Estem interessats en els efectes de la diversitat en els paràmetres per al moviment col·lectiu dels oscil·ladors.

Phase Transitions Induced by Diversity and Examples in Biological Systems

Niko Komin

Phase Transitions Induced by Diversity and Examples in Biological Systems

Niko Komin

PhD Thesis

Universitat de les Illes Balears

TESI DOCTORAL

Phase Transitions Induced by Diversity and Examples in Biological Systems

Tesi presentada per ***Niko Komin****, al Programa oficial de doctorat en Física de la Universitat de les Illes Balears, per optar al grau de Doctor en Física*

Palma, desembre 2010

Raúl Toral
Director

Niko Komin
Doctorant

Phase Transitions Induced by Diversity and Examples in Biological Systems

Niko Komin
Instituto de Fisica Interdisciplinar y Sistemas Complejos
IFISC (UIB-CSIC)

PhD Thesis

Director: Prof. Raúl Toral

This document was typeset with LaTeX 2_ε

Resumen

La presente tesis cubre varios aspectos de investigación que han sido motivados inicialmente por cuestiones relacionadas con procesos biológicos. Por un lado investigamos, desde un punto de vista matemático de la teoría de sistemas dinámicos, un modelo de absorción que es de amplio uso en farmacología. El estudio de las propiedades de absorción es un paso importante en el proceso del desarrollo de fármacos. Nuestro resultado aporta conocimiento sobre un modelo de absorción en concreto que puede mejorar el trabajo experimental al simplificar el proceso de análisis de los resultados. El estudio lleva a una solución aproximada del modelo que permite predecir fÃącilmente las observaciones del experimento para un amplio rango de parámetros. Además la solución puede ser usada para estimar la dispersión de la eficacia entre la población, conociendo la diversidad en sus parámetros fisiológicos entre diferentes pacientes.

La acción de un fármaco está sujeta a los diversos procesos dinámicos que ocurren dentro del cuerpo. Por ejemplo, se sabe que los niveles de una variedad de hormonas en el cuerpo humano y de otros mamíferos muestran cambios periódicos sincronizados con el

ritmo de 24 horas. Estos cambios pueden modificar (aumentando o disminuyendo) la acción de un fármaco. Los ritmos diarios de las funciones corporales, los denominados *ritmos circadianos de actividad*, están controlados por un reloj maestro situado en una región concreta del cerebro (el núcleo supraquiasmático). Allí unas veinte mil neuronas están acopladas entre sí y reciben la información sobre la luminosidad proveniente de los órganos visuales, cuyo cambio informa sobre el comienzo de un día nuevo. Las neuronas responsables de la generación de oscilaciones internas, y en última instancia, del acoplamiento de la actividad al ritmo externo, se han estudiado mucho en la última década. Se ha mostrado que neuronas aisladas pueden exhibir oscilaciones con periodos muy dispersos entre ellas. Nosotros estudiamos cómo diferentes niveles de dicha dispersión facilitan o dificultan la sincronización del conjunto con la señal periódica que viene de los ojos. Hemos mostrado cómo la diversidad lleva el conjunto a la "muerte de las oscilaciones" ("oscillator death") y cómo eso causa una mejora de la sincronización. Este resultado muestra un posible mecanismo por el que la diversidad, que ocurre de manera natural en los sistemas biológicos, puede ser un ingrediente fundamental para el funcionamiento óptimo del organismo.

El sistema matemático que forma la base de estas oscilaciones bioquímicas tiene un alto numero de variables y además aparecen de manera altamente no lineal. Sistemas abstractos con propiedades controladas tienen la ventaja de ser tratables con métodos analíticos en una manera que permite analizarlos por completo. De esta manera se pueden aprender detalles que están escondidos en el abanico de posibles comportamientos en un sistema bioquímico muy complejo. El modelo de "rotores activos" ("active rotators") es un simple sistema que puede mostrar conducta excitable u oscilatoria. Si las frecuencias propias de un conjunto de rotores activos están distribuidas aleatoriamente se puede observar un régimen coherente donde el sistema global entra en el estado oscilatorio a pesar de que una parte de los elementos están en el estado ex-

citable. La transición a las oscilaciones globales a causa de diversidad tiene propiedades similares a las de las transiciones de fase conocidas de la termodinámica y física estadística. Hemos estudiado las propiedades críticas y la dependencia con el tamaño de sistema, mediante simulaciones numéricas extensivas. La criticalidad de dicha transición muestra comportamientos inesperados por un sistema en el que el acoplamiento global parecería implicar una conducta de campo medio. En particular, los exponentes críticos de escala con el tamaño no coinciden con los de campo medio. La destrucción del régimen de oscilaciones globales se manifiesta en otra transición de fase. Hemos identificado el orden de la transición y encontrado condiciones en las cuales la transición es de primer orden.

Para un estudio más profundo de transiciones de fase inducidas por diversidad decidimos investigar otros modelos prototípicos de transiciones de fase térmicas o inducidas por ruido. Hemos reemplazado los términos de carácter térmico, es decir fluctuaciones temporales, por un parámetro de distribución aleatoria. Refinamos un método eficiente de tratar sistemas de ese tipo que nos permite obtener ecuaciones aproximadas que describen el comportamiento global. Dada su baja dimensionalidad, se pueden estudiar mediante métodos propios de la teoría de sistemas dinámicos las ecuaciones aproximadas. Así hemos obtenido el diagrama de fases para el modelo Ginzburg-Landau con diversidad aditiva y multiplicativa y para el modelo canónico de transiciones inducidas por ruido. Hemos comparado la solución dada por el método aproximado con la resolución de los modelos dentro del límite de campo medio. En los dos (Ginzburg-Landau aditivo y modelo canónico de transiciones de fase inducidas por ruido) el análisis de escala con el tamaño de sistema nos enseña que las transiciones muestran exponentes críticos parecidos a los de los rotores activos. El resultado analítico que hemos obtenido para el modelo de Ginzburg-Landau aditivo comprueba que pertenece a la clase de universalidad de campo medio, pero se aprecia una violación de la relación de fluctuación-

disipación que interpretamos en términos de un hamiltoniano efectivo en la que los términos de campo externo no aparecen en la manera usual.

"If you ever get close to a human
And human behaviour
Be ready be ready to get confused

There's definitely definitely definitely no logic
To human behaviour
But yet so yet so irresistible

And there's no map to human behaviour

They're terribly terribly terribly terribly moody
Then all of a sudden turn happy
But, oh, to get involved in the exchange
Of human emotions
Is ever so ever so satisfying

And there's no map
And a compass wouldn't help at all" — Björk: Human Behaviour (Debut, 1993)

Acknowledgments

Evolution and destiny gave me my senses to hear, see, touch, taste and smell the beauty of nature and my emotions to feel it. Curiosity drives the quest of live. The amount of people that has supported my way along the quest is huge.

The financial needs for food, shelter and joy and for travelling to meet teachers and colleagues during the years of working at my thesis has been provided by the people of the European Union via the BioSim research network and by the people of the Balearic Islands via a scholarship of the Government of the Balearic Islands. The academic surroundings – libraries, access to scientific journals, courses, computers, non electronic material and infrastructure – were given by the public University of the Balearic Islands (UIB) on one hand and the Institute for Cross-Disciplinary Physics and Complex Systems (IFISC) on the other. The latter is a joint research institute of the UIB and the Spanish National Research Council (CSIC). I am thankful for having had the honour to spend my time with scientific investigation in this environment.

I was adjoined to the IFISC research centre during the time of my doctorate. Here it was Professor Raúl Toral who invited me to come

to the place, who trusted in me in times when I missed advancements and who taught me and helped me with infinite patience. Moreover, he gave me a huge amount of freedom that allowed me to develop at my personal will. I am very grateful and I feel lucky to have had Raúl Toral as my doctoral thesis supervisor.

Many insights to formerly unknown fields I owe to the members of the BioSim network. At the BioSim conferences and meetings I learned much about pharmaceutical, medical and biochemical processes and how the methods that I have studied in physics can contribute valuable information. The cooperation with the pharmacologists Marival Bermejo, Isabel González Alvarez and Vicente Casabó, at that time all at the University of Valencia, made it possible to contribute to the field of pharmacology. Without their help this part of our investigation would not have happened. Another part of our investigation, about the biological clock in mammals, was only possible through the collaboration with Emilio Hernández García and Adrian Murza. The last result of the thesis would have been impossible without the work of and discussions with Lucas Lacasa. I am thankful for these people as an integral part of the scientific achievements presented here.

Due to its interdisciplinary approach the IFISC attracts scientists from a variety of fields. It is a good place to broaden the scientific horizon. Apart from the academic conditions it is equally necessary to find oneself in a pleasing environment. I had the chance to make very good friends at the institute. Friends to talk about scientific doubts, to amplify euphorias and damp depressions, to confront contradictions and to open up new ways of looking at life. Above all I want to express my thanks to my close friends Alessandro Scirè, Antonio Pérez-Serrano, Lucas Lacasa and Fernando Galve. It has been a pleasure meeting you. Others, that at any time have had an open ear to discuss anything – Alejandro Herrada, Xavier Castellò, Juan Carlos González-Avella and many more – have made their invaluable contributions to the thesis.

An immense part in my achievements had people outside of the labour environment. My close friends here in Mallorca and elsewhere; my friends that were once so close and who are still dear to me although so distant; and above all my family and Guadalupe, you all sharpened my senses, broadened my emotions and fed my curiosity – the beauty of nature in my live. I thank you all for what you are.

Palma 2010, Niko Komin

Contents

Part I

Introduction

Chapter 1

Preface

The present thesis covers various topics that range over different aspects of scientific research. On one end there is the specific analysis of a precise form that models some experimental observations. A good theoretical understanding of the mathematics that describe the observations can be a guide to the experimentalist and help estimate the validity of the measurements. On the other end there are abstract models whose relation to physical systems seem far but they are prototypic for a broad range of different systems and the drawn conclusions tend to be quite general. Depending on the abstraction and on the simplifications in use the distinction between both ends might not be sharp. The ordering of the research results presented in part II of this thesis somehow reflects the seamless transition from one end to the other. To introduce the reader into the context of the genuine results we provide introductory material in the chapters of the present part I.

Part I, the introduction

After first giving an overview of the arrangement of the thesis here we will go on to chapter 2 where the general aspects of **dynamical systems** are shown. In the beginning we will explain the main concept and the properties like **fixed points**, **stability** and **bifurcations** of dynamical systems. This will be of use in some cases of the thesis where we were able to give dynamical equations for the average behaviour that can be analysed with a typical bifurcation analysis. Then we will introduce **noise** into dynamical systems in general and present typical examples of the consequences of stochasticity. Furthermore we will see how **diversity**, as time independent random differences in the local dynamics, can be responsible for a qualitative change in the system. Some well known examples are presented which mark the territory of the forthcoming results. A **phase transition** is a collective phenomenon that arises purely from the interaction of many similar elements and is not present in the isolated system. It is the sudden change of a system from an 'ordered' to a 'disordered' state or vice versa. We will explain the main characteristics of such transitions and show known examples.

After having set up the mathematical framework that came to use in the presented research we want to use chapter 3 to provide the biological background that is the base for two of the presented results. The chapter starts with the demonstration of the dynamics of **enzyme reactions** where a non reactive molecule, the enzyme, has to be present and bound, to facilitate the reaction. In this way, as we will see in the chapter, they are formally ubiquitous on biochemical processes from **gene expression** to transport across membranes. We will show an example of the influence of noise on biochemical processes and examples of **biochemical oscillators**. Thereafter we summarise the constitution of the **cell membrane** and some possible **transport processes** across the membrane.

Part II, the results

The investigation that led to this thesis started with an interest in the description of biological systems. We started investigating two different systems: on one hand we were interested in mathematical models that are used by pharmacologists to estimate the **absorption** properties of pharmaceutics when ingested orally, i.e. those who are usually though the mono cellular layer of the intestinal wall. Our ambition was to give a deeper understanding of the model which could then help to state more precisely the conditions and the limits of an experiment. A transformation of the original system and an adequate approximation allow us to give an analytic solution of the equilibrium concentration and of the experimentally relevant efflux ratio. These functional dependencies give access to predictions for the propagation of errors and of the sensitivity of an experiment with respect to the different parameters. The results we obtained are presented in chapter 4. They comprise a direct contribution to the practical considerations in the process of drug development.

On the other hand we began working with a model that is a description of the daily pacemaker (the **circadian clock**) in mammals. The pacemaker is a region in the brain where coupled neurons send a periodic signal in synchrony with the day-light pattern. Rather than working with the latest models which describe many details known from the experiments, we were interested in how the diversity in these kind of biochemical oscillators in general affects the ability to synchronise with the light rhythm. We could show how the right amount of diversity leads to a better synchrony with the light rhythm as the slight differences lead the global system into the state of oscillator death where they are easier to entrain. We are confident that these results, presented in chapter 5, hold for other variations of the original model.

The main essence of many observation in nature can be described by an abstraction to a mathematical model which has the advantage that conclusions drawn from the model hold for different observa-

tions. The difficulty is to identify correctly the observed quantities with the variables of the model and to not oversimplify the model. The many variables for the chemical species in the circadian model hinder a complete solution of the problem. In chapter 6 we investigate a set of coupled one dimensional **excitable systems** which can be in an excitable or an oscillating regime. We coupled many **active rotators** with diverse intrinsic frequencies, such that some are excitable and others oscillatory. We found that the right amount of diversity induces coherent oscillations of all elements. The creation of this state as well as its destruction by too much diversity happen through a phase transition, much in the sense of magnetic systems, which can be of first or of second order depending on the distribution of the random parameters.

This led us to focus on abstractions of **magnetic systems** where an intrinsic bistability allows large coupled systems to be either in a globally ordered state or in a disordered state. The behaviour of classical phase transitions has been studied before in many different physical models. In most of them the thermal fluctuations contribute a random element to the system. We analysed some of the known models and added diversity to their local dynamics instead of using thermal fluctuations (at zero temperature, so to speak). Without the fluctuations the equations become deterministic and a system that comes to halt once will not start moving again. Again, globally ordered and disordered phases have been found and the transitions from one to the other have properties known from the classical systems. However, as these systems are fundamentally different we found differences from the classical case. Namely the **critical exponents**, describing the system's behaviour close to the transition point, are different than expected. The results of this investigations are presented in chapters 7 and 8.

Like at the end of every chapter, where we summarise the respective main results, we will give general conclusions and an outlook onto possible further studies in chapter 9, at the end of the thesis.

Chapter 2

Dynamical systems

2.1 Introduction

The history of dynamical systems, which are governed by mathematical equations that describe the evolution of a system in time, goes back to the late 17th century when both G. W. Leibniz and I. Newton independently developed infinitesimal calculus. Infinitesimal calculus made it possible for Newton to derive Kepler's laws of the planetary motion from Newton's own principles of forces and motion. Later, in the 19th century, J. C. Maxwell correctly identified the relations between the electric and the magnetic field, another dynamical system that gave a great insight into the nature of light.

If one wants to use a dynamical system to model some observations it is crucial to specify the state variables and the underlying rules. It needs thorough work and intuition, but depending on the focus and on the separation of relevant from irrelevant factors the resulting model might be a good or a bad description of the observed world.

By adequately identifying the dynamic variables and the rules of the system one obtains a mathematical model describing the temporal evolution of it. Many mathematicians, physicists, engineers and computer scientists have devoted their passion to shed light on ways to treat this formalism.

The basic mathematical concepts of dynamical systems is the focus of this chapter. We begin section 2.2 with an introduction of the mathematical language used in this thesis for the description of dynamical systems. It is far from complete and we restrict the considerations to differential equations. The section presents the analysis of the basic behaviour, the long term evolution, and some words about numerical solving techniques. Section 2.3 introduces the concept of noise into dynamical systems. Here, noise is understood as a rapidly fluctuating force term that is characterised by a probabilistic description in which averages over time: the mean and standard deviation, as well as temporal correlations play an important rule. Probabilistic predictions of the outcome of an experiment is the focus of study in systems under the influence of noise and we will see some explanatory examples. The collective behaviour of a large number of interacting variables that are governed by the same set of dynamic equations is presented in section 2.4. We will see basic concepts that are necessary for the understanding of these macroscopic effects not visible in the microscopic equations. A quantity that, although fixed in time, is randomly chosen at the beginning of an experiment, is usually called quenched noise, disorder or diversity. If no 'classic', or thermal, noise is present then the underlying equations become deterministic, i.e. the outcome is completely determined by the initial conditions. However, since one part (or more) of the equation is different in every trial one would have to ask for the probability of some result to occur. Questions arising for this kind of systems are put forward in section 2.5 of this chapter.

2.2

Basic concepts

Dynamical systems refer to equations describing the evolution of a system with time. One of the properties that distinguishes the different types of dynamical systems is the way time is described: it can be a continuous or a discrete process. On one hand there is the discrete measuring of an animal population size in a given area from year to year, on the other hand we have the example of Kepler's laws, where position and motion of the planets change continuously with time. The set of equations describing discrete systems are called **difference equations** or **recurrence equations**. A general form in one dimension could be written like:

$$x_{t+1} = f(x_t) \ . \tag{2.1}$$

The state x of the system at time $t+1$ is given by some function f of the state at time t. Continuous systems are described by **differential equations**. It is common to write:

$$\dot{x}(t) = f(x(t), t) \ , \tag{2.2}$$

where it is the infinitesimal change of state x at time t, written $\dot{x}(t) \equiv \frac{dx(t)}{dt}$, which is determined by the function f of the state x at time t. Both, difference and differential equations share some similarities, in language and properties. Throughout this thesis we will be concerned exclusively with differential equations. In this sense the following considerations will refer only to systems of latter type. A profound analysis of difference equations with applications can be found in dedicated textbooks like the one by Kelley & Peterson (2001) or by Cull *et al.* (2005).

In a more general form the system's state is described by a set of N variables, rather than just one. Then this N-dimensional system is given by the state vector (or **phase point**) $\vec{x}(t) = (x_1(t), \cdots, x_N(t))$

and the vectorial function $\vec{f}(\vec{x}(t), t)$. The space in which the $\vec{x}$ are defined is called the **phase space** and the function along which a given phase point $\vec{x}_0$ evolves is called the **trajectory** based in x_0. In some cases it is possible to write down explicit solutions of Eq. (2.2), i.e. a functional description of the trajectories. Many textbooks, for example Boyce & DiPrima (2001), are concerned with the analytic solution of differential equations. In such a case one knows exactly in which state a system will be at any given time for any given initial condition. In section 4.2 of the chapter about the absorption processes of pharmaceuticals we were able to find an appropriate reduction of the model for which a closed analytic solution can be given. Without such a solution one can still get an insight into the behaviour of the system by analysing the structure of the underlying equations. To this end it can become useful to find a function $V(\vec{x}, t)$ such that:

$$f_i(\vec{x}, t) = -\frac{\partial V(\vec{x}, t)}{\partial x_i} \quad \forall\, i = 1, \ldots, N\,, \tag{2.3}$$

called the **potential** of the dynamics (San Miguel & Toral 2000). If it exists, then one talks about the f_i as **forces**, in analogy to the Newtonian dynamics, although these do not necessarily refer to forces in the sense of mechanics. From now on only explicit dependence on time of the forces will be denoted by $f_i(\vec{x}, t)$, in all other cases we simply write $f_i(\vec{x})$.

In the case that a closed solution to Eq. (2.2) does not exist or is not known, which is usually the norm in physical sciences, one will have to use other means to get some insight into the system. One way is to ask for the system's behaviour on the long run. This will be addressed in the following.

2.2.1 Fixed points and stability

When the state of an observed system does not change through time, the dynamical system is said to be in a **fixed point**, **equilibrium**, or

in the **steady state**. We will use the common notation x^* for these points of the phase space. That the state does not change means, that the left hand side of Eq. (2.2) is zero:

$$f_i(\vec{x}^*) = 0 \quad \forall\, i = 1, \ldots, N\,. \tag{2.4}$$

Consequently, all phase points which do not fulfil Eq. (2.4), are not constant in time, they are changing. The trajectories can, but do not have to, end in one of the fixed points. If all trajectories starting in the vicinity of a fixed point tend towards it, the fixed point is called **asymptotically stable**. If, on the other hand, the trajectories depart from the point it is an **unstable** fixed point. If the point attracts trajectories from some directions but repels them from others it is called a **saddle**. Often, by simply drawing the respective potential or forces of the system, the fixed points and their stability can be identified easily (for an example, see figure 2.1).

A mathematically rigorous decision about the stability of a point can be made by considering the linearised equations near the fixed point. Let $\delta(t) = x(t) - x^*$ be a phase point at a small distance away from a fixed point, a small perturbation. Its trajectory is given by the dynamic equation $\dot{\delta}(t) = \frac{d(x(t)-x^*)}{dt}$, where x^* is constant, and therefore it is $\dot{\delta}(t) = \dot{x}(t) = f(x(t)) = f(x^* + \delta(t))$. To obtain a linearised equation we can now use the Taylor's expansion of f around x^* and write $\dot{\delta}(t) = f(x^*) + \delta(t)f'(x^*) + O(\delta(t)^2)$. By definition $f(x^*) = 0$. Quadratically small terms $O(\delta(t)^2)$ can be neglected if $f''(x^*) \approxeq 0$ so that we obtain the approximate equation for the evolution of the perturbation:

$$\dot{\delta}(t) = \delta(t) f'(x^*)\,, \tag{2.5}$$

from which we can conclude that the distance $\delta(t)$ of a trajectory close to a fixed point will exponentially decrease to zero with time if $f'(x^*) < 0$ and it is therefore a stable fixed point. If it is $f'(x^*) > 0$ then the distance grows exponentially with time and the fixed point is unstable. The sign of $f'(x^*)$ marks the stability (as is seen in the example of figure 2.1) and its magnitude is a marker for how strong

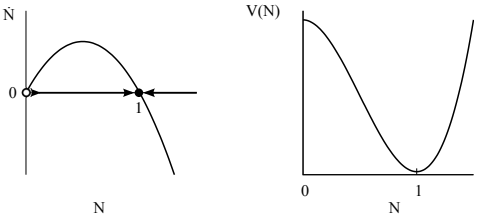

Figure 2.1: Example for a geometric analysis of a dynamical system: the parameter free logistic equation $\dot{N}(t) = N(t)\,(1 - N(t))$, a simple growth model, where the growth rate of a population decreases linearly with the population size. It is easy to see in the left panel, that for $N^* = 0$ and $N^* = 1$ the growth rate is zero. These are the two fixed points of the system. Populations larger than one have a negative effective growth and decrease towards $N^* = 1$. Populations between 0 and 1 have a positive growth and will increase. $N^* = 0$ itself is a fixed point, but any initial value close to zero but larger will have an increasing trajectory. The point $N^* = 0$ is unstable, whereas $N^* = 1$ is asymptotically stable. The potential $V(N) = N^3/3 - n^2/2$, shown in the right panel, displays a local minimum at $N^* = 1$ and a local maximum at $N^* = 0$.

the point attracts or repels trajectories. In the case that it is exactly zero a nonlinear analysis is needed to determine stability.

Systems with dimensions larger than one are linearised by the use of the **Jacobian matrix** $\mathcal{J}_{x_1,\cdots,x_N}$. The resulting equation

$$\dot{\vec{\delta}}(t) = \mathcal{J}_{x_1,\cdots,x_N}(x^*)\,\vec{\delta}(t) \tag{2.6}$$

describes an asymptotically stable (or unstable) fixed point if the maximum real part of all **eigenvalues** is negative (or positive). Imaginary parts different from zero indicate an oscillatory behaviour.

2.2.2 Bifurcations

If a dynamical system has a parameter, say μ, that can change the number of fixed points or the stability of a fixed point, then this change is called a **bifurcation**. μ is called the **bifurcation parameter** or **control parameter** and the value where the change occurs is the **bifurcation point**. Different underlying dynamics lead to different scenarios of bifurcation, the simplest are those in one-dimensional systems with one independent parameter. A nice textbook with a thorough view on bifurcations is the book by Strogatz (1994). The diagrams that we will see here, the bifurcations scenarios, will return when we analyse low dimensional differential equations that describe the averaged quantities of large coupled systems in chapter 7.

Saddle-node bifurcation

In systems that display a saddle-node bifurcation a change in the control parameter creates two fixed points or destroys them by a collision of a stable and an unstable steady state when the parameter is varied in the other direction. At the bifurcation point the steady state is attracting from one side and repelling from the other. A prototypic model, that is one with only polynomial force terms, that displays this behaviour can be written as:

$$\dot{x} = \mu + x^2 \,. \tag{2.7}$$

If $\mu < 0$ then the right hand side of (2.7) is zero for $x^* = \pm\sqrt{-\mu}$. Furthermore it is $f'(x^*) < 0$ for the negative solution and $f'(x^*) > 0$ for the positive solution. In $\mu = 0$ we find x^* as the only solution and for $\mu > 0$ we find none. The geometric analysis of the complete system is shown in the first row of figure 2.2.

A somewhat special kind of saddle-node bifurcation can be observed, when the phase space is a closed set, like the points on a

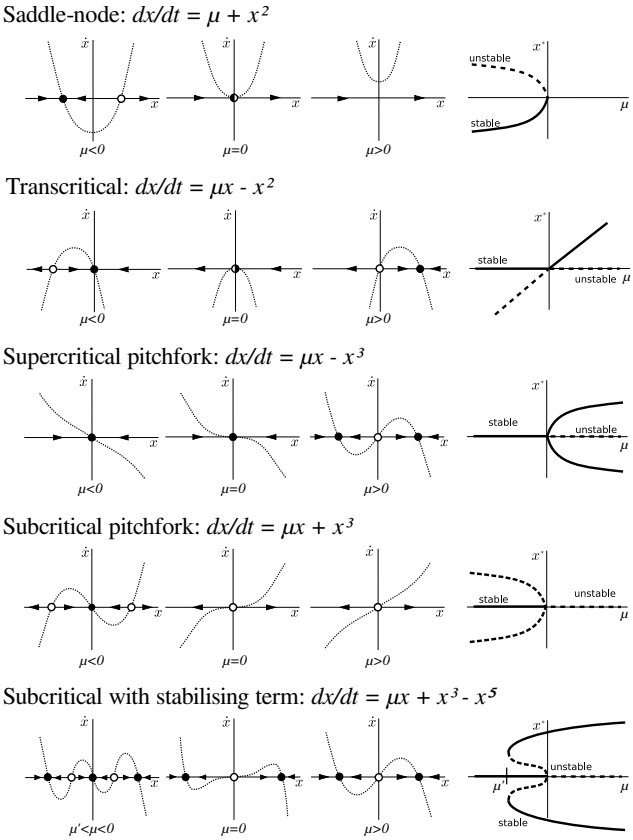

Figure 2.2: Geometric analysis of one-dimensional bifurcations discussed in the text. The derivatives $\dot{x}$ are drawn versus the position x for a control parameter below, at and above the bifurcation point (from left to right). The bifurcation diagrams in the column to the right show the fixed point x^* versus the control parameter. Stable solutions are drawn with a thick line, unstable solutions with a dashed line. (figure adapted from Tessone 2005, p. 8).

circle. The difference to a "normal" saddle-node bifurcation lies in its trajectories. Those which in an infinite space would diverge to infinity, will now be attracted into the stable fixed point. This can lead to interesting behaviour as a trajectory resting in the stable state can be perturbed over the unstable state and will return to the stable state via an excursion on the cycle. This saddle-node bifurcation on an invariant circle (SNIC) will play a role in the considerations of chapter 6. The normal form is the theta model (Ermentrout & Kopell 1986), the dynamics of the phase variable θ are governed by:

$$\begin{aligned} \dot{\theta}(t) &= (1 - \cos\theta(t)) + I\,(1 + \cos\theta(t)) \\ &= 1 + I + (I - 1)\cos\theta\,. \end{aligned} \tag{2.8}$$

This could be understood as a simple one-dimensional model for the spiking of a neuron. In this case I would be considered as a time-dependent input current. Here, however, we want to restrict ourselves to the simple form and take I as the control parameter of the bifurcation. If $I > 0$ then Eq. (2.8) has no fixed point and the phase grows continuously. For $I < 0$ two fixed points exist, a stable and an unstable equilibrium which are born at $I = 0$. As it becomes clear from the schematic of the bifurcation in figure 2.3 the dynamics for $I < 0$ are always approaching the stable equilibrium but if a perturbation out of it is large enough to overcome the threshold of the unstable fixed point, then the trajectory shows the large excursion along the limit cycle.

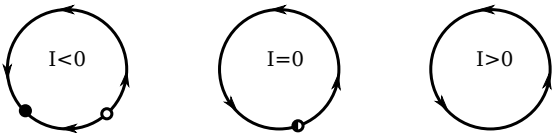

Figure 2.3: Saddle node bifurcation on an invariant cycle. Based on the theta model, Eq. (2.8).

Transcritical bifurcation

At a transcritical bifurcation the number of fixed points does not change but its stability does. The prototypic form is:

$$\dot{x} = \mu x - x^2 \,. \tag{2.9}$$

Easily we see that $x^* = 0$ is a solution of the fixed point condition (2.4) for any given μ and it follows from $f'(x^*) = \mu - 2x^*$ that $x^* = 0$ is stable if $\mu < 0$ and unstable otherwise. A second solution exists at $x^* = \mu$ whose stability is opposite to that of the first solution: it stabilises when μ changes from negative to positive. The geometric analysis and the bifurcation diagram are shown in the second row of figure 2.2.

Supercritical pitchfork bifurcation

Pitchfork bifurcations are known in two types and can occur in systems with a certain symmetry. For example the polynomial equation for dynamics undergoing a supercritical pitchfork bifurcation

$$\dot{x} = \mu x - x^3 \tag{2.10}$$

is invariant under a change of $x \to -x$. Again $x^* = 0$ is a fixed point and, again, it changes from stable to unstable (compare $f'(x^*) = \mu - 3x^2$). In contrast to the transcritical bifurcation, for $\mu \leq 0$ no other steady state can be found whereas for $\mu > 0$ two additional fixed points exist: $x^* = \pm\sqrt{\mu}$. Both are stable. The bifurcation diagram explains why it is called a 'pitchfork' bifurcation (see geometric analysis in third row of figure 2.2).

Subcritical pitchfork bifurcation

The second kind of pitchfork bifurcation is called subcritical and has the same symmetry as the last example, $x \to -x$, but the cubic

term acts destabilising:

$$\dot{x} = \mu x + x^3 \,. \tag{2.11}$$

The non-trivial steady states $x^* = \pm\sqrt{-\mu}$ exist only for $\mu < 0$ and are unstable, accompanying the stable solution $x^* = 0$. At values $\mu > 0$ where the non-trivial solutions disappear, the origin becomes unstable (see forth row of figure 2.2).

It is possible to add a stabilising term to Eq. (2.11) without breaking the symmetry:

$$\dot{x} = \mu x + x^3 - x^5 \,. \tag{2.12}$$

In contrast to system (2.11), in this equation the origin is the only equilibrium for $x < \mu' < 0$. At μ' two pairs of fixed points are born at a saddle-node bifurcations, whose unstable branches decrease and vanish at $\mu = 0$. The stable branches grow away from $x = 0$. See the fifth row of figure 2.2. Now a trajectory in $x = 0$ can be perturbed either weakly and relax back into the origin or strong enough to relax into a different equilibrium state.

Hopf bifurcation

The systems treated so far in this section were one-dimensional. A system state in two dimensional phase space can do more than just grow or shrink, it can come back to a state visited before and close the trajectory. A closed trajectory is called a **limit cycle** when all neighbouring trajectories are not closed, i.e. they are either attracted or repelled by the limit cycle.

A Hopf bifurcation is the creation of a limit cycle out of a fixed point. It can be understood by considering a dynamical system in polar coordinates of the following form:

$$\dot{r} = r(\mu - r^2) \tag{2.13a}$$

$$\dot{\phi} = 2\pi \,. \tag{2.13b}$$

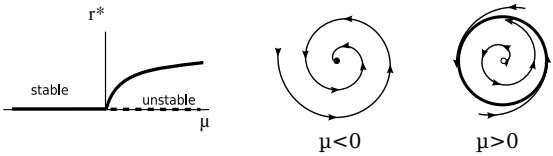

Figure 2.4: Hopf bifurcation. Bifurcation of the radial component r shown to the left. For $\mu < 0$ the origin is the only stable equilibrium, all trajectories spiral into it with constant angular momentum $\dot{\phi}$ (middle). Values $\mu > 0$ result in the unstable point $r^* = 0$ and the stable solution $r^* = \sqrt{\mu}$. All trajectories which do not start in the origin spiral towards the limit cycle (right).

The dynamics of the radial and angular coordinates (r, ϕ), with $r \geq 0$, are independent from each other and therefore can be analysed separately. The angular velocity $\dot{\phi}$ is constant, so a phase point will rotate around the origin with constant velocity.

The dynamics of the radial component, Eq. (2.13a), is identical to the prototypic pitchfork bifurcation, Eq. (2.10). We recall the results from the pitchfork bifurcation now with r confined to be positive: $\mu < 0$ leads to a stable steady state at $r^* = 0$ and $\mu > 0$ results in an unstable origin plus the stable equilibrium $r^* = \sqrt{\mu}$.

The interpretation of these results in the two-dimensional plane shows a phase point rotating around the origin with a constant angular velocity. The distance to the origin approaches the fixed point of Eq. (2.13a). Therefore in the case of $\mu < 0$ all trajectories will spiral into the origin whereas in the case of $\mu > 0$ the trajectories spiral towards the limit cycle at $r^* = \sqrt{\mu}$ (see figure 2.4). The Hopf bifurcation is the mechanism through which biochemical oscillations, as presented in section 3.3, arise and it is the way how oscillator death due to diversity is introduced into the circadian pacemaker cells of chapter 5 which enhances the ability of the system to synchronise with a perdiodic signal.

2.2.3 Solving differential equations numerically

So far we were able to derive analytic expressions of special solutions that reveal where the system ends up after very long times. When neither a full functional solution of Eq. (2.2) nor a fixed point solution can be found one has to fall back to approximative numerical methods. Two different classes of approximate algorithms have been used throughout the thesis. When the actual dynamical behaviour is of interest, rather than just the fixed point, or when there are many different fixed points and one wants to know how different initial conditions evolve one would use integration algorithms like a forth-order Runge-Kutta method. This method can become very costly when the time scales and the system size are very large. In cases where only the fixed point is of importance many root finding methods to solve the fixed point equation (2.4) are known. If a fixed point exists and convergence can be assured it might be much faster than integrating the dynamical equations for long times.

2.3 Noise induced phenomena

The dynamical systems of interest in section 2.2 were all deterministic: a selected initial condition always evolves along the same trajectory. Many observations in nature seem to lack this property, for example it has not been possible to predict neither the exact moment at which a radioactive atom spontaneously decays nor the exact place of a small particle immersed in water after some time. While the mechanism that controls the spontaneous decay is of quantum mechanic origin, the unpredictability of the particle in water originates in the 'uncountable' number of deterministic collisions the particle is subjected: a precise, deterministic, description of

this so called Brownian motion would require the formulation and solution of the equations of motion for every single water molecule in the system and full knowledge of the initial conditions. Instead one can ask for probabilities, rather than precise predictions, and base the reasoning on statistical properties.

2.3.1 A random process

Brownian motion has played a central role in the investigation of random processes and it seems natural to use this model to introduce random processes. In the year 1827 Robert Brown observed pollen floating in water under his microscope. The velocity of a particle of mass m submerged in a fluid should be damped with force that can be approximated by Stokes' law of friction $F(t) = -\alpha v(t)$. The equation of motion for such a particle without any additional forces reads:

$$m\dot{v}(t) = -\alpha v(t)\,. \tag{2.14}$$

The solution of above equation is well known. It tells us, that a particle of initial velocity v_0 will transfer its kinetic energy to the fluid and the velocity decays exponentially as $v(t) = v_0 e^{-tm/\alpha}$. However, this is not what Robert Brown observed: "While examining the form of these particles immersed in Water, I observed many of them very evidently in motion..." (Brown 1828, page 162)

The transfer of kinetic energy is due to the many collisions the particle will receive along its way. In this sense Eq. (2.14) is valid only if the mass of the particle is large. If the mass is small enough that the collisions alter the position macroscopically then the force has to be modified to account for them. One could argue that the collisions act as a small additional random force, sometimes accelerating the particle, sometimes decelerating it. Then the equation of motion reads:

$$\dot{v}(t) = -\gamma v(t) + \sigma\xi(t)\,, \tag{2.15}$$

with $\gamma = \alpha/m$. This stochastic differential equation is called a **Langevin** equation and $\xi(t)$ is called Langevin force or the noise term, σ is the noise strength or **diffusion constant** and $-\gamma v(t)$ the **drift**.

Since the average velocity $\langle v(t) \rangle$ should obey the deterministic form, Eq. (2.14), it is assumed that the average over the Langevin force is zero:

$$\langle \xi(t) \rangle = 0 \,. \tag{2.16}$$

Furthermore we assume that the collisions with different molecules are independent and that the collision time is small compared to the relaxation time $\tau = 1/\gamma$, therefore we can write:

$$\langle \xi(t)\xi(t') \rangle = \delta(t - t') \,. \tag{2.17}$$

The Langevin force defined in such a way is called white noise. The velocity of the particle, described by Eqs. (2.15-2.17), will vary from system to system since the random term $\xi(t)$ varies as well. Therefore, instead of looking for a solution to Eq. (2.15) one can ask for the probability $P(v) = W(v)\,dv$ that the particle's velocity is in the interval $(v, v + dv)$. The probability density W will depend on time t and the initial distribution, its evolution can be described by the respective **Fokker-Planck** equation (see for example Risken 1989):

$$\frac{\partial W}{\partial t} = \gamma \frac{\partial (vW)}{\partial v} + \frac{\sigma^2}{2} \frac{\partial^2 W}{\partial v^2} \,. \tag{2.18}$$

Derivations of the Fokker-Planck equation can be found in many textbooks for example the books by Risken (1989), Gardiner (1985) or van Kampen (2007). A full integration of this particular equation (2.18) can be achieved by an appropriate change of variables but the solution will not be presented here. The stationary solution of Eq. (2.18) recovers Maxwell's distribution of velocities. What we want to notice here is that the Fokker-Planck equation is a deterministic partial differential equation that describes how the probability density of the underlying stochastic dynamical system, here the velocity of a Brownian particle, evolves in time.

In the following we will present some examples, where the presence of stochastic elements in the dynamical systems can introduce drastic changes in their behaviour. Firstly we show how the introduction of noise can change the stability and number of equilibrium solutions, not unlike the phenomenon of phase transitions in statistical mechanics. Then we elaborate on the possible changes of the dynamic behaviour due to an intermediate level of noise.

2.3.2 Noise induced transitions

Consider the dynamical system of the Verhulst equation

$$\dot{x}(t) = \mu x(t) - x(t)^2 \,, \tag{2.19}$$

which originally goes back to a model proposed for the growth of biological populations but can be obtained from other problems too. For example the chemical Schlögl reaction (Schlögl 1972):

$$\begin{aligned} A + X &\rightleftharpoons 2X \\ B + X &\rightarrow C \,, \end{aligned} \tag{2.20}$$

where an autocatalytic reaction (the first step) interacts with a sink mechanism of the product X (the second step), can be expressed in the form of Eq. (2.19) when the concentration of species A and B are kept constant and C is removed from the system by the experimentalist. It can be shown that, under the so-called mean-field approximation where correlations are neglected, the population $x(t)$ of product X follows Eq. (2.19). In section 2.2 we have seen that Eq. (2.19) undergoes a transcritical bifurcation, i.e. a stable fixed point turns unstable and an unstable fixed point gets stable (see fig. 2.2, second row). In the present case, where X is a chemical substance or the size of a population, it has to be $x(t) \geq 0 \,, \forall t$, therefore the trajectories approach $x^* = 0$ for $\mu < 0$ and $x^* = \mu$ otherwise, perturbations from the steady state return in the characteristic time μ^{-1}.

If we now consider the case that the environmental fluctuations, the perturbations, act on the parameter μ with a time scale faster then μ^{-1} then we will find an example of the remarkable effects which noise can have on dynamical systems: the stationary solution obtains qualitatively different forms, depending on the strength of the fluctuations. As we have done with the friction in the model of Brownian motion we will replace the parameter by a sum of a constant term and a varying term $\mu(t) = \mu + \sigma\xi(t)$ with $\xi(t)$ defined in the sense of the Langevin force, Eqs. (2.16) and (2.17). Now we can write the stochastic equation:

$$\dot{x}(t) = \mu x(t) - x(t)^2 + \sigma x(t)\xi(t)\,. \tag{2.21}$$

By following an appropriate calculus * the respective Fokker-Planck equation can be obtained:

$$\partial_t W(x,t) = -\partial_x \left[\left(\mu x(t) - x(t)^2 + \frac{\sigma^2}{2} x(t) \right) W(x,t) \right] + \frac{\sigma^2}{2} \partial_{xx} x(t)^2 W(x,t)\,. \tag{2.22}$$

The analysis of the above equation and of the boundary conditions of the process reveal three possible regimes. Consider that the limit $x \to \infty$ acts like a natural boundary, i.e. it is not reached even in $t \to \infty$ and the process therefore will not explode. The other end of the state space, $x = 0$, changes its properties depending on the value of μ: for negative μ it represents an attracting boundary, i.e. it will be attained in the asymptotic limit $t \to \infty$. Furthermore, the drift and diffusion terms at $x = 0$ are both zero. As a consequence the stationary distribution $W_{st}(x)$ for $\mu < 0$ is a delta-distribution such that all probability is concentrated at zero. At $\mu = 0$ the picture changes, as the lower boundary becomes natural and is no longer attracting.

*The different interpretations of an integral of a random term (namely the Ito calculus or the Stratonovich calculus, see (Risken 1989), (Gardiner 1985) or (van Kampen 2007)) can lead to different Fokker-Planck equations. In the presented case both interpretations lead to the same *qualitative* result, thus we limit our considerations to the Stratonovich interpretation.

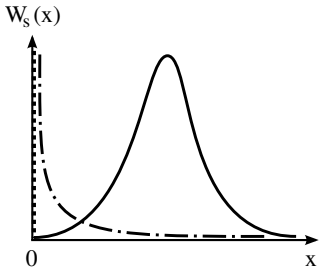

Figure 2.5: Sketch of the stationary probability density for the stochastic Verhulst model: $\mu < 0$ (dotted curve), $0 < \mu < \sigma^2/2$ (dash-dotted curve) and $\mu > \sigma^2/2$ (continuous curve). The curve changes from a delta distribution at $x = 0$ over a monotonously decaying distribution to a distribution with a single maximum at $x \neq 0$.

Although the most probable value in the stationary state, the maximum of $W_{st}(x)$, is still $x = 0$ it is not attained by any sample path, so that some probability has 'leaked' out of the delta-distribution to the side (compare the dotted and the dash-dotted curves in figure 2.5). The third regime is observed when $\mu > \sigma^2/2$, where the maximum of $W_{st}(x)$ is no longer in $x = 0$. It changes abruptly to $\mu - \sigma^2/2$ such that the stationary distribution is now decaying to both sides of the maximum. A continuous curve sketches this case in figure 2.5.

The dynamical system of Eq. (2.19) shows two noise-induced transitions, one at $\mu = 0$ and another one at $\mu = \sigma^2/2$. The mean and variance of the population in the stationary state for $\mu > 0$ follow from the solution W_{st} of Eq. (2.22) as:

$$\langle x \rangle = \int_0^\infty x W_{st}(x) dx = \mu \tag{2.23}$$

$$\langle (x - \langle x \rangle)^2 \rangle = \mu \sigma^2/2 \,. \tag{2.24}$$

The change of the stationary probability distribution at $\mu = 0$ is not reflected in the mean and variance. However, it can be seen,

that for $\mu = \sigma^2/2$ the standard deviation $\sqrt{\langle(x - \langle x\rangle)^2\rangle}$ and the mean coincide, a result which can be interpreted as follows: for values $0 < \mu < \sigma^2/2$ the fluctuations dominate over autocatalytic growth and extinction is the most probable outcome*. For larger values of μ the autocatalytic growth overcomes the fluctuations and a non-zero population size is most probable.

The transition of the behaviour in the Verhulst-system with fluctuating parameter at $\mu = \sigma^2/2$ is already present in the deterministic case. At $\mu = 0$ the fixed point $x = 0$ gets unstable and a new solution appears. The noise term only shifts the transition towards larger values. A thorough introduction into noise-induced transitions, a complete analysis including the stationary solution and the Fokker-Planck equation considering both Ito and Stratonivoch calculus for the Verhulst model and other systems with more profound modifications of the macroscopic behaviour of a dynamical system under the influence of fluctuations can be found in (Horsthemke & Lefever 1984). Other effects of fluctuations on dynamical systems, that do not change the fixed point but rather the dynamical behaviour, will be introduced in the following.

2.3.3 Resonance effects

When an oscillator is periodically fed with energy and the driving period is close to (one of) the intrinsic period(s) of the oscillator, the whole system is said to be in **resonance**. If the oscillator's damping is small enough then even very small amplitude driving lets the oscillator accumulate energy and lead to high amplitude oscillations. Common examples of this effect include the guitar's body that resonates with the vibration of a string or the centre of mass of someone sitting on a swing and moving the legs back and

*Note that the value $x = 0$ is never achieved due to the natural boundary of the continuous system but population size will fall below any given ϵ. Therefore, if x were discrete, distinction would be observed.

forth. These systems show oscillatory behaviour even in the absence of a periodic forcing, when energy is only applied once.

Benzi *et al.* (1981) proposed and showed that a system which simply dissipates a one time energy supply can show resonances to oscillatory forcing of small amplitude. The effect they termed **stochastic resonance** and it has attracted a lot of attention ever since.

Stochastic resonance

To characterise this effect various measures have been proposed. The **signal-to-noise ratio** (SNR) is a notion from the formalism of data analysis. It interprets the forcing as an input signal and compares the system's reaction to its noisy background. To this end one starts by defining the power spectral density of the signal:

$$S(\omega) = \int_{-\infty}^{+\infty} \mathrm{e}^{\imath\omega\tau} \langle\!\langle x(t+\tau)x(t) \rangle\!\rangle d\tau \,, \tag{2.25}$$

which is the Fourier transform of the correlation function $\langle\!\langle x(t+\tau)x(t) \rangle\!\rangle$, the average over noise and over the initial phases of the input. For unforced stochastic systems it should be a continuous function decaying with large frequencies. In the case that a periodic force drives the system it is expected that $S(\omega)$ is the sum of a background spectrum $S_N(\omega)$ and delta spikes at multiples of the driving frequency. The signal-to-noise ratio is the proportion of the power in the output spectrum at the driving frequency to its background activity at that frequency (Gammaitoni *et al.* 1998):

$$SNR = \frac{2}{S_N(\Omega)} \lim_{\Delta\omega \to 0} \int_{\Omega-\Delta\omega}^{\Omega+\Delta\omega} S(\omega) d\omega \,. \tag{2.26}$$

An alternative approach that will be used in chapter 5 is the spectral power amplification (Jung & Hänggi 1991) which compares the output power p_{out} to the power of the input signal p_{in}. In the case of

an harmonic driving $A_0 \cos(\Omega t + \phi)$ the output power is $p_{in} = \pi A_0^2$ and then the spectral power amplification reads:

$$\eta = \frac{p_{out}}{p_{in}} = \frac{\lim_{\Delta\omega \to 0} \int_{\Omega-\Delta\omega}^{\Omega+\Delta\omega} S(\omega) d\omega}{\pi A_0^2} . \tag{2.27}$$

The spectral density can be expressed with the Fourier series of the correlation function, then the limit in Eq. (2.27) reduces the integral to the first Fourier coefficient M_1:

$$\eta = \frac{4|M_1|^2}{A_0^2} = \frac{4}{A_0^2} \left| \frac{\Omega}{2\pi} \int_{-\pi/\Omega}^{\pi/\Omega} \langle\!\langle x(t) \rangle\!\rangle e^{-i\Omega t} dt \right|^2 \tag{2.28}$$

In this form it is a measure that is readily accessible and it has been applied to calculate resonance effects in the numerical simulations of chapter 5.

A generic model that exhibits stochastic resonance and that was proposed by Benzi *et al.* (1981) can be constructed when we consider a stochastic extension of the prototype model for the supercritical pitchfork bifurcation in the bistable regime (Eq. (2.10), $\mu = 1$) and apply a time periodic forcing to it:

$$\dot{x}(t) = x(t) - x(t)^3 + A_0 \cos(\Omega t + \phi) + \sqrt{2}\sigma\xi(t) . \tag{2.29}$$

A_0 and Ω denote the forcing's amplitude and frequency respectively, ϕ its initial phase. Without any forcing, $A_0 = 0$, the particle's position will fluctuate around one of the two minima $x_m = \pm 1$ of the time independent double well potential:

$$V(x) = -\frac{1}{2}x^2 + \frac{1}{4}x^4 \tag{2.30}$$

and occasionally a large perturbation will make the particle jump over the barrier into the other minimum. The jump rate will depend on the noise intensity and the form of the potential, an approximation was given first by Kramers (1940), a review on the widespread

uses of this result was written by Hänggi *et al.* (1990). The jump rate reads:

$$r_K = \frac{1}{\sqrt{2}\pi}\exp\left(-\frac{\Delta V}{\sigma^2}\right). \tag{2.31}$$

The precise form of the potential is approximated by the height of the barrier $\Delta V = V(0) - V(x_m)$. A high barrier or low noise results in few jumps whereas a low barrier or high noise provokes many jumps.

When the periodic forcing is switched on, $A_0 \neq 0$, then the potential becomes time dependent, $V = V(x,t)$. The forcing breaks the symmetry of the potential as it periodically rises one minimum and lowers the other and vice versa after half a period. This favours a jump towards the lower lying minimum, hence it leads to a periodically modulated jump rate. If the average waiting time $T_K = 1/r_K$ is about twice the period of the signal then it comes to a resonance between the statistic jumps and the periodic rocking of the potential.

If we consider only the jumps between minima and ignore the local dynamics we can straightforwardly imagine a model of just two possible states, $\pm x_m$, with periodically changing jump rates. This simplified system is the first for which a full analysis of the stochastic resonance was achieved (McNamara & Wiesenfeld 1989). In this case, the SNR in leading order reads:

$$SNR = \pi\left(\frac{A_0 x_m}{\sigma^2}\right)^2 r_K \tag{2.32}$$

$$\sim \sigma^{-4}\mathrm{e}^{-\Delta V/\sigma^2}. \tag{2.33}$$

An example of the SNR in dependence of noise strength, according to Eq. (2.33), is shown in the left panel of Figure 2.6. The SNR grows with rising noise strength and passes through a maximum to then decline with large noise strengths. The maximum marks the stochastic resonance, the noise strength where the output is best 'seen' against the background noise. Interesting in this result, and differing from the classic understanding of resonance, is the

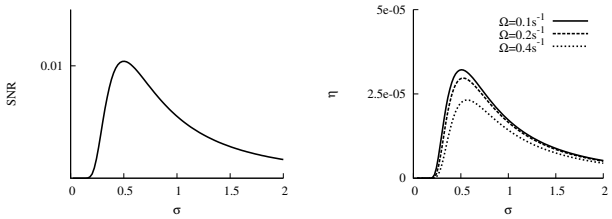

Figure 2.6: left: Signal-to-noise ratio for a particle in a discrete two-state potential with weak periodic forcing, Eq. (2.32), and parameters $A_0 x_m = 0.1$. right: Spectral power amplification, Eq. (2.34), for three different driving frequencies.

independence of the driving frequency Ω: any frequency will resonate. A look at the spectral power amplification η of the two-state model (see, e.g. Anishchenko *et al.* 2007)

$$\eta = \frac{4r_K^2 x_m^4}{\sigma^2(4r_K^2 + \Omega^2)} \tag{2.34}$$

shows that a maximum exists for all frequencies (compare figure 2.6, right). The maximum in the SNR and in η do not coincide. After reaching the maximum in the SNR a higher noise strength yields more power in the output signal, however the noise background is higher as well which means that the SNR is going down where the spectral power still is rising.

The field of stochastic resonance is well-known by now and the effect has been found experimentally in a large variety of systems. They range from physical systems like Schmitt triggers and ring lasers over chemical systems like the Schlögl reaction to biological systems like sensory neurons, ion channels or animal behaviour (see Anishchenko *et al.* 2007; Gammaitoni *et al.* 1998, and therein).

Coherence resonance

The main ingredient for the appearance of ordered behaviour in the scope of stochastic resonance is the external forcing whic lies outside of the system. We now want to consider a situation where noise enhances the coherence of oscillatory modes already present within the system. The first reports on that effect concerned enhancement of limit cycle oscillations near the Hopf bifurcation by Ebeling *et al.* (1986) or for limit cycles that (dis-)appear via a saddle-node bifurcation (Gang *et al.* 1993; Rappel & Strogatz 1994). In the work by Pikovsky & Kurths (1997) this effect was studied on excitable systems and the phenomenon was termed **coherence resonance**, although the technically more correct term of **stochastic coherence** was coined by Zaikin *et al.* (2003).

Typically an excitable system has one stable fixed point and an unstable fixed point nearby. Small perturbations of the resting system are damped out but a perturbation large enough to pass the unstable fixed point lead to a return via a large excursion in phase space, usually called a pulse, a spike or firing. After a pulse the system is in a refractory state for a while, in which perturbations do not lead to a new pulse. The precise form of the excursion is largely independent on the strength of the perturbation.

The system of choice in (Pikovsky & Kurths 1997) is a reduced form of the Fitzhugh-Nagumo model, which reads:

$$\begin{aligned} \epsilon\dot{x}(t) &= x(t) - \frac{x(t)^3}{3} - y(t) \\ \dot{y}(t) &= x(t) + a + \sigma\xi(t)\,. \end{aligned} \tag{2.35}$$

It can be thought of as a model that imitates the generation of action potentials in nerve cells, lacking the complexity of more biological models such as Hodgkin-Huxley type models or others (see, e.g. Izhikevich 2007). The small parameter $\epsilon \ll 1$ separates fast dynamics, $x(t)$, from slow ones, $y(t)$. Eqs. (2.35) have a limit cycle when

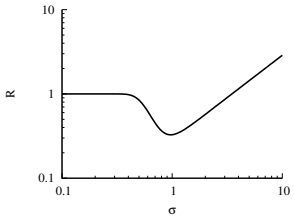

Figure 2.7: Coherence Resonance: for intermediate noise values the jitter is low. Less noise lets the activation time t_a dominate the spike interval, therfore $R = 1$. At higher noise the fluctuations $\mathrm{Var}(t_e) \sim \sigma^2 \langle t_e \rangle^2$ dominate the jitter and it is $R \sim \sigma$. Compare Eq. (2.36). Here we have set $\langle t_e \rangle = 1$ and $\langle t_a \rangle = \exp(1/\sigma^2)$.

$|a| < 1$ or show excitable dynamics with one attracting fixed point if $|a| > 1$. In the excitable regime one observes noise induced pulses whose frequency and regularity depend on the noise strength.

The time between subsequent pulses, the interspike interval t_{ISI}, is composed of the activation time t_a it needs for a pulse to be generated and the time it takes for an entire excursion in phase space, t_e. On average the activation time can be estimated by Kramers rate (2.31), $\langle t_a \rangle \sim \exp(const/\sigma^2)$, and its fluctuations by $\mathrm{Var}(t_a) \approx \langle t_a \rangle^2$. For a uniform velocity along the excitation the average excursion time $\langle t_e \rangle$ is only weakly dependent on the noise amplitude but it fluctuates with $\mathrm{Var}(t_e) \sim \sigma^2 \langle t_e \rangle^2$. The phenomenon of coherence resonance becomes clear by looking at the normalised fluctuations of the interspike interval (or **jitter**):

$$R = \frac{\sqrt{\mathrm{Var}(t_{ISI})}}{\langle t_{ISI} \rangle} \approx \frac{\sqrt{\langle t_a \rangle^2 + \sigma^2 \langle t_e \rangle^2}}{\langle t_a \rangle + \langle t_e \rangle} \,. \tag{2.36}$$

Figure 2.7 shows a hypothetical curve of the jitter versus the noise strength, where we have set $\langle t_e \rangle = 1$ and $\langle t_a \rangle = \exp(1/\sigma^2)$. Low values of R resemble a highly ordered pulse sequence whereas high

values of R are a consequence of unordered spiking. In the low noise limit t_a dominates the time between pulses and the jitter is $R \approx 1$. High noise lets t_a decrease dramatically such that its contribution to the interspike interval is negligible. It is dominated by t_e and the jitter grows with $R \sim \sigma \langle t_e \rangle^{-1/2}$. In between both regimes coherence resonance is found: $R(\sigma)$ passes through a minimum and the correlation time through a maximum, both signatures of a more regular spiking behaviour.

2.4 Collective phenomena

So far we have read about isolated dynamical systems governed by a set of differential equations. They can be used, for example, to describe chemical reactions (see chapter 3) or particle transport processes (chapter 4) or to describe the classical motion of objects with interacting forces. In several cases, however, the system under study is composed by a very large number of variables (degrees of freedom) in constant interaction. This is for instance the case for the atoms forming a gas or as well for the more abstract systems we investigate in chapters 6, 7 and 8. In such a situation, a dynamical system's approach (which reduces to solve Newton's equations) is computationally unaffordable as there are of the order of 10^{23} units and it is analytically intractable for the collisions between particles, which introduce nonlinear interaction terms into the dynamics.

On the other hand, as we will see in the above mentioned chapters and in the somewhat 'smaller' system of coupled neurons in chapter 5, the behaviour that multicomponent systems evidence as a byproduct of the interaction between many individual dynamics cannot be inferred from the behaviour of a single unit in many cases: it is a purely collective phenomenon that arises due to the nonlinear interactions. As a matter of fact, collective phenomena are ubiq-

uitous in nature: from the bird and fish flocks to the stock market evolution, from the large scale weather or the turbulent behaviour of a fluid to the brain activity, all are multicomponent systems whose units interact locally and nonlinearly and whose global behaviour is an emergent and collective property of the system.

Alternative paths to describe the phenomenology of such systems are needed, ways that connect the microscopic dynamics, i.e. the dynamical systems, with their global emergent properties. This is indeed the framework of statistical mechanics, whose guiding motif is to connect the dynamics of each variable (the so-called microphysics) with the system's global behaviour through a statistical description. In such a framework, global variables (such as the pressure, the volume, or the global magnetization in a material, or the average speed in a bird flock, to cite some) allow several microscopic states with equivalent global variables. Accordingly, global variables (that describe collective behaviour) are quoted macrostates, and the number of different microstates that lead to the same macrostate is a measure of the probability of a system to evidence a given global property. Macroscopic deterministic laws arise insofar some macrostates appear with a probability that differs from 1 by terms of order $N^{-1/2}$ (being N the number of variables).

2.4.1 Phase transitions: generalities

An important example of a collective phenomenon is the dramatic change in the macroscopic state of a system when a certain parameter (control parameter) is smoothly varied: one says that the system has evidenced a phase transition, where the different macroscopic states are called different phases.

A system will always tend to minimize its energy and maximize its entropy in order to reach a thermodynamic equilibrium, what in the language of statistical mechanics corresponds to the min-

imisation of its free energy (incidentally, the free energy is derived from the Hamiltonian of the system, which encodes the local dynamics of each variable, therefore connecting microphysics with macroscopic behaviour). By changing a control parameter (such as temperature or in general an intensive variable) the thermodynamic system will evolve into a new equilibrium state. A phase transition takes place when such equilibria are related for instance to different sets of symmetries. Such is the case in the solid-liquid transition of water: below the freezing temperature $T_0 \approx 0°C$, the equilibrium state (i.e. the state minimizing the free energy) is such that molecules arrange in a hexagonal crystal with discrete rotational symmetry (ice), whereas above T_0 the equilibrium state has continuous rotational symmetry, corresponding to a liquid phase. Of course other evidences than symmetry changes can take place in phase transitions, and the classification of such transitions has received several descriptions. The distinguishing feature of most phase transitions is the appearance of a non-zero value of an **order parameter**, i.e. a macroscopic variable which is non-zero in the ordered phase (or equivalently, the lower symmetrical phase) but identically zero in the disordered (highly symmetrical) phase. The natural order parameter of a multicomponent system is not always straightforwardly found and in some cases it is not even an observable. Examples of order parameters include the difference in the density between phases (solid-liquid-gas transitions), the net magnetization (ferromagnetic transitions), or the degree of orientational order (liquid crystals) to cite a few.

If the order parameter suffers from a discontinuity in the vicinity of a phase transition, it is named **first order**, and both phases are in equilibrium at the transition. An example is the solid-liquid transition of water, where the density evidences a discontinuity at the freezing temperature $T_0 \approx 0°C$. If, on the other hand, the order parameter vanishes continuously then the transition is suspected to be **second order** or **continuous**: the state of both phases at the transition is the same. Note at this point that as the order parameter

vanishes in the transition, it can serve as an expansion parameter to describe the nature of the transition, as will be shown in forthcoming chapters.

The change of stability of a certain phase is a **collective phenomenon** since it arises from the interaction among the elements. A proper connection between the microscopic dynamics and the macroscopic observables is obtained from the principles of statistical mechanics. It starts by defining the Hamiltonian $\mathcal{H}$ of the system, which corresponds to the total energy and describes the evolution of the system on a microscopic scale according to its internal and external interactions. It is usually impossible to obtain even a numerical solution to that Hamiltonian of a high number of variables necessary to describe the phase transition, say the boiling of a litre of water. To overcome this difficulty, statistical mechanics aims at the statistics of such a system and obtains solutions for macroscopic variables as a statistic consequence of the interaction of a large number of elements. One considers a large (virtual) ensemble of systems in different microstates representing the same macrostate. This leads to the **partition function**

$$\mathcal{Z} = \int \exp(-\beta \mathcal{H}) \,, \tag{2.37}$$

where $\beta = 1/kT$ and k is Boltzmann's constant and T the temperature. The partition function allows to derive all macroscopic properties of the system, such as the free energy

$$\mathcal{F} = -kT \ln(\mathcal{Z}) \,. \tag{2.38}$$

With the definition of the free energy the distinction between first order and second order transitions can be made more rigorous: If a first derivative of the free energy shows a discontinuity then the transition at that point is named first order. The jump of the entropy, $S = -\partial \mathcal{F} / \partial T$, corresponds to a latent heat, energy that is applied (or freed) when the system passes from one phase to the other. The

change in energy does not result in a change of the macroscopic observables. If, on the other hand, the first derivatives are continuous but the higher derivatives are discontinuous or infinite, then the transition is named as higher order, continuous or critical transition. This corresponds to a divergence of the susceptibility and correlation length. Interestingly, the magnitude of the discontinuity is unimportant in terms of the classification of the phase transition. In the next section we provide a quick overview of the most important features of second order phase transitions, namely their critical behaviour and the universality of their critical exponents.

2.4.2 Criticality and universality at second order phase transitions

In the last section we have argued that second order phase transitions evidence discontinuities in the second derivative of the free energy, corresponding to divergences of the susceptibility and correlation length. Interestingly, data from multiple experiments and results from exactly solvable models have shown that several thermodynamic quantities can be described by a set of power laws in the vicinity of the critical temperature. The theory of critical phenomena states that near the critical point, the order parameter m, the susceptibility χ, the specific heat C and the correlation length ξ, which is defined through the exponentially decreasing correlation function $\Gamma(r) = \langle \rho(0)\rho(r) \rangle \sim r^{-\tau} \exp(-r/\xi)$ of some microscopic quantity ρ at locations with distance r, vary as:

$$m \sim |\epsilon|^{\beta}, \tag{2.39a}$$

$$\chi \sim |\epsilon|^{-\gamma}, \tag{2.39b}$$

$$C \sim |\epsilon|^{-\alpha}, \tag{2.39c}$$

$$\xi \sim |\epsilon|^{-\nu}, \tag{2.39d}$$

where we used the definition of a reduced temperature:

$$\epsilon = 1 - T/T_c\,. \tag{2.40}$$

At the critical temperature T_c itself two more relations can be found. The order parameter m varies with its conjugate field H as

$$m \sim H^{1/\delta} \tag{2.41}$$

and the correlation $\Gamma(r)$ varies with distance as

$$\Gamma(r) \sim r^{-(d-2+\eta)}\,, \tag{2.42}$$

with d being the dimension of the system.

The constants denoted by small Greek letters are called **critical exponents**. The sign in the exponents of above relations can be reasoned with thermodynamic arguments that can provide relations between the exponents. The definitions of the thermodynamic properties show that the six exponents are not independent of each other.

It turns out that, whereas the critical temperature T_c depends sensitively on the details of the microscopic interactions, the critical exponents are to a large degree universal, depending only on a few fundamental properties such as dimensionality or symmetries. Accordingly, two systems undergoing a second order transition can be very different in context but share the same critical exponents: one says that both systems belong to the same universality class and hence share similar behaviour near the transition. Examples of different universality classes include the $2D$ and $3D$ Ising, the $3D$ XY, the $3D$ Heisenberg or the $2D$ q-state Potts, where the names characterize the simpler models of each class.

A first approximative theory to derive the critical behaviour in the vicinity of second order transitions was introduced by Landau, and is based in the concept of a **mean field**. Conceptually speaking, the main idea of a mean field theory is to replace all interactions in a N body system to a single body with an average or effective interaction. A first step is therefore to state an effective, coarse-grained Hamiltonian. In order to describe the phenomenology behind a second order (ferromagnetic) transition, by making use of

arguments based solely on locality and symmetries, Ginzburg and Landau introduced such an effective Hamiltonian. Then, a very simple expression for the free energy can be estimated from this Hamiltonian through a mean field approximation, that essentially assumes that the free energy is analytic and shares the same symmetries of the coarse-grained Hamiltonian. Critical exponents can be found accordingly, yielding values $\beta = 1/2$, $\gamma = 1$, $\alpha = 0$, $\nu = 1/2$, $\delta = 3$. While the Landau theory turns to be wrong quantitatively speaking (essentially, the mean field approximation removes the presence of fluctuations, which become very important close to the critical point), mean field theory is always a good starting point for analysing different systems undergoing second order transitions, in order to gain analytical understanding of the specific phenomenology (concretely, the theory makes specific predictions for what kind of non-analytic behaviour one should see when the underlying free energy is analytic.) Landau theory turns to be correct when the dimensionality of the system is large enough (larger than the so called upper critical dimension), since in this situation fluctuations are not that relevant. For lower dimensionalities, a rigorous derivation of the critical exponents requires the renormalization group theory. This theory as well provides justification for using the absolute value of the reduced temperature in Eqs. (2.39), (2.41) and (2.42), which effectively means that the exponent is the same if one approaches the transition from one side or from the other side. Renormalisation group theory proved that this indeed is the case.

2.4.3 Finite size scaling

The singularities in the thermodynamic functions in a critical point, and the associated power law scaling, are only well defined in the thermodynamic limit, and therefore do not hold in finite systems due to finite-size effects. For instance, in finite systems the correlation length cannot diverge, simply because the system is not infinite. Indeed, it can be argued that no singularity can take place in finite

systems since in that case the partition function, the free energy, the average energy and others are analytic functions of the inverse temperature β and so do not have singularities at finite temperature. Accordingly, one finds that close to the transition, the correlation length is no longer a diverging quantity, but rather is of the order of system length L. The theory of finite size scaling (Cardy 1988; Ferdinand & Fisher 1969; Fisher & Ferdinand 1967) tells us how to modify the power laws in (2.39) and (2.41) in order to take into account (and accordingly, how to detrend) these finite size effects that remove true criticality in finite systems. Consider a d-dimensional euclidean system with linear size L. Then the susceptibility χ (which diverges with the correlation length as $\xi^{\gamma/\nu}$ in the infinite system) follows

$$\chi = \xi^{\gamma/\nu}\phi(\xi/L), \tag{2.43}$$

where $\phi(u)$ is a scaling function, with the property that $lim_{u\to 0}\phi(u) = const$. Now, since the correlation length itself scales with the reduced temperature as $\xi \sim |\epsilon|^{-\nu}$, one finds that the (finite size) scaling for the susceptibility is

$$\chi = L^{\gamma/\nu}\tilde{\phi}(L^{1/\nu}\epsilon), \tag{2.44}$$

where $\tilde{\phi}$ is another scaling function. A plot of χ versus T will be peaked around $T = T_c + v_0 L^{-1/\nu}$, with a width $v_1 L^{-1/\nu}$ and height $L^{\gamma/\nu}$. Thus, assuming the validity of the finite-size scaling hypothesis, studies of finite systems of different sizes (i.e. a so called finite size analysis) can give information about the critical exponents of the infinite system (for mean field analysis where the system size is characterized by the number of variables N, one assumes homogeneity and therefore $N = L^d$). This theory can be derived heuristically using again the renormalisation group, and systematically through field-theoretic renormalisation group.

2.4.4 A phase transition induced purely by noise

We have seen that under certain conditions a change of temperature or of some external field can make a collective system undergo a phase transition with special characteristics like the critical exponents. In addition we have seen how a random force term in isolated dynamical systems yields a tremendous change of the equilibrium state. As we will be investigating phase transitions in collective systems under the effect of quenched noise in chapters 6, 7 and 8, we want to present now a kind of prototype model for phase transitions induced purely by the presence of a noise term.

Consider dynamics in a regular lattice of dimension d where the local steady state of an uncoupled element varies continuously with the noise term $\xi(t,\vec{r})$, defined as in section 2.3:

$$\begin{aligned}\dot{x}(t,\vec{r}) &= -x(t,\vec{r})\left(1+x(t,\vec{r})^2\right)^2 + \left(1+x(t,\vec{r})^2\right)\sigma\xi(t,\vec{r}) \\ &= -\left.\frac{\partial V(x,\xi)}{\partial x}\right|_{t,\vec{r}}\end{aligned} \tag{2.45}$$

Figure 2.8 shows, for a better understanding, some instantaneous potentials $V(x)$ for given values of ξ. In this case of uncoupled elements the average position $\langle x(t)\rangle$ in an ensemble approaches zero for long times. However, on short time scales the dynamics favour non-null values such that $\langle x(t)\rangle$ initially grows away from zero. This means, as van den Broeck *et al.* (1997) argue and show, that the "destabilisation" of the zero solution can be responsible for the formation of local ordered regions if the elements are coupled to their neighbourhood $\mathcal{N}(\vec{r})$:

$$\begin{aligned}\dot{x}(t,\vec{r}) = -x(t,\vec{r})\left(1+x(t,\vec{r})^2\right)^2 + \left(1+x(t,\vec{r})^2\right)\sigma\xi(t,\vec{r}) \\ + \frac{C}{2d}\sum_{\vec{r}'\in\mathcal{N}(\vec{r})}\left(x(t,\vec{r}')-x(t,\vec{r})\right).\end{aligned} \tag{2.46}$$

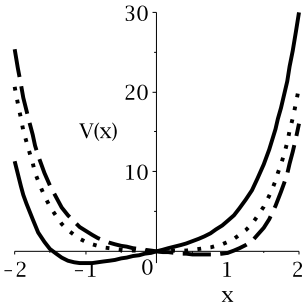

Figure 2.8: Local instantaneous potential for the dynamics of Eq. (2.45) for $\xi < 0$ (solid line), $\xi = 0$ (dotted line) and $\xi > 0$ (dashed line). The steady state varies continuously with ξ.

The ordered regions might subsequently grow, i.e. for a sufficiently high coupling constant C the system exhibits a phase with broken symmetry in the steady state $\langle x \rangle \neq 0$ for intermediate values of noise strength σ. Numerical calculations at the phase transitions show that typical criticality is observed: the fluctuations of the order parameter rise according to a power law with system size and the critical exponents suggest that the model belongs to the universality class of Ising models.

2.5 Diversity in collective dynamical systems

We have seen in section 2.2 how the value of a single parameter can change significantly the stationary solution of a dynamical system and in section 2.3 how the stationary solution is changed when the strength of a rapidly fluctuating force term is varied. In both cases we were looking at uncoupled systems and only in section 2.4 the

interest went for systems with a large number of coupled variables. As one possible source of the rapidly fluctuating forces we identified the collisions of particles due to their thermal motion which corresponds to a linear stochastic term in the microscopic equations.

Scientists in the seventies of the 20th century started to consider magnetic systems with impurities or heterogeneity. This results in varying interactions instead of (or apart from) a fluctuating force. As the impurities do not change in time, or in a time scale much slower than the spin dynamics, they are usually called by the term **quenched disorder**. When the variations are applied to the local interactions between the elements the systems are called spin glass systems, in the case of a varying coupling to the external field one talks about random field Ising-models. A wealth of literature has addressed the phenomenology behind spin glasses and random field models including phase diagrams, ageing and other dynamical behaviour and comparison with their equilibrium counterparts (see Calabrese & Gambassi 2005; Crisanti & Ritort 2003; Young 1998, and references therein).

Quenched disorder is not limited to the interaction terms. Interacting oscillators could have diverse natural frequencies or biological cells in an absorbing tissue could have different volumes. Many different causes for heterogeneity are possible. If the microscopic dynamics lack a time dependent stochastic term, i.e. they are deterministic, the system can be understood as a zero temperature system in terms of statistical mechanics. Quenched noise systems without any time dependent noise term are the main scope of this thesis. In the following we will see some exemplary results from recent studies of non magnetic systems.

2.5.1 Diversity-induced resonance

If we remember the case of stochastic resonance we stated that a (overdamped) particle in a double-well potential can amplify an

input signal of low amplitude when subjected to the right amount of noise. The prototype (as given in Eq. (2.29)) has a polynomial potential of fourth order, a sinusoidal input signal and an additive stochastic force term. By considering a large number of bistable systems coupled through the mean position of all particles Tessone *et al.* (2006) discovered the ability of diversity to enhance the system's answer to a periodic signal. The dynamics:

$$\dot{x}_i = x_i - x_i^3 + \eta_i + \frac{C}{N}\sum_{j=1}^{N}(x_j - x_i) + A_0 \sin(\Omega t)\,, \tag{2.47}$$

differs from Eq. (2.29) in two aspects: First, we now have N elements coupled to each other with a coupling strength C and, second, the stochastic force term is replaced by an additive force η_i which is constant in time. The extra forces are chosen randomly from a probability distribution that satisfies the conditions $\langle \eta_i \rangle = 0$ and $\langle \eta_i \eta_j \rangle = \delta_{ij}\sigma^2$. The variance σ of that distribution is referred to as **diversity**.

It was found by Tessone *et al.* (2006), that the spectral power amplification of the input frequency (Eq. (2.34)) passes through a maximum with respect to the diversity, meaning a maximal response to the external signal for intermediate values of diversity, an effect analogue to that of stochastic resonance. It is not limited to bistable systems. In the same work the authors analysed the response of coupled excitable systems to an external signal. To this end they coupled a number of Fitzhugh-Nagumo systems (Eq. (2.35)), replaced the stochastic force term by a constant force taken randomly from a distribution and added the periodic signal in the slow variable. Again a spectral power amplification was found for intermediate diversity levels. In a later work Toral *et al.* (2009) showed the possible amplification of a sinusoidal forcing in coupled linear oscillators with diversity in the natural frequencies.

2.5.2 Diversity-induced effects without forcing

In section 2.3 we have seen resonance effects caused by a stochastic force term in the presence and in the absence of an external forcing. The same effects have been observed in systems without a stochastic term. The diversity-induced effect described above is a reaction to an external periodic forcing, therefore more similar to stochastic resonance. We will now summarize two examples, one in an electronic system, the other in a biological, for which it has been shown theoretically that an enhancement of coherence can happen due to the presence of intermediate levels of diversity without the presence of any periodic forcing. In this sense it is similar to the reported effect of coherence resonance.

The Chua circuit is an electronic circuit consisting of a few elements that exhibits chaotic behaviour and can be modelled by a set of three differential equations. By changing the inductance of the components the circuit can be brought into a regime where the trajectory jumps chaotically between two domains of a chaotic attractor. If one considers only the residences in the two domains of the attractor one can define a jitter in the sense of Eq. (2.36). Chen & Zhang (2008) showed that the jitter passes through a maximum with respect to the introduced diversity, which means that the diverse elements lead the system from the chaotic regime to more or less regular jumps between the domains. Only a very high diversity brings the system back into a chaotic state.

The second example we will present here is quite different from the one before as it considers a spatially extended model. Goldbeter *et al.* (1990) proposed a minimal model to explain calcium oscillations induced by a signal transmitter. The signal transmitter *InsP3* (the principal phosphorus storage in many plant and animal tissues as well as in microorganisms) can trigger calcium oscillations by the interplay of calcium released from an InsP3 sensitive calcium pool which in turn triggers the release of calcium from an InsP3 insensitive calcium pool. The work has gained considerable attention. A

large number of cells with calcium dynamics in the sense of Goldbeter *et al.* (1990), arranged on a regular two-dimensional lattice and with diversified InsP3 saturation constants, have been investigated by Gosak (2009). The mean of the saturation constant is set to a value such that the single system is in a steady state, just below the Hopf bifurcation. The interaction between the cells is achieved by letting the calcium diffuse across the cells. Obviously a zero diversity leads the whole system into a steady state. However, a perturbation can trigger a calcium spike and in this way a distributed variation of the saturation constant acts like a distributed perturbation. As a consequence a rising diversity brings the extended system from a steady state into a state of coherent spiral waves which are destroyed for higher values of diversity where only fractions of wave fronts exist. A well defined spatial correlation function shows a pronounced maximum for intermediate diversity values, again underlining the ability of noise or diversity to induce coherent behaviour.

2.5.3 Synchronisation of diverse Kuramoto oscillators

When different things happen at the same time then the events are said to be synchronous. In an ensemble of oscillating elements the investigation of synchrony among them is a huge field that has attracted a lot of interest. A model for synchronising oscillators that was analysed extensively was presented by Kuramoto (1975, 1984). As it is the base for the investigations of chapter 6 we want to collect the main features of the original Kuramoto oscillators here. They are phase oscillators with random frequencies that are coupled to each other through the sine of their phase differences. The dynamical variable is the phase ϕ and its dynamics is governed by:

$$\dot{\phi}_i(t) = \omega_i + \sum_{j=1}^{N} K_{ij} \sin\left(\phi_j(t) - \phi_i(t)\right). \tag{2.48}$$

For a vanishing coupling matrix K_{ij} a single element simply rotates with a constant angular velocity. To see what happens in the coupled case it is instructive to consider the easiest case where coupling between all elements is equal: $K_{ij} = K/N, \forall i, j$. This reduces the model to a mean-field coupled one. When defining a complex order parameter as

$$\rho(t)\, \mathrm{e}^{\imath\Psi(t)} = \frac{1}{N} \sum_{j=1}^{N} \mathrm{e}^{\imath\phi_j(t)}\,, \tag{2.49}$$

which can be understood as the position of the centre of mass of all oscillators, then it becomes obvious how the local dynamics gets coupled to the global phase $\Psi(t)$:

$$\dot{\phi}_i(t) = \omega_i + K\rho(t) \sin\left(\Psi(t) - \phi_i(t)\right). \tag{2.50}$$

Now it is interesting to ask for the overall behaviour when the intrinsic frequency is taken from some probability distribution $g(\omega)$.

If the centre of mass, Eq. (2.49), is close to the unit circle ($\rho(t) \approx 1$) than we know that the single units are concentrated close to another whereas a vicinity to the origin ($\rho(t) \approx 0$) means that the oscillators are spread out widely along the circle. The first case is, where all oscillators have the same phase $\theta_i(t) = \Psi(t), \forall i$ is called global synchronisation. In between the extremal situations partially synchronised behaviour is observed. An analytic view of synchronisation in coupled Kuramoto oscillators is obtained by supposing infinite system size, $N = \infty$, and calculating the probability density $P(\theta, \omega, t)$ to find an oscillator with frequency ω at time t at the phase θ. For a symmetric distribution $g(\omega) = g(-\omega)$ Kuramoto (1975) found that a non-trivial order parameter, i.e. $\rho \neq 0$ arises for $K > K_c$ with $K_c = 2/[\pi g(0)]$. Kuramoto (1975) found not only the critical coupling strength but could give the solution of the order parameter in case a Lorentzian distribution $g(\omega) = \frac{\gamma/\pi}{\gamma^2+\omega^2}$ is used. It is then (for large times t):

$$\rho = \sqrt{1 - (K/K_c)}\,; \tag{2.51}$$

it grows with an exponent of $\beta = 1/2$ (see section 2.4.2), as it could be expected for the mean field approximation. This supercritical bifurcation turns into a subcritical in the case that $g''(0) > 0$. Stability of the synchronised state was analysed by Strogatz *et al.* (1992). A complete review of the Kuramoto model in the presence of noise, extended models and numerical methods for their treatment as well as applications can be found in (Acebrón *et al.* 2005).

2.6 Summary

This chapter has been written in an attempt to pave the way to the understanding of the results in the forthcoming chapters of part II. It is concerned with the basic mathematical and physical concepts known to the science of dynamical systems and nonlinear dynamics. It starts with a short and fairly general introduction to differential equations as a possible representation of a dynamical system, section 2.2. Different terms, such as the steady state and its stability, bifurcations, forces and their corresponding potentials are introduced. We show ways to analyse the behaviour of dynamical systems.

Subsequently, in section 2.3, the notion of stochastic processes is introduced by means of the well known example of Brownian motion. We sketched how a qualitative change of an equilibrium state can arise due to an additional random force with the example of the chemical Schlögl-reaction. Then we have summarised resonance effects that can be caused by noise: remarkable observations in stochastic dynamics, that have attracted a lot of attention since the eighties of the 20th century and are called stochastic and coherence resonance. Here an intermediate level of noise enhances a weak external signal (stochastic resonance) or enhances an intrinsic oscillatory mode without external forcing (coherence resonance).

Effects that arise solely from the interaction of a high number of dynamical systems are found in the section 2.4 about collective phenomena. These effects include the observation of phases that are fundamentally different in their symmetries. The transitions between phases can be classified according to the way the order changes from one phase to the other. Universal properties (critical exponents) are explained and the method of finite-size scaling, which allows the estimation of critical exponents in the thermodynamic limit, is introduced. The section closes with an example of a phase transition that is induced by the presence of a random force term.

Collective phenomena in diverse systems, i.e. systems that owe their randomness to time independent noise, are presented in section 2.5. Here the interacting elements possess some property that is randomly distributed along the population but does not change with time. Resonance effects, similar to those observed in stochastic dynamical systems, may arise with the 'right amount' of diversity: the switching in a bistable potential in resonance with a periodic driving; regular jumps between two domains of a chaotic attractor without a periodic forcing; induction of coherent spiral waves and synchronisation of phase oscillators with diverse natural frequencies.

We will now proceed with the introduction of the more biological background, both introductory chapters together mark the context of the chapters of part II.

Chapter 3

Applications in biochemistry

3.1 Introduction

Some of the chapters further down study nonlinear processes that are observed in a biological context. Deterministic and stochastic dynamical systems, as well as collective phenomena are concepts presented in chapter 2 that all can be observed in many different essential processes of living systems. The variety of studied fields is huge, they range from the description of organism abundance in predator-prey relationships (Hoppensteadt 1982), the active and passive motion of agents like animals, plankton or pollen, within moving media (Okubo & Levin 2001) or the electrochemical potentials in neurons (Izhikevich 2007).

In chapter 4 we will study the absorption of pharmaceuticals across a layer of intestinal cells. The drug molecules have to pass two cell membranes which are loaded with pumps that keep the molecules

out. It is the aim of section 3.4 to formulate the main properties of cell membranes and the main ways of possible transport.

The synchronisation of biochemical oscillations that master the daily rhythms of mammals is investigated in chapter 5. There, many oscillators are coupled among themselves and with an external light. The oscillations are the result of a periodic regulation in the expression of a gene which is what section 3.3 is going to introduce. It explains shortly the process of protein synthesis from DNA, presents an example of the influence of noise and shows biochemical oscillators that are based on the regulation of gene expression.

Both, gene regulation and some membrane transporters, can be approximated by the dynamics of enzyme reactions. To understand why these processes are so similar in their dynamics we will start this chapter with an introduction to enzyme reaction in section 3.2.

Textbooks that cover the presented topics from a biological perspective are for example (Nelson & Cox 2000) or (Alberts *et al.* 2002). A profound mathematical perspective of some of the processes and many physiological applications can be found in (Beuter *et al.* 2003).

3.2 Enzyme reactions

The micro-organism yeast has been used by humans for thousands of years to bake bread or ferment alcohol. With the invention of the microscope at the beginning of the 17th century it was possible to actually see yeast cells. It took until 1850, when Louis Pasteur (1822-1895) proved that alcoholic fermentation is conducted by living yeast. He went as far as postulating that alcoholic fermentation is in fact inseparable from the "live" in the yeast, a vital principal as a reason for the fermentation. However, Eduard Buchner (1860-1917) discovered that yeast extract, a substance free of any living

organism, is able to ferment sugar into alcohol, thus pure chemical reactions of molecules are responsible for the reaction. His work on fermentation processes was honoured with the Nobel Prize in Chemistry in 1907. The molecules responsible for facilitating the fermentation process were called **enzymes**.

The first enzyme to be isolated and crystallized was urease, a molecule catalysing the hydrolysis of urea, in 1926 by James B. Sumner (1887-1955). Urease is a protein, a polymer of amino acids, and with the exception of some catalytic RNA molecules all enzymes are proteins with molecular weights between 12000 and more than one million atomic mass units. Thousands of different enzymes have been identified and catalogued, some of them requiring only integrity of their amino acids, others rely on the presence of inorganic ions or of more complex substructures called coenzymes. The principle of all enzymes is catalysing a chemical reaction, i.e. they lower the activation energy necessary for the two or more molecules to react. The substances before reaction are called **substrates**, the substances at the end of the reaction are called **products**.

The existence of catalysts is essential for living systems. Many reactions, relevant for example for food digestion, nerve signalling or motoric action, are very slow under normal biological conditions. By binding the substrate molecule(s) to the active site of the enzyme an enzyme-substrate complex is formed. It provides an environment which energetically favours the reaction and thus accelerates the rate of production. A schematic view of the function of enzymes is depicted in figure 3.1, where an imaginary enzyme catalyses the breaking of a metal stick.

3.2.1 Simple kinetics

If we now look at a very simple enzymatic reaction, where one substrate molecule S binds to the enzyme E which then decays into

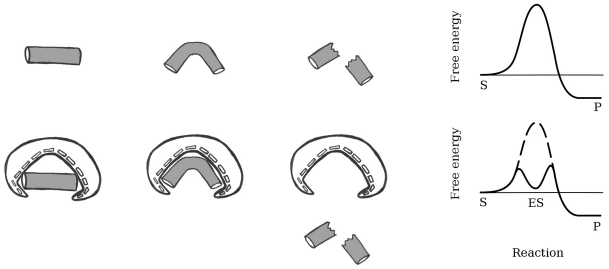

Figure 3.1: The breaking of a stick (top row, from left to right): A metal stick (the substrate) is first bent to an intermediate state. Then it breaks (product). The energy diagram (on the right) shows the energy barrier of the intermediate state. The broken stick has less free energy than the original one. The catalysed breaking of a stick (bottom row, from left to right): The enzyme has a binding site formed like the intermediate state of the stick. It is equipped with little magnets which lower the free energy of the intermediate state (enzyme-substrate complex, ES). Energy diagram on the right. (adapted from Nelson & Cox 2000, page 252)

one product P plus an uncombined enzyme, one might write

$$S + E \rightleftharpoons ES \rightleftharpoons P + E\,. \tag{3.1}$$

In 1913 the two scientists Maud L. Menten (1879-1960) and Leonor Michaelis (1875-1949) published a famous work on the function of invertase (or saccharase) (Michaelis & Menten 1913). Invertase is an enzyme, found for example in yeast, which catalyses the breakdown of sucrose. What Menten and Michaelis postulated and reasoned was the following: the reaction starts with the relatively fast combination of the complex

$$S + E \underset{k_{-1}}{\overset{k_1}{\rightleftharpoons}} ES \tag{3.2}$$

and is followed by a rather slow decay into the product and the enzyme

$$ES \underset{k_{-2}}{\overset{k_2}{\rightleftharpoons}} P + E\,. \tag{3.3}$$

By assuming a high energy barrier for the combination of a product with an enzyme the backwards rate k_{-2} can be neglected. In this way one can write down a set of differential equations for the dynamical variables $s(t), e(t), c(t)$ and $p(t)$, resembling substrate, enzyme, complex and product concentration respectively:

$$\begin{aligned}
\dot{s}(t) &= k_{-1}c(t) - k_1 s(t)e(t) && \text{(3.4a)}\\
\dot{e}(t) &= (k_{-1} + k_2)c(t) - k_1 s(t)e(t) && \text{(3.4b)}\\
\dot{c}(t) &= -(k_{-1} + k_2)c(t) + k_1 s(t)e(t) && \text{(3.4c)}\\
\dot{p}(t) &= k_2 c(t) && \text{(3.4d)}
\end{aligned}$$

After a short time of rapid complex building the rates of complex formation and breakdown will be in a steady state of flow, leading

to a constant concentration $c(t)$ meaning $\dot{c}(t) = 0$. The sum of bound and unbound enzyme molecules is constant $c(t) + e(t) = e_0$ and one can eliminate $e(t)$ in (3.4c). The steady state concentration of complexes is

$$c(t) = \frac{e_0 s(t)}{s(t) + \frac{k_{-1}+k_2}{k_1}} \equiv \frac{e_0 s(t)}{s(t) + K_M} \tag{3.5}$$

and K_M is called the Michaelis-Menten constant. When this equation is substituted into the dynamics of the product one finds:

$$\dot{p}(t) = \frac{k_2 e_0 s(t)}{s(t) + K_m} \equiv V_{max} \frac{s(t)}{s(t) + K_m}\,, \tag{3.6}$$

which is a form that can easily be compared with an experiment. For large substrate concentrations the production velocity saturates at V_{max} whereas low substrate concentrations lead to velocities of $V_{max}s/K_M$. The constants K_M and V_{max} have been determined for many enzymes. A graphical analysis of the parameters can be achieved by plotting the production rate $\dot{p}$ versus the substrate concentration (Michaelis-Menten plot) or by plotting the reciprocal of both sides of Eq. (3.6) (Lineweaver-Burk plot):

$$\frac{1}{\dot{p}} = \frac{K_m}{V_{max} s} + \frac{1}{V_{max}}\,. \tag{3.7}$$

A scheme of how both methods are applied can be seen in left and right panel of figure 3.2.

3.2.2 Enzyme cooperativity

The kinetics we have seen until now refer to reactions with single substrate molecules only. When the enzyme has more than one binding site for the substrate one talks about **cooperativity**. It comes in different flavours: *Positive* cooperativity is when the first

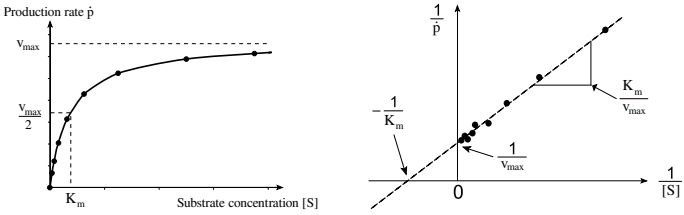

Figure 3.2: A Michaelis-Menten plot of an enzyme reaction. The maximal production rate v_{max} can only be approximated since it is reached at infinite substrate concentration. The Michaelis-Menten constant K_m is the concentration at which the production rate is half its maximum (left panel). The double reciprocal Lineweaver-Burk plot allows determination of V_{max} to a higher degree of accuracy than the Michaelis-Menten plot (right panel). (figures adapted from Wikipedia 2010*a*,*b*).

substrate bound to the enzyme increases the binding rate for the next substrate molecule, *negative* cooperativity is the opposite case and in *independent* cooperative enzymes no influence on the binding rate by previously bound molecules is seen. Depending on the number of binding sites different dynamics are observed. For two binding sites we can write:

$$S + E \underset{k_{-1}}{\overset{k_1}{\rightleftharpoons}} SE \xrightarrow{k_2} P + E \tag{3.8}$$

$$S + SE \underset{k_{-3}}{\overset{k_3}{\rightleftharpoons}} S_2E \xrightarrow{k_4} P + SE \tag{3.9}$$

As before we assume a large substrate concentration (so $s(t) \approx \text{const}$) and a "quasi-steady-state" where complex production is equal to its decay: $\frac{d}{dt}[SE](t) = \frac{d}{dt}[S_2E] \approx 0$ (flow equilibrium). This means

$e_0 = [SE] + [S_2E] + [E]$. From this we obtain:

$$\dot{p}(t) = \frac{[k_2\Lambda_2 + k_4 s(t)]\, e_0 s(t)}{\Lambda_1\Lambda_2 + \Lambda_2 s(t) + s(t)^2} \tag{3.10}$$

with

$$\Lambda_1 = \frac{k_{-1} + k_2}{k_1} \quad \text{and} \quad \Lambda_2 = \frac{k_{-3} + k_4}{k_3} \tag{3.11}$$

This is a general result. Let's have a look at some examples.

Example: independent binding sites

Independent means that the binding rates are not influenced by the number of bound molecules. Since the first molecule to come has two sites to choose from and dissociation can start with either one of the two bound molecules we have:

$$\begin{aligned} k_1 &= 2k_3 \\ k_{-3} &= 3k_{-1}\,, \end{aligned} \tag{3.12}$$

hence $\Lambda_2 = 4\Lambda_1$ and

$$\dot{p}(t) = \frac{2e_0 k_2 s(t)}{2\Lambda_1 + s(t)}\,. \tag{3.13}$$

The reaction velocity of an enzyme with two independent binding sites is twice that of an enzyme with one binding site.

Example: positive cooperativity

In this case the binding of the first molecule favours the binding of the second, so the rates are $k_3 \gg k_1$, which is approximated by

the limits $k_1 \to 0$ and $k_3 \to \infty$ and the product $\Lambda_1\Lambda_2 = \text{const}$. As a consequence the production rate of Eq. (3.10) reduces to:

$$\dot{p}(t) = V_{max}\frac{s(t)^2}{\Lambda_1\Lambda_2 + s(t)^2} \tag{3.14}$$

Example: higher numbers of binding sites

When there are more than one binding site the derivation of the production velocity yields:

$$\dot{p}(t) = V_{max}\frac{s(t)^n}{\prod_{i=1}^{n}\Lambda_i + s(t)^n} \tag{3.15}$$

This is called the Hill-equation (Hill 1910). The production rate shows a sigmoid shape as a function of substrate concentration.

We see that by now the investigation of enzymatic reactions can look back on a 100 years of history. It is a wide field and the kinetics presented here treat only the simplest cases. The production rates of many enzymes, called **allosteric enzymes**, are controlled by molecules (the **ligands**) other than the substrate. In this case the kinetic equations above have to be altered.

In an example of a biochemical oscillator further down (section 3.3.2) we will make use of a reaction rate modeified in a simple way to model an allosteric enzyme. A review on the kinetics of cooperative and allosteric enzymes was written by Ricard & Cornish-Bowden (1987), a more recent, comprehensive and accurate enzyme kinetic theory can be found in many modern textbooks.

3.3

Gene expression and biochemical oscillators

The central dogma of molecular biology is a simplified explanation of protein synthesis from their genes. Although it is now known to be a far more complex process it can be reduced to four main processes. The first step is called **transcription**, the duplication of the information stored within the nucleobases of the DNA. This is achieved by the enzyme RNA-polymerase which copies the genetic code into a messenger RNA (mRNA) molecule. Since the amount of genes is not changing, the rate at which translation happens can be assumed to be constant. When the completed mRNA finds its way to one of the many ribosomes then the ribosome **translates** the mRNA piecewise into the complete protein by chaining together the amino acids in the right order as it is coded in the mRNA and therefore in the DNA molecules. If one thinks of the very high number of ribosomes but limited number of mRNA then it is a valid assumption that the translation rate is proportional to the number of mRNA molecules. The image has to be completed by taking into account that the degradation of both, the mRNA and the protein. As a whole the central dogma can be written down as a number of reactions with different reaction rates:

$$r, p \xrightarrow{k_R} r+1, p \tag{3.16}$$

$$r, p \xrightarrow{r\,k_P} r, p+1 \tag{3.17}$$

$$r, p \xrightarrow{r\,\gamma_R} r-1, p \tag{3.18}$$

$$r, p \xrightarrow{p\,\gamma_P} r, p-1\,, \tag{3.19}$$

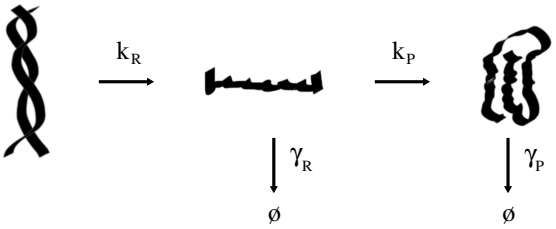

Figure 3.3: Sketch of the central dogma of molecular biology. The gene is part of the DNA (left) and transcribed to the mRNA (middle). Then the protein (right) is translated from the mRNA. Both, the mRNA and the protein, decay with a given rate.

where p, k_P and γ_P denote the protein number, production and decay rate and r, k_R and γ_R the respective quantities for the mRNA (see figure 3.3). The whole idea goes back to the ideas of Francis Crick (Crick 1970), co-discoverer of the DNA molecule structure.

This model is very simple as it does not account for the interaction of various genes or proteins. Apart, a modern, more precise, description of protein synthesis has to include the intermediate steps of mRNA maturation and posttranslational modification of the protein into the active molecule. With molecule numbers being integer numbers and their changes given by (average) reaction rates (s^{-1}), Eqs. (3.16-3.19) refer to a stochastic dynamical system with a discrete phase space. Stochastic in nature it will not be possible to predict exact numbers of molecules in the cell. As usual one has to rely on probabilities. In the following section we will present a steady state solution and a remarkable conclusion from the central dogma of molecular biology.

3.3.1 Noise suppression by negative feedback

As pointed out the protein synthesis is a stochastic process so one can only ask for probabilities or mean values. Under above assumptions of a single gene transcription without any interaction the steady state probability has been given in (Thattai & van Oudenaarden 2001). It turns out that the mRNA distribution in equilibrium is that of a Poisson distribution: $\langle r \rangle = k_R/\gamma_R$ and $\sigma^2[r]/\langle r \rangle = 1$. It is only dependent on the mRNA production and decay rates. The resulting number of proteins is:

$$\langle p \rangle = \frac{k_R}{\gamma_P}\frac{k_P}{\gamma_R}, \tag{3.20}$$

$$\frac{\sigma^2[p]}{\langle p \rangle} = 1 + \frac{\frac{k_P}{\gamma_R}}{1+\frac{\gamma_P}{\gamma_R}} \approx 1 + \frac{k_P}{\gamma_R}. \tag{3.21}$$

The approximate value for the normalised fluctuations, Eq. (3.21), is a result from the observation that typical lifetimes of mRNA is larger than that of proteins, thus the ratio $\gamma_P/\gamma_R \approx 0$. We see that the protein's normalised fluctuations are larger than 1 which means that the distribution is broader than a Poisson distribution. That would result in very large fluctuating molecule numbers.

We pointed already out that the central dogma as described above is a simplified version of what is going on in reality. It is very well known, that proteins can regulate the expression of genes, both positively or negatively. If a given protein acts upon its own gene one talks about autoregulation. It has been shown that in regulatory network of *E. coli* the majority of feedback circuits are negatively (or repressively) autoregulated circuits (Thieffry *et al.* 1998). A negative gene regulation (see figure 3.4) can be modelled by a modification of the mRNA production rate k_R. One possibility to do so is that we assume that the unregulated rate is decreased linearly by the presence of protein p: $k'_R = k_R(1 - \epsilon p)$. The factor ϵ is a measure for how strong the inhibition is. Using this rate in the system of protein

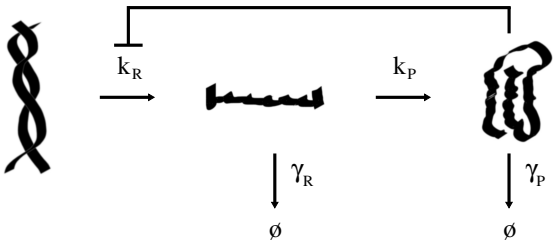

Figure 3.4: Negative gene regulation. The standard of gene expression (as in fig. 3.3) is extended by an inhibition of transcription, denoted by the arrow ending in a bar over the rate k_R, due to the presence of protein molecules. The result is that the fluctuations of the process are decreased.

synthesis one finds the following result:

$$\begin{aligned} \langle p \rangle &= \langle p \rangle_0 \frac{1}{1 + \langle p \rangle_0 \epsilon} \\ &= \langle p \rangle_0 - \epsilon \langle p \rangle_0^2 + O(\epsilon^2) \end{aligned} \tag{3.22}$$

for the regulated mean protein number and

$$\frac{\sigma^2[p]}{\langle p \rangle} = 1 + \frac{\frac{k_P}{\gamma_R}}{1 + \frac{\gamma_P}{\gamma_R}} - \epsilon \langle p \rangle_0 \frac{k_P + \gamma_R}{\gamma_P + \gamma_R} + O(\epsilon^2) \tag{3.23}$$

for its fluctuations. Here $\langle p \rangle_0$ denotes the unregulated protein number, Eq. (3.20), so we can see that the negative autoregulation shifts the mean to smaller values and reduces the width of the distribution. The fluctuations of protein molecule number is reduced.

Although the fluctuations can be reduced by autoregulation, the gene expression is an inherently noisy process, mainly due to the low molecule number in cells. A lot of experimental studies have shown the stochasticity in gene expression and they have investigated the different sources of it (see for example the works by Elowitz *et al.* (2002), Ozbudak *et al.* (2002) or Blake *et al.* (2003)).

3.3.2 Biochemical oscillators

Observations of oscillatory behaviour are ubiquitous in biological systems. Reported time scales and levels of organisation range from milliseconds in the periodic discharge of neuron membrane potentials via seconds in the beating of a heart, tens of minutes in the oscillating transpiration and water uptake of the cereal grain oat to the various hours of the periodic spore release in fungi (for a collection of data see Rapp 1979). Even longer time scales can be observed in mammalian hormone levels oscillating over weeks or mating activities over years. It is therefore of large interest to study the mechanisms leading to such behaviour.

Probably the first biochemical oscillation identified experimentally is the periodic conversion of sugar to alcohol, called glycolysis, reported by many studies in the 1960s in yeast cell extract (see e.g. Pye & Chance 1966) or in yeast cell populations (Gosh *et al.* 1971). It can be understood when looking at an intermediate enzymatic step that donates phosphorus from an ATP molecule to the reaction and thus produces an ADP molecule, which in turn activates the enzymatic reaction. The corresponding reaction network prototype of two chemical species, as seen in figure 3.5, leads to the **Substrate-Depletion Oscillator**: a constantly supplied substrate Y turns with help of an enzyme into product X at a low rate. The rate is substantially increased by the binding of product molecules to the enzyme (see section 3.2). We will use a Hill equation to modify the reaction rate of $Y \to X$ thinking of two binding sites for the ligand. With an appropriate transformation one can derive dimensionless equations for the rescaled concentrations of the chemical species (Tyson 2002):

$$\dot{x}(t) = \nu\,(z(t) - x(t))\,\frac{\epsilon^2 + x(t)^2}{1 + x(t)^2} - x(t)\,, \tag{3.24a}$$

$$\dot{z}(t) = \kappa - x(t)\,. \tag{3.24b}$$

In the remaining parameters ν stands for the reaction rates of the fully activated enzyme, $\epsilon^2\nu$ is the rate in absence of the product.

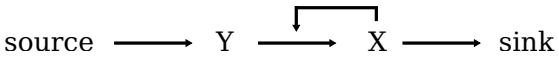

Figure 3.5: The reaction network of a Substrate-Depletion Oscillator where the product X activates its own production. The more X is present, the faster is its production until Y is reduced faster than it is (constantly) fed into the system. Without Y no more X is produced and its concentration goes down.

The rate at which the substrate flows into the system κ is the parameter with which we will control the reaction. Both, ν and κ are normalised by the rate at which the product X is cleared from the reaction. Variable $z(t)$ is the sum of substrate plus product.

With a short algebra one obtains the steady state

$$x^* = \kappa \quad \text{and} \quad z^* = \kappa \frac{1 + \kappa^2}{\nu(\epsilon^2 + \kappa^2)} \,. \tag{3.25}$$

Stability of the equilibrium is only assured for very large or very small values of κ, intermediate inflows of substrate lead to an unstable steady state and the creation of a stable limit cycle through a Hopf bifurcation (page 17). See figure 3.6 for example trajectories.

With just two variables the presented system is one of the simplest models capable of oscillatory trajectories. Others can be found but we want to go on to a three dimensional system as it is the basis for modelling the oscillations of cells that work as pacemaker in animals and plants.

3.3.3 The Goodwin oscillator

The oscillator named after Goodwin (1965, 1966) is based on proteins that can inhibit their own synthesis. In this idea the translation and activation of the protein follows a linear production rate and

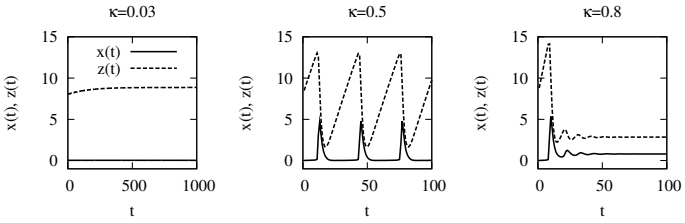

Figure 3.6: Trajectories of a Substrate-Depletion oscillator. Product X (continuous line) and the sum of product plus substrate Z. For intermediate substrate inflow κ stable oscillations can be observed. Small values for κ leads to a continuous approach of the equilibrium (left panel, note the extended time span), whereas too large inflows lead to damped oscillations around the steady state (right). Parameters: $\nu = 1.0, \epsilon = 0.05$. The curves were obtained from numerical integration of Eqs. (3.24).

degradation. The transcription rate of *mRNA* is, however, a term that saturates at zero with rising protein concentration. Figure 3.7 displays the reaction network, a set of equations could read:

$$\dot{x}(t) = \frac{1}{1+z(t)^p} - bx(t)\,, \tag{3.26a}$$

$$\dot{y}(t) = b\,(x(t) - y(t))\,, \tag{3.26b}$$

$$\dot{z}(t) = b\,(y(t) - z(t))\,. \tag{3.26c}$$

In this dimensionless form variable x represents the *mRNA* concentration, y the protein concentration and z that of the activated protein. For simplicity we assume here that the linear parameter $b, b > 0$ is equal in all three equations. Then it turns out that the steady state $x_1^* = x_2^* = x_3^*$, the fixed point of the equation $1/(1+(x^*)^p) = bx^*$ destabilizes through a Hopf bifurcation for $bx^* < (p-8)/8$. It shows us that, since x is a positive number, oscillatory behaviour requires a minimal value for the binding cooperativity p, that is p needs to be

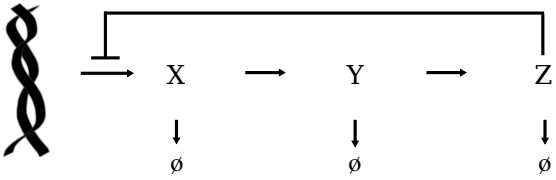

Figure 3.7: Reaction network of the Goodwin oscillator. The transcription of *mRNA* (X) is suppressed by the presence of the activated protein (Z). The unprocessed protein Y is not active in the inhibition of *mRNA* transcription.

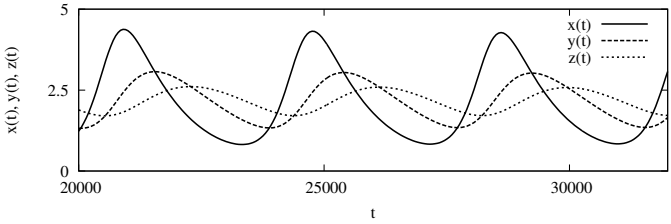

Figure 3.8: Trajectories of *mRNA* (X), unprocessed (Y) and activated protein Z for parameters in the oscillatory regime: $p = 9, b = 10^{-4}$.

bigger than 8. Goodwin wasn't aware of that, it was Griffith (1968) who did this analysis and writes that Goodwin "now considers his result (oscillations with $p = 1$, N.K.) to have arisen erroneously out of errors in the analogue simulation which he employed" (page 207). A typical oscillatory trajectory of Eqs. (3.26) can be seen in figure 3.8. It can be shown that the minimal exponent p decreases when more chemical species are involved. That is, for example, if the chain of figure 3.7 is extended with a fourth species then one can find a limit cycle already for $p > 4$ (Tyson 2002).

This kind of oscillator plays a major role in the modelling of the pacemakers for the rhythmic activity of animals and plants. In-

vestigation of the *per* gene in *Drosophila* and the discovery of its essential role in generating circadian (nearly daily) rhythms has led to remarkable advances in the understanding of the underlying molecular mechanisms of biological clocks. A model for *per* transcription and translation has been put forward by Goldbeter (1995) and is the base for many subsequent works. In chapter 5 we will analyse a model for the pacemaker neurons in mammals that is based on the Goodwin oscillator. It is, however, made up of two activating and one inhibiting regulation.

3.4 The cell membrane and transport processes

In chapter 4 we will analyse a specific model for the absorption of drugs across a mono-cellular layer of epithelial cells into the blood stream. As the substance enters and leaves the cells it has to pass twice a cell membrane. To prepare the reader with the needed understanding of the biological processes this section introduces the main aspects of the cell membrane and the mechanisms that lead to an interchange of substances or information between the inside and the outside of a living cell. It is kept phenomenological as the details of the interactions, the consequences of the thermodynamic principles, can not be presented here and the reader is referred to the literature.

3.4.1 Historical notes

The biological cell is the basic unit of all known organisms: both unicellular or multicellular. Knowledge of cells as such starts with microscopic observations. Robert Hooke (1635-1703) published a book called *Micrographia* in 1665 where he gave account of his observations with various lenses where he, among other things, described

cork as he saw it under his microscope (fig. 3.9). The elementary units of the structure he called **cells**.

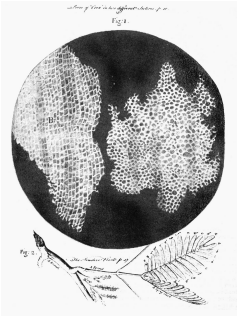

Figure 3.9: Cork oak cells and mimosa leaves. Robert Hooke, Micrographia, 1665. (taken from Wikipedia 2010*d*).

If we look at a living cell from the outside, we basically see a closed and more or less rigid container with selectively permeable walls and macromolecules sticking out of it. These walls are called **cell membranes**. (Cells with a different outermost cover, the cell wall, are not relevant within the scope of this thesis.) When we go into the container, into the **cytoplasm**, we can see that one group of cells holds smaller containers, the **organelles**, made of the same kind of membrane. Cells of this group are called **eukaryotes** and form the base of animals, plants and fungi. Cells without membrane-bound containers, like those of bacteria, are called **prokaryotes**. The macromolecules sticking out of the membrane are called **membrane proteins**. Some are docked onto one side of the membrane, others penetrate it from one side to the other. The membrane proteins are used to communicate the cytoplasm with the outer world.

The plasma membrane defines the periphery of the cell and it separates its content from the environment. Nowadays it can be isolated from other cell constituents by centrifugal techniques and then

chemically analysed. Its composition turns out to vary between kingdoms, species, tissues and cell types but among all known kind of cells certain structural similarities and therefore properties are shared: Biological membranes are impermeable to most polar and charged solutes and permeable to nonpolar compounds, probably their most remarkable and important feature.

At the end of the 19th century, before the dawn of electron microscopy, it was hypothesised, that a living cell is an electrolyte surrounded by a membrane, impermeable to ions. It was lead by the discovery that **lipid**-soluble molecules pass easily into cells (see Robertson 1981, and therein). Hugo Fricke measured the electric capacity of red blood cell membranes around the year 1925. He supposed that the membrane is formed by a thin oil film and calculated its thickness to 3.3*nm* (Fricke 1925). A great deal of understanding biomembranes was achieved by studying lipids and the monomolecular films they form on surfaces in the years before Fricke's findings.

Lipids are a class of molecules found in organisms which are not soluble in water. They are either **hydrophobic**, which means they are repelled by water, or consist of both a **hydrophilic** and **lipophilic** part, thus combining "water-loving" and "fat-loving" properties in one molecule. The latter are called **amphiphilic** and are, as we will see in a few paragraphs, the key to understanding the biomembranes.

Amphiphilicity of some of the lipids was deduced by measuring the thickness and the surface tension of oil films in confined areas on water surfaces (Devaux 1932; Rayleigh 1890, and therein). The surface tension goes through a sharp transition when measuring its dependence on oil film thickness. Irving Langmuir (Langmuir 1917) interpreted this observation as a transition from a phase where the molecules are randomly arranged on the water to a phase of a closed structure, with the polar heads in the water and the nonpolar carbon chains in the air. It is known now, that the amphiphilic

constituents of the cell membrane are mainly **phospholipids**, where the hydrophilic head is a phosphate group and the hydrophobic tail a number of hydrocarbon chains.

In the same year when Fricke published his observations on red blood cells, Gorter and Grendel did an interesting experiment, as well with extracted red blood cells. They measured the cells' surfaces and then separated the membrane from the plasma with washing techniques. When they measured the amount of molecules contained in the membrane they found that it is "exactly sufficient to cover the total surface of the chromocytes [red blood cells] in a layer that is two molecules thick" (Gorter & Grendel 1925, pg. 439). A remarkable conclusion if one considers the modern view of the cell membrane, as we present in the following subsection and depict in figures 3.10 and 3.11.

3.4.2 A modern view on the cell membrane

These classical experiments, the use of electron microscopy and thermodynamic considerations lead to what is known as the **fluid mosaic model** (Singer & Nicolson 1972). Expenditure of free energy is necessary to transfer nonpolar molecules into water and likewise to transport polar, or ionic, molecules from water into a nonpolar medium. The same can be assumed for the respective groups in amphiphilic molecules. Therefore a number of phospholipids submerged in water can minimise the free energy by forming various structures. Cylindrical molecules for example can minimise energy by aligning in two layers side by side, with the nonpolar tails pointing at each other and the polar heads being surrounded by water (see figure 3.10, left). Such planar layers are studied experimentally by meeting the boundary conditions with a rigid wall between two compartments (see for example Winterhalter 2000). Without the conditions the edges are in contact with water and the bilayer sheet is therefore unstable. When the bilayer closes on itself due to local

curvature it can form a stable vesicle, called **liposome** (fig. 3.10, middle). They can enclose other aqueous solutions. Other phospholipids, with a rather wedge shaped geometry, can build a closed structure around nonpolar substances. These structures are called **micelles** (fig. 3.10, right).

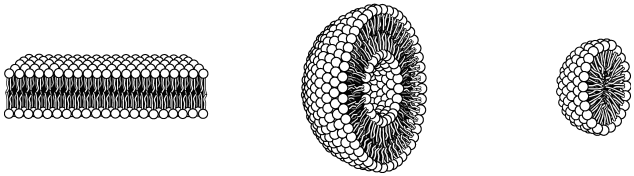

Figure 3.10: The three main structures amphiphilic molecules can form in an aqueous solution: a homogeneous bilayer (left); a closed bilayer forming a separate volume within the aqueous solution called liposome (middle); wedge shaped molecules can form a stable structure by what is called a micelle (right), (pictures adapted from Wikipedia 2010*c*)

A large variety of phospholipids has been found and the composition of the membranes varies among the species, cell types and tissues and even between the inner and outer leaflet of one and the same membrane. Apart from the phospholipids other components have been found as part of the biological membranes: large proteins whose total weight can be up to four times the total weight of the lipids (Korn 1969). They are held in place by interactions between the hydrophobic part of the lipids and the hydrophobic **transmembrane domains** of the protein. Depending on the exact form and the length of the hydrophobic domain the proteins can be present only on one side or can span the lipid bilayer (see figure 3.11). Different functions of the proteins have been identified. Some can provide identification of the cells from the outside, others provide signal transduction between the inside and the outside of the cell. The proteins that transport substances actively or passively across the

membrane are subject of section 3.4.3. **Tight junctions** are a class of membrane proteins that span not only one cell membrane but two membranes of two neighbouring cells, thus creating a rate-limiting barrier to diffusion of solutes that holds the adjacent cells firmly in place. Tight junctions are expressed, for example, in the epithelial cells of the small intestine (see Mitic & Anderson 1998, and therein).

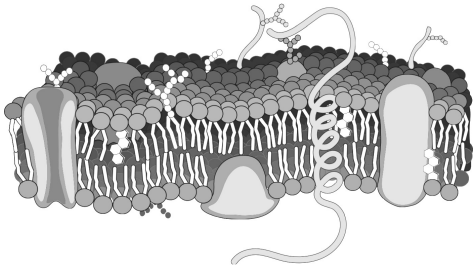

Figure 3.11: Schematic view of proteins embedded in the lipid bilayer. Some are present only on one side, others span the entire layer. A great range of functions have been identified, from active and passive transport through cell identification to signal transduction, (adapted from Wikipedia 2010*e*).

In an experiment with a cell that was combined artificially, one half from a human cell and the other half from a mouse cell, it has been observed that the membrane proteins spread along the surface and intermix completely after about 40 minutes (Frye & Edidin 1970), such that mouse proteins and human proteins are distributed equally. This means, that under physiological conditions the mosaic of lipid and protein units move around freely and the bilayer is in a fluid state. The transition temperature from a fluid to the crystalline state depends on the composition of the membrane. Saturated fatty acids pack well into the crystalline state whereas the kinks in the unsaturated fatty acids hinder the crystallisation, therefore

the proportion of saturated and unsaturated phospholipids (and the content of other molecules) controls the liquidity and the transition temperature of the membrane. It has been shown that, for example, *E. coli* bacteria can adjust the membrane's composition depending on the temperature during the growth process. As a result the fluidity of membranes from bacteria grown at low temperature is about the same as that of bacteria grown at high temperature (Marr & Ingraham 1962). In spite of their liquidity the membranes form a reliable container for the cell constituents. The shape of a cell is determined by the local elasticity of the membrane (Sackmann 1994) as a consequence of minimisation of free energy. Elasticity can be controlled by the distribution of different lipids in the membrane and the presence of embedded proteins.

The cell membrane isolates the cytoplasm from the outside of the cell. Its structure allows only lipophilic and small, uncharged molecules to pass through. Only a flow equilibrating a concentration difference is thermodynamically possible. The transport of other substances or the creation of gradient required for the cellular processes are facilitated with the help of transporter proteins.

3.4.3 Transporter proteins

Molecules or ions that cross the membrane via transporter proteins can do so either passively, without the expenditure of energy along their electrochemical gradient, or actively. Various mechanisms that provide energy to cell processes are known: absorption of light, oxidation reactions, the electrochemical gradient of a substance and the hydrolysis of **ATP**. Some of the known transporters are rather selective on the transported substances.

Aquaporins

An example of passive transport are water pores. Due to the hydrophobic part of the phospholipids, water molecules diffuse through the membrane at a very low rate. In the 1950s and 60s, observations of water permeabilities of different cells led to the conclusion that some membrane protein has to act as a water pore, enhancing permeability significantly. Peter Agre identified such a pore for the first time and his work on the nowadays so-called **aquaporins** was honoured with the Nobel Prize of chemistry in 2003. Some aquaporins conduct only water, others are known to let pass other small molecules, for example CO_2 or glycerol. However, all aquaporins have in common that they are impermeable for charged species, especially protons, thus maintaining an existing electric potential. The traffic in the water pores can be regulated by different mechanisms, such as the presence of hormones or certain levels of pH. A recent review of aquaporin structure and function can be found in (Gonen & Walz 2006) and therein.

Ion interchange

The electric potential and the resultant possibility of a flow of charge across the membrane is crucial for a variety of processes in an organism, such as the signalling in neurons or the contraction of muscles. The potential is built up with the help of **ion transporters**, transmembrane proteins that pump ions against their gradient across the membrane. They gain the necessary energy either by hydrolysis of ATP or by the transport of another ion along its respective gradient. The action potentials, rapidly rising and falling membrane potentials, that play a central role in cell-to-cell communication of neurons, in the contraction of muscle cells and in the insulin release of beta cells, are a consequence of opening **ion channels**. Opening (and closing) of such a channel can be controlled by the membrane potential itself (voltage-gated ion channels, e.g. for sodium (Mar-

ban *et al.* 1998)) or by the binding of a ligand. An example of such a ligand is the neuro-transmitter Acetylcholine whose binding to the according receptor results in the opening of the channel (Miyazawa *et al.* 2003). An introduction to channels can be found in a book by Aidley & Stanfield (1996). It covers the function and structure of ion channels, as well as the investigation techniques and the effects of drugs, toxins or genetic mutations on the proper functioning of ion channels within the body.

ABC transporters

Another important role in the transport across membranes is played by the ATP-binding cassette transporters (ABC-transporters). They belong to a huge protein superfamily that is found across species from prokaryotes to eukaryotes (Jones & George 2004). They consist of a transmembrane domain and a nucleotide-binding domain. Most of them have the transmembrane domain composed of twelve subunits ('α-helices') that embed the protein in the membrane (see figure 3.12). The α-helices are heterogeneous in structure and their precise form and winding determines the substrates that the protein is affine to. It is believed that the change between two protein confirmations can translocate the substrate across the membrane and a net flux into a preferred direction is achieved by differences in the binding affinity of the inward and outward facing confirmation (Rees *et al.* 2009). The energy is provided by the hydrolysis of ATP to ADP at the nucleotide-binding domain or ATP-binding cassette.

This large class of transporters is an important part of physiological processes. On one hand, they can provide essential nutrients to the cell and, on the other hand, they can expel toxics out of it. This means that many antibiotics and anticancer drugs will not reach the place of action in time, as we will see in chapter 4. There we will also see why the transport dynamics are such that they can

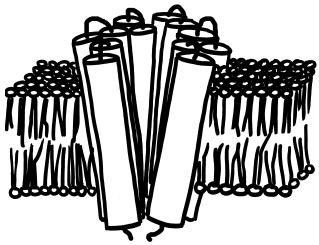

Figure 3.12: Schematic view of an ABC-transporter with its twelve α-helices that penetrate the inner and outer leaflets of the cellular membrane.

be approximated with enzymatic dynamics in the way shown in section 3.2 of the present chapter.

3.4.4 Other means of transport

For completeness we want to present shortly two other transport mechanisms. One of them is a consequence of the remarkable properties of the cell membrane: two membranes can undergo fusion without losing any of the integrity of the membranes. For example a vesicle, a closed phospholipid bilayer enclosing an aqueous solution, can combine with the cell membrane and release its content into the cytoplasm, the membrane of a sperm cell unites with that of the egg or some viruses infect a cell by docking onto the membrane. On the other hand, organelles within the cell can enclose proteins or lipids into a vesicle and thus transport the load to other organelles or to the cell membrane to release its content to the outside of the cell. We see, **membrane fusion** is central to many biological processes.

The other transport does not refer to substances in the chemical sense. In the beginning of this section we named the exchange of information, and although information can be exchanged by a

flux of ions or neurotransmitters, some membrane proteins are only transporting information. **Receptor enzymes** are embedded in the membrane with a ligand-binding domain on one side of the membrane and a domain with an active site of enzymatic reaction on the other. This means that a bound ligand changes the conformation of the protein and has a result on the other side of the membrane without any actual substance flow. A widely studied example of such a receptor enzyme is the insulin receptor which plays an essential role in the glucose equilibrium in higher organisms (Ward & Lawrence 2009).

3.5 Summary

The intention of this chapter is to get the reader closer to the conditions that govern the biological processes analysed in chapters 4 and 5. A fundamental ingredient is the saturating dynamics that is known from enzyme reactions, which are presented in section 3.2. The same formulas can be used to express the regulation of genes that are enhanced or blocked by the presence of certain proteins and to express the dynamics of transporters that are embedded in the cell membrane to pump chemical compounds molecule by molecule.

In the beginning of section 3.3 we have a short glance at a simplified dynamical system describing gene expression and show how gene regulation can be introduced into the model to suppress fluctuations in the process. It then follows a description of how biochemical oscillations can arise from the regulated expression of genes. This kind of oscillators is used in chapter 5 to model the neurons that regulate the daily rhythms in mammals.

An overview over the constituents of the cell membrane is presented in section 3.4. It firstly shows how a stable membrane can be formed

to enclose aqueous solutions, which in the end is responsible for the formation of the isolated cell as a living unit. Its chemical composition allows only certain molecules pass through. All others, wanted or unwanted, have to pass through specialised channels. The channels are either openings that allow passive passage to certain substances or molecular pumps that transport material under the usage of energy in a specified direction, even against the gradient. A coarse classification of the different channels based on their functioning is presented. The section is thought to set the mind for chapter 4, where a tightly bound mono layer of epithelial cells is the barrier for drugs to get into the body and ABC transporters accompany the passive transport.

Part II

Results

Chapter 4

Compartment models in drug absorption

4.1 Introduction

The research presented in this chapter was initiated by a cooperation with pharmacologists from the University of Valencia (Marival Bermejo Sanz, Vicente Casabó-Alós y Isabel González Álvarez) within the BioSim network. The BioSim network was established by the European Commission and initiated in 2004.

> "The main objective of the Network is to demonstrate how the use of modern simulation technique through a deeper and more qualitative understanding of the underlying biological, pathological and pharmacological processes can lead to a more rational drug development process, improved treatment procedures, and a reduction in the needs for animal experiments." (BioSim 2010)

CHAPTER 4. MODELS IN DRUG ABSORPTION

Drugs are substances that alter the bodily functions when absorbed into the organism, pharmaceutical drugs are intended for medical diagnosis, cure, treatment or prevention. Apart from a fundamental interest in understanding the basic mechanisms by which a drug is assimilated by the human body and how it unfolds its desired action, the kinetics of drug absorption is also a topic of much practical interest. Detailed knowledge of this process, resulting in the prediction of the drug absorption profile, can be of much help in drug development stage (Eddershaw *et al.* 2000; Zhou 2003). To this end, several kinetic models for drug absorption within the body have been established (see e.g. Yu & Amidon 1999). The main focus of this chapter lies on the detailed analysis of a previously developed model of drug absorption, belonging to the category of the so-called three-compartment models (Kramer *et al.* 1974; Skinner *et al.* 1959). The presented case deals with three compartments connected in a row, allowing passive, diffusion-like exchange of substances among adjacent volumes. Between two of the three compartments an additional, non-linear transport is active.

In the first section of this chapter we will briefly introduce the cell culture experiments used in experimental pharmacology to measure absorption properties of new chemical compounds. Subsequently a short overview of compartment models, used to study the flow and accumulation of substances in different parts of the body, is presented. Then we focus on the peculiarities of antibiotic absorption.

In section 4.2 we will define the used model precisely and provide an analytical solution to an (adequate) approximation of the model. The approximative method facilitates the analysis of the absorption characteristics as a whole, without requiring repetitive numerical integration of the differential equations and allows a fast and easy insight into how physiologically meaningful parameters influence quantities available from experiment in three-compartment models.

The method will be applied to a special form of non-linear flux, where the transporter protein is described by Michaelis-Menten

dynamics. The results are compared with absorption experiments of a selected broad spectrum antibiotic (section 4.3). Most of the results from sections 4.2 and 4.3 were published in (Komin & Toral 2009). The chapter closes with some concluding remarks and an outlook in section 4.4.

4.1.1 Oral absorption pathway

To get the desired drug into the body, a variety of methods with different advantages and disadvantages are known. For most patients oral application is probably the most accepted form, it is usually painless and can be taken by the patient itself at his or her home, without the need of a specialised person or sophisticated facilities.

Orally administered drugs are mainly absorbed by the small intestine; they are mediated upon by a variety of processes (Hunter & Hirst 1997). The inner wall of the small intestine is lined with **epithelial** cells, so the drug passes from the **lumen** (the inner, intestinal volume) through the epithelial cells and the **lamina propria** into the blood stream in the capillaries (fig. 4.1 (left)). On its way it can be metabolised, transported away from the tract where absorption is possible or accumulate in organs other than those of treatment.

Due to the **tight junctions**, which are rows of transmembrane proteins embedded in both membranes of neighbouring epithelial cells to connect them with each other, only very small and hydrophilic molecules can pass along the contact of two neighbouring cells (this is called the **paracellular** route). Therefore transport along this pathway is very small except for when a modulator of tight junctions is present. If the compound has the appropriate physical and chemical properties it can cross the cell's membranes passively (**transcellular passive diffusion**). These compounds may be substrate for intracellular metabolism and they are more likely to be substrate for efflux transporters, extracting them from the cell back into the intestine. However, the transcellular passive way (limited by efflux

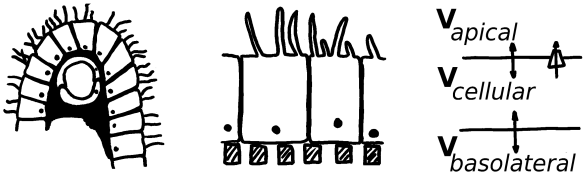

Figure 4.1: Left: Schematic view of a section of an intestinal wall. Epithelial cells with *microvilli* and a capillary embedded in the *lamina propria*. Middle: Sketch of the epithelial cells when seeded on a filter. Right: Simplified mathematical model of three compartments, as used in the text, with an efflux pump indicated on the apical side.

transporters) is the main route of absorption for orally taken drugs. In other cases transcellular absorption can be mediated by naturally occurring carriers which normally transport vitamins or nutrients. A rather seldom pathway in adult small intestine absorption is via endocytosis, where the transported material is coated with part of the cell membrane on one side, incorporated into the cell and then released from the cell on the other side.

In this chapter we will be concerned with the transcellular pathway that is limited by efflux transporters.

4.1.2 In vitro experiments and compartment models

Much experimental activity aimed at analysing the kinetic aspects of the process of drug absorption has been pursued recently. For better control, a variety of **in vitro** methods of drug absorption have been developed (Balimane *et al.* 2000). The limiting barrier in the transcellular pathway is the layer of epithelial cells. To measure the absorption of a given substance in a large range of external conditions (overall drug amount, presence of other substances etc.)

it comes handy that epithelial cell cultures can be seeded in a monolayer, forming the contact surface between two chambers (fig. 4.1 (middle)). The concentrations of a substance can then comfortably be measured over time in both chambers.

Two of the well-known cell lines used in drug absorption experiments are **Caco-2** cells (Artursson & Borchardt 1997; Artursson *et al.* 2001) and **MDCK** cells (Irvine *et al.* 1999). Caco-2 cells were derived from a human colon carcinoma. After they are seeded they differentiate into an "...highly functionalized epithelial barrier with remarkable morphological and biochemical similarity to small intestine columnal epithelium." (Irvine *et al.* 1999) (p. 28). The MDCK cell line was derived from canine kidney cells and as well differentiates into epithelium and forms tight junctions. Both cell lines are used to asses transport properties of new developed compounds. The main disadvantage of the well characterised human Caco-2 cell line is its relatively long growth period, limiting the throughput of screened compounds and/or conditions. MDCK cells are faster growing and thus allowing for a reduction of culture time, cost and effort (Irvine *et al.* 1999). A downside of both of these cell lines is that they are seeded on a flat surface, whereas the intestine forms folded walls with much higher surface area than just the inside of a tube. As a consequence only high permeability drugs are well represented by this model, whereas the permeability for low permeability drugs is underestimated when compared with **in vivo** values (Artursson *et al.* 2001).

When the monocellular layer is seeded on a semipermeable membrane it is in contact with the liquids above and below and allows mass flow from one side to the other. In the next section we will go into the details of the used **compartment model** and describe the assumptions necessary to obtain it. Before we want to have a few words about the general concept of compartment models. In pharmacology these models are used to break systems of drug action down into smaller units. A number of compartments are connected with each other in different ways and the mass flux of

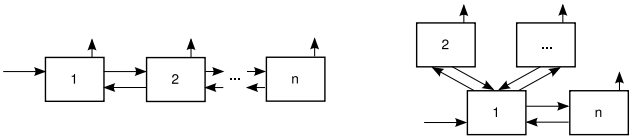

Figure 4.2: Comparison between catenary (*left*) and mammillary (*right*) compartment models. Arrows between chambers 1..*n* depict the mass flow between them. Degradation within a chamber is symbolised by the small arrow pointing up. The single arrow pointing into the first chamber represents the introduction of the substance into the system.

a given substance through the system is the object of interest. The models can be split into classes according to their topology. The **catenary** models (from 'catena', latin word for 'chain') are compartments connected in a row whereas the **mammillary** models have a central compartment with others surrounding it (fig. 4.2). A mix of both types is possible as well. A different form of classification is concerned with the level of abstraction, i.e. that if the compartments correspond to a well defined volume in the organism the model is said to be **physiological** whereas other models, where no such correspondence exists, are called **mechanistic** models (Holz & Fahr 2001).

The considerations in section 4.2 will concern a purely catenary model. A distinction between physiological and mechanistic model is not necessary, the presented method applies to both classes. However, the experimental work we have chosen to compare our theory with (section 4.3) is about a physiological one.

4.1.3 Antibiotics and the multidrug transporter

Antibiotics are drugs which are used to treat bacterial infections. There is a huge variety of different antibiotics, they can be synthetic,

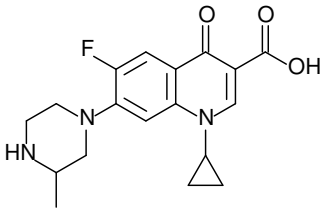

Figure 4.3: Structure of antibiotic CNV97100

of natural origin or semi-synthetic, where a natural compound is chemically modified. Some are active against a broad spectrum of bacteria, others only against a narrow spectrum. Infectious diseases are the second major cause of death worldwide but the use of antibiotics results inevitable in the development of resistant bacterial strains. Only persistent discovery of new compounds can fight the problem of ever new resistant bacteria (von Nussbaum *et al.* 2006).

A family of synthetic, nowadays broad-spectrum, antibiotics are the **quinolones**, also sometimes called **fluoroquinolones**. Since their first generation in the 1960's they developed from being effective in a very limited spectrum (predominantly anti-Gram-negative) to a broad-spectrum antibiotic which, in most cases, can be applied orally (Ball 2000). The novelty about this family of substances is its direct inhibition of DNA synthesis (Hooper 2001). **Ciprofloxacin** is a fluoroquinolone patented in the 1980's and still in wide use for a variety of indications. It is particularly, but not only, effective against Gram-negative bacteria. It exists as an oral as well as intravenous formulation (Davis *et al.* 1996). A new ciprofloxacin derivative (CNV97100, see fig. 4.3) is the subject of the absorption study (González-Alvarez *et al.* 2005) and we will use it to apply the method developed in this chapter.

Typical absorption experiment places different amounts of the investigated drug on either side of the cell culture. By measuring the amount on the receiving sides the apparent permeabilities can

be derived. In the CNV97100 experiment a *pH* of 7.0 was used in both the **apical** chamber (which resembles the lumen) and the **basolateral** chamber (oriented away from the lumen) to avoid any bias due to ionisation effects. If the *pH* were different in the two chambers it would be necessary to include these effects into the model by estimating the fraction of ionised and non ionised compound and to model separately the permeation of both species in both directions in each chamber. The unstirred water layer had not been considered to be the limiting diffusion step, an assumption justified by taking into account the molecular weight and the lipophilicity of CNV97100. This had been checked experimentally *in situ* in rats (Bermejo *et al.* 1999) and *in vitro* in Caco-2 cells (Bermejo *et al.* 2004). As a consequence the three compartment model was chosen to be an adequate picture of the underlying processes.

Absorption of many drugs (Raviv *et al.* 1990) is seriously limited by P-glycoprotein (P-gp), the so-called multidrug transporter. This particular protein is expressed on the apical membrane of intestinal epithelium cells (Ruiz-García *et al.* 2002; Troutman & Thakker 2003*a*,*b*). The molecule to be transported must bind with the protein and will then be "flipped" (Hunter & Hirst 1997) onto the other side of the membrane, where it is no longer available for the "reaction". This makes its dynamics similar to enzyme reactions and is often represented by the sigmoid shape of a Michaelis-Menten-reaction rate (Michaelis & Menten 1913):

$$\mathcal{J}(Q_C) = \frac{S V_M Q_C/V_C}{K_M + Q_C/V_C} \,. \tag{4.1}$$

V_M determines the maximal reaction velocity, S is the surface area and K_M is the concentration for which the velocity extends halfway towards the maximum. In this case of an **intracellular binding** site, the relevant variable is the concentration Q_C/V_C around the binding site of the transporter, inside the cell.

In other cases, the efflux pump possesses an **extracellular binding** site. Consequently, transport is determined by the drug concen-

tration, Q_A/V_A, in the apical compartment and the corresponding Michaelis-Menten expression is:

$$\mathcal{J}(Q_A) = \frac{SV_M Q_A/V_A}{K_M + Q_A/V_A} \,. \tag{4.2}$$

Both situations will be considered in this thesis. For reasons of simplicity, we have considered that the efflux pumps depend on concentration on one of the two sides of the membrane (González-Alvarez *et al.* 2005; Ruiz-García *et al.* 2002). However, new results suggest that the transporter binding site for the molecule is inside the inner leaflet of the membrane (Hennessy & Spiers 2007). If we consider the space inside the phospholipid bilayer to be an additional volume with two permeable walls on either side, the concentration in that volume would be between those in the adjacent volumes.

4.2 Three compartments, one non-linear flux

Compartment models describe the behaviour of solutions or emulsions in connected volumes by analysing the molecule flux between them and all sources and sinks. They are used to explain data from absorption experiments. When applied to drug absorption in above mentioned cell culture experiments, some specific simplifications can be made. In the following work it is considered that two volumes (e.g. gastrointestinal lumen and blood plasma *in vivo* or apical and basolateral chamber *in vitro*) are connected through a third, *in vitro* the cellular, volume. The absorbed substance should have low lipophilicity such that the unstirred water layer can be neglected. Furthermore it is assumed that the compound does not ionise and that the concentrations in the different intestinal cells of the mono-layer are equal (which is exact only if all cells have the

same parameters). With these assumptions the absorption can be seen as a transport from one large volume to another through a third (the cellular) volume (González-Alvarez *et al.* 2005). Figure 4.1 (right) sketches the simplifications of the model. There is no spatial dependency and molecules can pass through the two cell membranes. The overall amount of drug molecules is considered to be constant, a hypothesis that assumes a closed system and that metabolism does not occur. For an *in vitro* experiment of short duration this is a reasonable assumption.

Passive transport across the membrane is mediated, to a first approximation, by the concentration gradients according to Fick's law (Fick 1855), which specifies a linear relation between the flux of particles and the concentration gradient. When passive absorption is accompanied by energy-consuming efflux transporters, it is represented by a non-linear function term in kinetic transport equations. A variety of transporter types could be involved in the absorption of the molecules. In our work we consider that the non-linear transporters are present only on one (the apical) cell membrane, but our results could be extended directly to the case that those transporters are located on the basolateral membrane (or even in both membranes). Incorporating both linear and non-linear terms, the time evolution of the amount of diluted molecules ($Q_{A/C/B}$) in the three compartments can be described as follows:

$$\frac{dQ_A(t)}{dt} = +Cl_{AC}\left(\frac{Q_C}{V_C} - \frac{Q_A}{V_A}\right) + \mathcal{J} \tag{4.3a}$$

$$\frac{dQ_C(t)}{dt} = -Cl_{AC}\left(\frac{Q_C}{V_C} - \frac{Q_A}{V_A}\right) - \mathcal{J} - Cl_{CB}\left(\frac{Q_C}{V_C} - \frac{Q_B}{V_B}\right) \tag{4.3b}$$

$$\frac{dQ_B(t)}{dt} = +Cl_{CB}\left(\frac{Q_C}{V_C} - \frac{Q_B}{V_B}\right) \tag{4.3c}$$

$$Q_0 = Q_A + Q_B + Q_C, \tag{4.3d}$$

where equation (4.3d) stands for conservation of the overall molecule number, Q_0. The indices denote the corresponding compartment

(*Apical, Cellular, Basolateral*), $V_{A/C/B}$ are the respective volumes. The apical, cellular and basolateral concentrations are given respectively by $a = Q_A/V_A$, $c = Q_C/V_C$ and $b = Q_B/V_B$. The passive, linear, diffusion terms are proportional to the concentration difference, being Cl_{AC} and Cl_{CB} the clearances indexed with their respective membrane index. In the equations, $\mathcal{J}$ represents the non-linear contribution due to specific efflux transporters. As it is an energy-consuming process, this can happen both along or against the gradient.

The conservation law Eq. (4.3d) reduces the number of independent variables from three to two concentrations. In other words, the system described by first-order differential equations (4.3) only has two degrees of freedom, which implies that it can be replaced by a single differential equation of second order. In the next section we will show that it can be put into the form:

$$\ddot{x} = -\Gamma(x)\,\dot{x} + F(x). \tag{4.4}$$

Variable x represents a rescaled concentration in one of the compartments (the cellular compartment if $\mathcal{J}$ depends on Q_C and the apical compartment if $\mathcal{J}$ depends on Q_A); the speed, $\dot{x}$, and acceleration, $\ddot{x}$, are, respectively, the first and second derivatives of x with respect to a rescaled time s, and $\Gamma(x)$ and $F(x)$ are functions to be described below. A qualitative understanding of these dynamics can be had by acknowledging that the previous equation corresponds to the equation of motion (Newton's second law) for the position x of a particle of unit mass upon which a force $F(x)$ and a friction, proportional to the particle speed $\dot{x}$ act. The force $F(x)$ and the friction coefficient $\Gamma(x)$ contain all of the parameters of the system as well as the particular form of the non-linear flux.

4.2.1 Model transformation

The conservation law (4.3d) allows the elimination of one of the three equations of the set (4.3a-4.3c). We have chosen to eliminate

either Q_A or Q_C, depending on whether the non-linearity depends on Q_C (intracellular binding site) or Q_A (extracellular binding site), respectively. More precisely: if $\mathcal{J} = \mathcal{J}(Q_C)$, we define the dimensionless normalised concentration $x(t) = \dfrac{Q_C(t)}{V_C\mathcal{N}}$ where $\mathcal{N}$ is a normalisation constant with units of concentration to be specified later; in the other case, when $\mathcal{J} = \mathcal{J}(Q_A)$, we define $x(t) = \dfrac{Q_A(t)}{V_A\mathcal{N}}$. In both cases, we also define $y(t) = \dfrac{Q_B(t)}{V_B\mathcal{N}}$. The initial drug concentration $C_0 = Q_0/V_I$ (being $V_I = V_A$ or $V_I = V_B$ according to whether the drug is initially loaded on the apical or the basolateral volume, respectively) is also rescaled to $c_0 = \dfrac{C_0}{\mathcal{N}}$. We finally define a rescaled dimensionless time variable $s = \dfrac{Cl_{CB}}{V_B}t$. It turns out that, with these definitions, the resulting two-degree system can be written in the common form:

$$\dot{x}(s) = \frac{dx(s)}{ds} = a_{11}x + a_{12}y + a_{13} + j(x) \tag{4.5a}$$

$$\dot{y}(s) = \frac{dy(s)}{ds} = a_{21}x + a_{22}y + a_{23}\,, \tag{4.5b}$$

with $j = \dfrac{V_B}{Cl_{CB}V_A\mathcal{N}}\mathcal{J}(Q_A)$ in one case, and $j = -\dfrac{V_B}{Cl_{CB}V_C\mathcal{N}}\mathcal{J}(Q_C)$ in the other. The dimensionless constants a_{ij} depend on the clearances, volumes, overall concentration, as specified in table 4.1.

By differentiating $\dot{x}(s)$ with respect to s using Eq. (4.5a) and, in the resulting expression, replacing $\dot{y}(s)$ by Eq. (4.5b) and $y(s)$ by its isolation from Eq. (4.5a), we get the form (4.4):

$$\ddot{x} = -\Gamma(x)\,\dot{x} + F(x), \tag{4.6}$$

with friction coefficient $\Gamma(x)$ and force $F(x)$ given by:

$$\Gamma(x) = \Gamma_0 - j'(x), \quad F(x) = \alpha - \beta x - a_{22}j(x). \tag{4.7}$$

Γ_0, α and β are dimensionless, positively-defined constants, whose relation to the coefficients a_{ij} are also detailed in table 4.1.

4.2.2 Approximate solution

If we now introduce the potential function $V(x)$ from which the force derives as $F(x) = -\dfrac{dV}{dx}$, the evolution of x can be visualised as the relaxation of a ball rolling downwards within a well of shape $V(x)$ under the combined effects of gravity and friction. It is known from mechanics that the particle will eventually stop at the minimum of the potential (stable equilibrium state) and that relaxation towards this final state will proceed via damped oscillations or monotonously, depending on the relative strength of the friction and potential contributions. Figure 4.4 visualises this *ball-in-a-well* approach. For very general non-linear transporters, including the Michaelis-Menten form used in section 4.3, the corresponding potential function $V(x)$ displays a single minimum, although its exact shape depends both on the linear and the non-linear terms in Eqs. (4.3).

If the potential $V(x)$ has a single minimum, the equlibirum value x_{eq}, we can approximate it by a parabola around this minimum $V(x) = V_{eq} + \frac{1}{2}V''_{eq}\left(x - x_{eq}\right)^2$. We will call $V''_{eq} = \omega^2$. Furthermore, we also approximate the friction coefficient $\Gamma(x)$ by its value at equilibrium $\Gamma_{eq} = \Gamma(x_{eq})$. The resulting linear differential equation $\ddot{x} = -\Gamma_{eq}\dot{x} - \omega^2(x - x_{eq})$ has the solution (Boyce & DiPrima 2001):

$$x(s) = \tilde{C}_1 e^{-s/\tau_1} + \tilde{C}_2 e^{-s/\tau_2} + x_{eq} \tag{4.8}$$

with time constants:

$$\tau_1 = \frac{2}{\Gamma_{eq} - \sqrt{\Gamma_{eq}^2 - 4\omega^2}} \quad \text{and} \quad \tau_2 = \frac{2}{\Gamma_{eq} + \sqrt{\Gamma_{eq}^2 - 4\omega^2}} \tag{4.9}$$

Table 4.1: Coefficients for equations (4.5) using parameter values from (González-Alvarez *et al.* 2005). Values are given for intracellular binding ($\mathcal{J} = \mathcal{J}(Q_C)$) and for extracellular binding ($\mathcal{J} = \mathcal{J}(Q_C)$). Only parameter γ depends explicitly on the exact form of $\mathcal{J}$, here the according MICHAELIS-MENTEN form was chosen.

Parameter	INTRAcellular	numerical	EXTRAcellular	numerical
a_{11}	$-\left[\frac{V_B}{V_C} + \frac{Cl_{AC}}{Cl_{CB}}\left(\frac{V_B}{V_C} + \frac{V_B}{V_A}\right)\right]$	-213.8	$-\frac{Cl_{AC}}{Cl_{CB}}\left(\frac{V_B}{V_C} + \frac{V_B}{V_A}\right)$	-173.1
a_{12}	$\frac{V_B}{V_C}\left(1 - \frac{Cl_{AC}}{Cl_{CB}}\frac{V_B}{V_A}\right)$	-209.8	$-\frac{Cl_{AC}}{Cl_{CB}}\frac{V_B^2}{V_A V_C}$	-250.4
a_{13}	$\frac{Cl_{AC}}{Cl_{CB}}\frac{V_B V_I}{V_A V_C}c_0$	$2.220\times10^8 V_I C_0$	$\frac{Cl_{AC}}{Cl_{CB}}\frac{V_B V_I}{V_A V_C}c_0$	$2.220\times10^8 V_I C_0$
a_{21}	1	1	$-\frac{V_A}{V_C}$	-27.10
a_{22}	-1	-1	$-\left(\frac{V_B}{V_C} + 1\right)$	-41.65
a_{23}	0	0	$c_0\frac{V_I}{V_C}$	$3.604\times10^8 V_I C_0$
γ	$-\frac{SV_M}{Cl_{CB}K_M}\frac{V_B}{V_C}$	-79.41	$\frac{SV_M}{Cl_{CB}K_M}\frac{V_B}{V_A}$	2.930

Γ_0	$-a_{11} - a_{22}$	$=$	$\frac{V_B}{V_C} + \frac{Cl_{AC}}{Cl_{CB}}\left(\frac{V_B}{V_C} + \frac{V_B}{V_A}\right) + 1$	214.8
α	$a_{12}a_{23} - a_{13}a_{22}$	$=$	$\frac{Cl_{AC}}{Cl_{CB}}\frac{V_B V_I}{V_A V_C}c_0$	$2.220\times10^8 V_I C_0$
β	$a_{11}a_{22} - a_{12}a_{21}$	$=$	$\frac{Cl_{AC}}{Cl_{CB}}\frac{V_B}{V_A V_C}(V_A + V_B + V_C)$	423.6

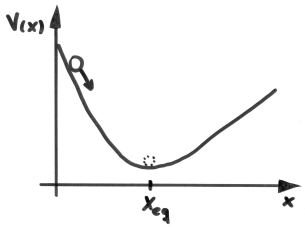

Figure 4.4: Visualisation of the particle-potential picture. The position of the "ball" represents the concentration which will eventually end up in the minimum. The exact shape of the potential depends both on the linear and the non-linear terms in Eqs. (4.3).

The coefficients $\tilde{C}_1$ and $\tilde{C}_2$ are determined by the initial conditions x_0 and $\dot{x}_0$, the latter being determined through Eq.(4.5b) by x_0 and y_0 as $\dot{x}_0 = a_{11}x_0 + a_{12}y_0 + a_{13}j(x_0)$. The resulting formulas are summarised in table 4.2. The initial values x_0 and y_0 depend on the particular model used. For example, for intracellular binding we have $x_0 = \frac{Q_C(t=0)}{V_C N} = 0$ and $y_0 = \frac{Q_B(t=0)}{V_B N}$. This latter value, in turn, has to be adjusted according to where the drug is loaded: for apical loading $y_0 = 0$, while for basolateral loading $y_0 = \frac{C_0}{K_M}$. Note that τ_1 and τ_2 will be complex if $\Gamma_{eq} < 2\omega$. In this case the system would relax to the steady state by performing damped oscillations. However, for the values of the parameters drawn from experiments, this case does not arise, τ_1 and τ_2 are positive real numbers and the decay to the equilibrium state is governed by real exponentials.

The time evolution of y can be obtained by a direct integration of the linear equation (4.5b):

$$y(s) = e^{a_{22}s}\left[y_0 + \int_0^s ds'\, e^{-a_{22}s'}\,(a_{21}x(s') + a_{23})\right] \tag{4.10}$$

Table 4.2: Coefficients of dimensionless solution Eqs. (4.8) and (4.11).

$\tilde{C}_1$	$\left(x_0 - x_{eq} + \tau_2\left(a_{11}x_0 + a_{12}y_0 + a_{13} + \gamma'\frac{x_0}{1+x_0}\right)\right)\frac{\tau_1}{\tau_1-\tau_2}$
$\tilde{C}_2$	$x_0 - x_{eq} - \tilde{C}_1$
$\tilde{D}_1$	$-\dfrac{a_{21}\tilde{C}_1\tau_1}{a_{22}\tau_1+1}$
$\tilde{D}_2$	$-\dfrac{a_{21}\tilde{C}_2\tau_2}{a_{22}\tau_2+1}$
$\tilde{D}_3$	$y_0 - y_{eq} - \tilde{D}_1 - \tilde{D}_2$

which yields

$$y(s) = \tilde{D}_1 e^{-s/\tau_1} + \tilde{D}_2 e^{-s/\tau_2} + \tilde{D}_3 e^{-s/\tau_3} + y_{eq}\,. \tag{4.11}$$

with a new time constant:

$$\tau_3 = -\frac{1}{a_{22}} \tag{4.12}$$

and coefficients $\tilde{D}_{1/2/3}$, whose relation to other constants is detailed in section 4.3, where an explicit form of efflux is analysed. The evolution of $z(s)$ is obtained by means of the conservation law. It is worth recalling that the time scales in real units are

$$t_1 = \frac{V_B}{Cl_{CB}}\tau_1\,, t_2 = \frac{V_B}{Cl_{CB}}\tau_2\,, t_3 = \frac{V_B}{Cl_{CB}}\tau_3\,. \tag{4.13}$$

4.2.3 Interpretation

By treating the original model in the way we described above we obtained a linear equation $\ddot{x} = -\Gamma_{eq}\dot{x} - \omega^2(x - x_{eq})$. It describes the damped pendulum of frequency ω. Its corresponding solution, as

found in many elementary books of mechanics, can be written as the sum of exponential functions of time (Eqs. 4.8 and 4.11). When the change of variables is undone and the third solution obtained via the conservation law, then we can write the solution of any mass-conserving, three-compartment-model, independent from the exact form of non-linearity, as:

$$Q_A(t) = Q_A^{eq} - A_1 e^{-t/t_1} - A_2 e^{-t/t_2} - A_3 e^{-t/t_3} \quad (4.14a)$$

$$Q_B(t) = Q_B^{eq} - B_1 e^{-t/t_1} - B_2 e^{-t/t_2} - B_3 e^{-t/t_3} \quad (4.14b)$$

$$Q_C(t) = Q_C^{eq} - C_1 e^{-t/t_1} - C_2 e^{-t/t_2} - C_3 e^{-t/t_3} \quad (4.14c)$$

where t_1, t_2 and t_3 define three time-scales and Q_A^{eq}, Q_B^{eq} and Q_C^{eq} are the equilibrium asymptotic quantities of the diluted substance in each compartment. These and the constants $(A/B/C)_{(1/2/3)}$ adopt different expressions, depending on the non-linearity. If given a specific expression for the non-linear transport terms and numerical values for the parameters, one can calculate the above constants and compare the result with the numerical integration of the non-linear system (4.3) or with experimental data. This explicit type of solution for a Michaelis-Menten flux J constitutes one of the main results of this chapter and is the basis for the subsequent analysis. In section 4.3 we will carry out this program explicitly for the model and data taken from (González-Alvarez *et al.* 2005).

Experimentally, it is rare to measure the complete variation of $Q_A(t)$, $Q_B(t)$ and $Q_C(t)$ with respect to time. A typical experiment (Balimane *et al.* 2004; Faassen *et al.* 2003; González-Alvarez *et al.* 2005; Lentz *et al.* 2000; Ruiz-García *et al.* 2002) starts by placing an initial concentration C_0 of a drug in either the apical or in the basolateral compartment. The so-called apparent permeability $P^{app} = \dfrac{dQ/dt}{SC_0}$, with $Q(t)$ the amount of material on the receiving side, is measured in both directions and the values are compared.

The explicit solution, Eqs. (4.14), identifies three different **characteristic time scales**, t_1, t_2 and t_3, within the evolution of these con-

centrations. Each one of them separates well defined regimes in the evolution of the concentrations: if time is much smaller than the characteristic time scale, the corresponding exponential term comes close to being linear; it changes exponentially at times close to it and is almost constant at much larger times. This information helps the experimenter to decide if the chosen sampling interval is adequate or not. Furthermore, it is mathematically possible to observe oscillatory behaviour in the presented system, if one of the $t_{1,2,3}$ is complex.

We would like to stress that our way of approximating the problem has allowed us to identify these natural time scales and to find their relationship to other constants that are experimentally accessible. It appears that in many cases (one example in the next section and table 4.3) one time-scale (t_2) is much smaller than the interval between measurements. Measurements of the apparent permeability are usually carried out within a time frame of between 15-30 min and a couple of hours (González-Alvarez *et al.* 2005; Lentz *et al.* 2000; Yamashita *et al.* 2000), whereas t_2 seems to be of the order of a few minutes. Hence, measurement times satisfy $t \gg t_2$ and the exponential term e^{-t/t_2} can be neglected. Analysis of the experiments (González-Alvarez *et al.* 2005) indicates that transport is mediated by transporters with an intracellular binding site. In this case, and according to table 4.3, both t_1 and t_3 are much larger than the measurement times, allowing us to perform the linear approximations $e^{-t/t_1} \approx 1 - t/t_1$ and $e^{-t/t_3} \approx 1 - t/t_3$ to obtain explicit expressions for the apparent permeability:

$$P_{BA}^{app} = \frac{1}{SC_0}\left(\frac{A_1}{t_1} + \frac{A_3}{t_3}\right) \tag{4.15}$$

in the case that the drug is initially delivered in the basolateral side, and

$$P_{AB}^{app} = \frac{1}{SC_0}\left(\frac{B_1}{t_1} + \frac{B_3}{t_3}\right) \tag{4.16}$$

when the drug is delivered in the apical side. It seems that even in the case of very fast-absorbing drugs (tested for permeabilities such as those in (Korjamo *et al.* 2007)) times are well separated into those of around an hour and those of less than a minute (data not shown). However, when it occurs that the time scales are all of a similar order, one can easily extend Eqs. (4.15) and (4.16) by the required term.

4.3 Application to MICHAELIS-MENTEN type transporters

Our mathematical treatment of the evolution equations has provided us with explicit expressions for the evolution over time of the amounts $Q_{A/B/C}(t)$, Eqs. (4.14), and the apparent permeabilities, Eqs. (4.15) and (4.16), for a three-compartment model with a non-linear flow. This section we want to use to apply the findings from above to a selected absorption study (González-Alvarez *et al.* 2005), where the non-linear flux can be expressed by MICHAELIS-MENTEN dynamics, as indicated in section 4.1.

Firstly we will carry out the necessary transformations explained in section 4.2 to the model with the explicit form of non-linear transport function $\mathcal{J}$. Then, by comparing theoretical predictions with the full results of numerical simulations of the evolution equations, we will show that our approximate treatment has a range of validity that covers typical experimental situations. Next, once this validity has been established, we will use our approximation to make comparisons to experimental data from above mentioned study. We will investigate how large is the influence of single parameters in the model on the quantities measured in absorption experiments. From this we can derive how errors in the parameters propagate

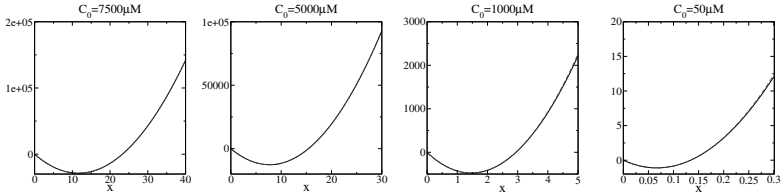

Figure 4.5: *Continuous* line: Original potential Eq. (4.20), *dashed* line: approximated parabola. For different amounts of loaded drug. Differences are of the order of the line width.

to the final result. The section closes with a possible extension of the non-linear flux, considering that part of the substance does not diffuse but stay bound in the cell.

4.3.1 Coefficients in case of Michaelis-Menten efflux transporter

Finally, when we undo the changes of variables we obtain coefficients as given in table 4.5 and together with Eq.(4.9) we derive Eqs. (4.14).

The second derivative with respect to x is:

$$V''\left(x_{eq}\right) = \omega^2 = \beta + \frac{a_{22}\,\gamma}{\left(1 + x_{eq}\right)^2}\,. \tag{4.17}$$

The approximated and original potentials are drawn in figure 4.5 in the case of apical loading of a system with intracellular binding site. From this figure, it can be seen that the parabolic form constitutes an excellent approximation for a wide range of initial concentrations C_0.

This presentation has so far been very general. In the case of the Michaelis-Menten form for the non-linear efflux transport function

$\mathcal{J}$, formulas (4.1) or (4.2), we identify K_M as a characteristic concentration and simply adopt the normalisation constant $\mathcal{N} = K_M$. Therefore the current is

$$j(x) = \gamma \frac{x}{1+x} \tag{4.18}$$

where γ is shown in table 4.1. The friction coefficient and force are:

$$\Gamma(x) = \Gamma_0 - \frac{\gamma}{(1+x)^2}, \quad F(x) = \alpha - \beta x - \gamma a_{22} \frac{x}{1+x}. \tag{4.19}$$

Note that the initial concentration C_0 is contained only in α and that the influence of the efflux transporter is found completely in γ. Γ_0, α and β are independent of the location of the pump. The values used for numerical calculations are taken from (González-Alvarez *et al.* 2005) and can be seen in table 4.4.

The potential from which the force $F(x) = -\frac{dV(x)}{dx}$ derives is:

$$V(x) = (-\alpha + \gamma a_{22})x + \frac{\beta}{2}x^2 - \gamma a_{22} \ln(1+x)\,. \tag{4.20}$$

The equilibrium concentration x_{eq} is the minimum of the potential, obtained by setting the force in Eq.(4.19) equal to zero. In the present case of a Michaelis-Menten type non-linearity, the solution is obtained without using any further approximations or simplifications other than stated for the original model:

$$x_{eq} = \frac{\alpha - \beta - \gamma a_{22} + \sqrt{4\alpha\beta + (\alpha - \beta - \gamma a_{22})^2}}{2\beta}\,. \tag{4.21}$$

Inserted into (4.5b) the equilibrium value for $y(s)$ is the solution of $\dot{y}(s) = 0$:

$$y_{eq} = -\frac{a_{21}x_{eq} + a_{23}}{a_{22}} \tag{4.22}$$

Through the conservation law one gets z_{eq}:

$$z_{eq} = \frac{Q_0}{V_z \mathcal{N}} - x_{eq}\frac{V_x}{V_z} - y_{eq}\frac{V_B}{V_z}\,, \tag{4.23}$$

where, to unify notation, we have labelled the volumes' meaning $V_x = V_C$ and $V_z = V_A$ for intracellular binding, and $V_x = V_A$ and $V_z = V_C$ for extracellular binding.

4.3.2 Concentration evolution and binding site location

We obtained expressions for the equilibrium amounts $Q^{eq}_{A/B/C}$ and the constants $(A/B/C)_{(1/2/3)}$ for non-linear transporters of the MICHAELIS-MENTEN type, in cases of transport mediated by both intracellular and extracellular binding. The corresponding expressions are summarised in table 4.5 of the Appendix as a function of parameters of the model. Using the numerical values of those parameters as derived in the absorption study of reference (González-Alvarez *et al.* 2005), we can extract precise numerical values for the equilibrium amounts $Q^{eq}_{A/B/C}$ and the constants $(A/B/C)_{(1/2/3)}$. Those numerical values are also listed in table 4.5. Finally, the numerical values of the time constants $t_{1/2/3}$ are listed in table 4.3. Using these numerical values, extracted from a real experiment and thus corresponding to a case of interest, we now proceed to check the accuracy of our approximation. To this end, we plotted in figures 4.6 (for two different initial conditions) the results of the direct numerical integration* of Eqs.(4.3) and our approximation, Eqs.(4.14). The most noticeable feature is that, at the scale of the figures, the two approaches are nearly indistinguishable and, in fact, the difference is of the order of the thickness of the lines. We conclude that our treatment provides a simple, yet very precise, expression for the evolution of the amounts $Q_{A/B/C}(t)$ and can be used instead of the less transparent numerical integration of the equations.

Table 4.3 lists the apparent permeabilities and the resulting *efflux ratios*, $P^{app}_{BA}/P^{app}_{AB}$, as obtained from Eqs.(4.15-4.16) in the cases of in-

*For this numerical integration we used a fourth-order Runge-Kutta algorithm with a time step of 1*s*.

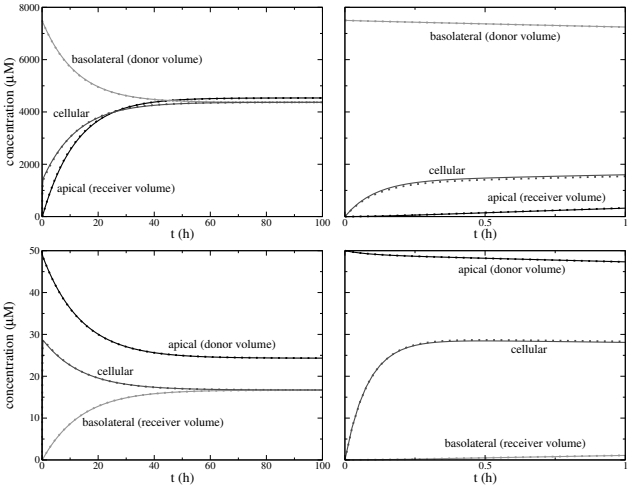

Figure 4.6: Time evolution of concentrations on either side of the cells and inside. *Dotted* line: Numerical integration of full dynamical system (Eqs. 4.3). *Continuous* line: Explicit expression of approximate solution (Eqs. 4.14). Parameters taken from (González-Alvarez *et al.* 2005), intracellular binding site with MICHAELIS-MENTEN dynamics (4.1) is considered. (top) Initial concentration $C_0 = 7500\mu M$, applied on the basolateral side. (bottom) Initial concentration $C_0 = 50\mu M$ applied apically. (left) Evolution over $t = 100h$, (right) Amplification of the first hour.

ternal and external binding site and different initial concentrations. The analysis of the three time scales $t_{1/2/3}$, listed in the same table, shows that t_2 is well below the time of the first measurement (30min) for all cases studied and the duration of experiment ($t \sim 2\,\mathrm{h}$) satisfies $t \ll t_1, t_3$, hence validating the approximations that led to Eqs.(4.15-4.16). The same analysis justifies the validity of the linear fit used in the experimental studies to extract the apparent permeabilities from the data. To avoid overloading the text with too many results, we have omitted the time scales for basolateral loading since they are of similar order.

Table 4.3: Time scales (when loaded apically) and apparent permeabilities predicted for different initial concentrations and different models (internal/external binding site).

C_0	binds	t_1	t_2	t_3	P^{app}_{BA}	P^{app}_{AB}	$\frac{P^{app}_{BA}}{P^{app}_{AB}}$
(μM)		(h)	(min)	(h)	($cm\,s^{-1}$)	($cm\,s^{-1}$)	
7500	int	12.3	6.38	23.6	6.70×10^{-6}	6.37×10^{-6}	1.05
	ext	11.9	6.67	0.567	6.80×10^{-6}	4.12×10^{-6}	1.65
5000	int	12.5	6.27	23.6	6.73×10^{-6}	6.26×10^{-6}	1.07
	ext	11.9	6.67	0.567	6.86×10^{-6}	3.97×10^{-6}	1.73
1000	int	13.5	5.59	23.6	6.88×10^{-6}	5.57×10^{-6}	1.24
	ext	12.5	6.70	0.567	7.18×10^{-6}	3.10×10^{-6}	2.32
50	int	13.8	4.90	23.6	7.10×10^{-6}	4.88×10^{-6}	1.45
	ext	15.7	6.73	0.567	6.94×10^{-6}	2.07×10^{-6}	3.35

To end the comparison with experimental data, we plot the results of the CNV97100 study in figure 4.7, superimposing on the data a line with a slope equal to the apparent permeability from table 4.3 (multiplied by SC_0). If the antibiotic is loaded apically (top row in fig. 4.7) the prediction of the model is good for all initial concentrations. If the loading is basolateral (bottom row); the prediction for low initial concentration underestimates the measured slope. As a

consequence, the predicted efflux ratio differs from experiment at lower concentrations, which makes a more detailed analysis of this difference necessary. The MICHAELIS-MENTEN kinetics used seem to provide an insufficient representation of P-gp efflux at lower initial concentrations when loaded basolaterally. The model underestimates the pump's efficiency in a basolateral to apical set up. We stress that our approximate solution still yields very accurate results for the apparent permeabilities and that this observed difference is a direct consequence of the model or the parameters used. To make this point clear, we have plotted the result of the numerical integration of (4.3) for the lowest concentration of $50\mu M$ in figure 4.7. The deviation from the experimental data is clearly observable in the case of basolateral loading of the drug. Considerations of other efflux pathways in the P-gp transporter protein are found for example in (Acharya *et al.* 2006).

4.3.3 Parameter dependence

Once we had determined the validity of our approach, we wished to use the explicit expressions to determine the dependence on the system parameters of some quantities which are of experimental interest. Here lies one of the strengths of our solution: In figure 4.8 we plot the characteristic time scale for absorption t_1, the equilibrium concentration ratio on both cell sides b_{eq}/a_{eq} and the efflux ratio $P_{BA}^{app}/P_{AB}^{app}$ as a function of the clearances Cl_{AC} and Cl_{CB}, the pump parameters V_M and K_M and the initial concentration of drug C_0. Analytic formulas give access to these results much easier than repetitive integration throughout parameter space plus extracting the data from the resulting trajectories.

Again, for reasons of simplicity, we have limited our presentation to the case of a secretory pump located apically with intracellular binding site; the best model according to analysis by (González-Alvarez *et al.* 2005). As observed in this figure, an increase in the initial con-

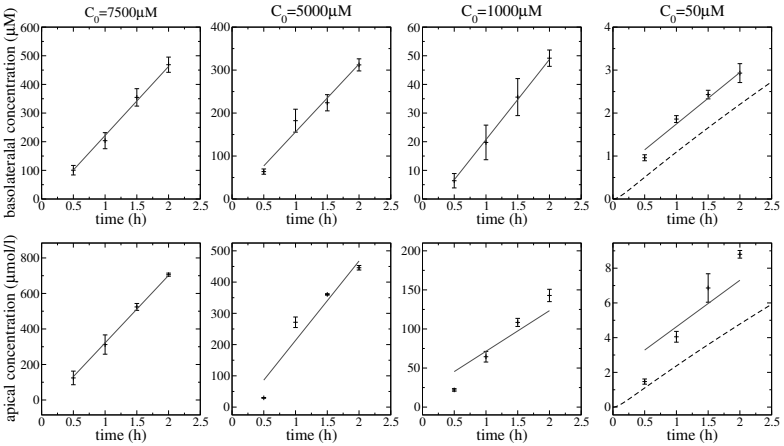

Figure 4.7: Antibiotic's concentration on the receiving side. (*Top*: drug loaded in apical compartment, *bottom*: basolateral loading.) Experimental values are from CNV97100 study. The *solid* line's slope is the prediction from the theoretical solution (shown in table 4.3) for intracellular binding, which was considered to be the model of best fit. The *dashed* line in the graphs on the right shows the numerical integration of the full system (4.3).

centration C_0 implies a decrease in the characteristic time t_1 from a finite value to a minimum value, limiting t_1 to a certain range. Raising C_0 increases the equilibrium concentration ratio b_{eq}/a_{eq}. Although this ratio varies significantly, steady concentration in the basolateral site, b_{eq}, shows a good linear dependence with C_0 (not shown in the figure). Note that the efflux ratio $P_{BA}^{app}/P_{AB}^{app}$ also decreases with increasing initial concentration, a feature supported by the experimental data, although the theoretical values deviate from the experimental results at low concentrations, a fact already discussed in the previous section. The clearance Cl_{CB} of the membrane where the pump is not situated has no influence on the equilibrium concentration and efflux ratios, but an increase of Cl_{CB} decreases the characteristic time t_1, indicating a faster transport of the drug. On the other hand, an increase in the clearance Cl_{AC} of the cell membrane where the pump is located has the effect of decreasing the efflux ratio and increasing the equilibrium concentration ratio. For large initial concentrations, $C_0 = 7500\mu M$, the characteristic time t_1 shows interesting behaviour with Cl_{AC} since it first increases and then decreases, indicating very slow drug absorption for some intermediate values of the clearance.

At large concentrations, the three quantities analysed show small dependence with respect to the pump parameters V_M and K_M, since the corresponding curves are almost flat. This makes it difficult to extract from the data accurate values of the pump parameters at those large concentrations. This suggests that lower concentrations would allow for a better experimental determination of the pump parameters - a practise used by experimentalists - however, we have to take into account, as discussed above, that the accuracy of the model might worsen with decreasing concentration. In the graph, we have included negative values for V_M, which is equivalent to a change in the flow direction of the pump.

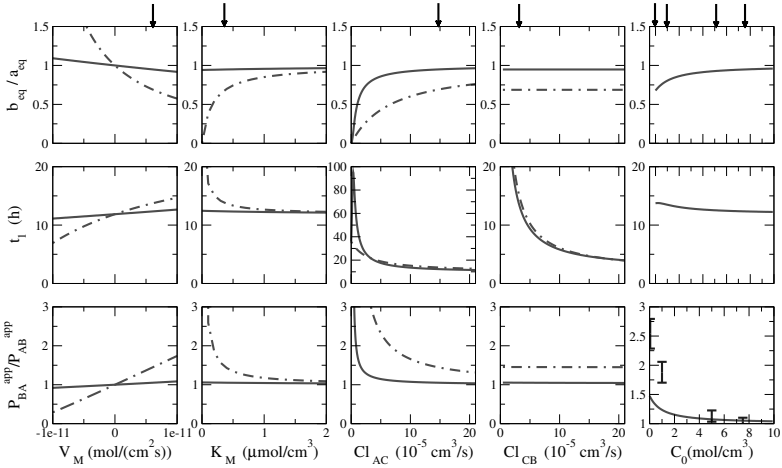

Figure 4.8: Secretory pump, intracellular binding site - *Top* and *middle*: equilibrium concentration ratio (basolateral/apical) and characteristic time (both for apical loading), *bottom*: efflux ratio $P_{BA}^{app}/P_{AB}^{app}$. Dependence on V_M and K_M (transporter parameters) and clearances $Cl_{AC/CB}$. *Continuous* line: $C_0 = 7500\mu M$, *dot-dashed* line: $C_0 = 50\mu M$. On the very *right*: dependence on initial concentration C_0. Arrows on top mark the experimentally derived value. (Values for the respectively fixed parameters taken from table 4.4.)

4.3.4 Error propagation

Apart from the considerations above, the analysis of parameter dependence is the first step towards examining the propagation of errors into the experimentally available quantities. For example it is clear from figure 4.8 (third and fourth column), that small differences in Cl_{AC} would be nearly unnoticed, due to the rather flat curve around its measured value (marked by the black arrow on top of the figures). On the other hand a small change in Cl_{CB} yields a big variation of time scale t_1. We want to use an example to make this clear. Again we will use parameters derived in the CNV97100 absorption study and evaluate in which way a change in parameter influences the measurable quantities. This can be imagined as the variability in different sample cultures.

The distribution f_x of a value x in function of the distribution f_α of the parameter α is given by:

$$f_x(x) = f_\alpha(\alpha) \left| \frac{d\alpha(x)}{dx} \right| . \tag{4.24}$$

Knowing the distribution of value x, the mean value of x is defined by:

$$\langle x \rangle = \int_{x_1}^{x_2} x f_x(x) dx . \tag{4.25}$$

Alternatively, if this integration cannot be solved, one uses Eq. (4.24) and writes:

$$\langle x \rangle = \int_{\alpha(x_1)}^{\alpha(x_2)} x(\alpha) f_\alpha(\alpha) d\alpha . \tag{4.26}$$

Correspondingly one can also compute in a similar way the second moment $\langle x^2 \rangle$ and the standard deviation σ. Due to the nonlinearity it is not always easy to derive explicit expressions but having found the parameter dependencies before, above integrations are easily done numerically up to arbitrary precision.

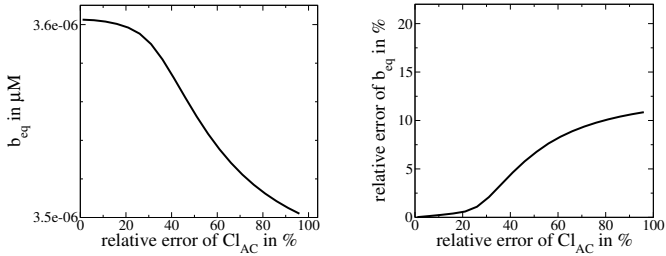

Figure 4.9: The mean basolateral concentration (*left*) and its relative error (*right*) in the case of $7500\mu M$ loaded apically, depending on the relative error of Cl_{AC}. A Gaussian distribution of clearance was assumed.

Now we use the parameter set from González-Alvarez *et al.* (2005), as done before. We chose an experimental set up (apical loading, $C_0 = 7500\mu M$) and the "model of best fit" (apical pump, intracellular binding) and can calculate for example the equilibrium concentration, or rather its distribution, on the receiving side. Figure 4.9 shows the mean value and the relative error versus the relative error of Cl_{AC}, the clearance of the apical membrane. Clearly one sees that the mean value itself is biased towards lower values by a (symmetric) error in the clearance. The relative error of the b_{eq} is a rising function with the remarkable feature of a range of very high slope. At a diversity in the clearance of about 30% the rise of the concentration's error is much higher than for other values. How large the diversity of the cell membrane's clearance is, is not the concern of this work but it allows to estimate the reasons for fluctuations in measurements.

4.3.5 Michaelis-Menten with cellular retention

To account for the amount of drug which retains bound in the cell and is not available as substrate anymore, Korjamo *et al.* (2007) used

an additional constant K which rescales the intracellular concentration. In this case the dynamical equations (4.3a-4.3c) and the flux definition (4.1) become

$$\frac{dQ_A(t)}{dt} = +Cl_{AC}\left(\frac{Q_C}{V_C}\frac{1}{K} - \frac{Q_A}{V_A}\right) + \mathcal{J} \tag{4.27a}$$

$$\frac{dQ_C(t)}{dt} = -Cl_{AC}\left(\frac{Q_C}{V_C}\frac{1}{K} - \frac{Q_A}{V_A}\right) - \mathcal{J} - Cl_{CB}\left(\frac{Q_C}{V_C}\frac{1}{K} - \frac{Q_B}{V_B}\right) \tag{4.27b}$$

$$\frac{dQ_B(t)}{dt} = +Cl_{CB}\left(\frac{Q_C}{V_C}\frac{1}{K} - \frac{Q_B}{V_B}\right) \tag{4.27c}$$

$$\mathcal{J} = \frac{SV_M\frac{Q_C}{V_C}\frac{1}{K}}{K_M + \frac{Q_C}{V_C}\frac{1}{K}} \tag{4.27d}$$

When our transformation is applied to this system (here only intracellular binding is considered), the matrix element a_{21} is multiplied with a factor $1/K$ and the same factor rescales the parameter γ. With these changes the obtained results can be used. We will not go into much detail but the **efflux ratio** (ratio of (4.15) to (4.16)) as the value of main interest to the experimentalist has been calculated. For a parameter set as derived in the CNV97100 study one sees a lowering of the whole curve for rising retention (fig. 4.10). Retention of values smaller than one would raise the curve, but this is not reasonable. The curve does not change its shape much. We conclude that this extension of the three-compartment model is not good for a better fitting to the experiment.

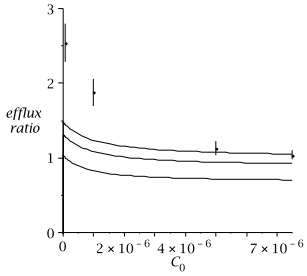

Figure 4.10: Efflux ratio versus initial concentration for different retention constants ($K = 1, 1.1, 1.3$, from top to bottom). The rest of parameters is taken from the CNV97100 experiment (table 4.4). $K = 1$ represents the case with no retention like in fig. 4.8, bottom, right. The experimental values are overlaid

4.4 Conclusions

Three-compartment models are widely used in drug absorption studies. The one treated here consists of a linear part, representing passive absorption (for example through cell membranes), and a non-linear part which models other means of transport, such as ABC-transporter proteins embedded into the cell membrane. In this work we have shown a way to transform this model into the picture of a *ball in a well* (fig. 4.4), which is a general form of equations facilitating analysis of mathematical structure. The lowest point of the "well" gives the value of the **equilibrium concentration** after saturation of the process. With an adequate approximation, one can derive the **absorption profile** as the sum of three exponentials and identify their **characteristic time scales** dividing the process into phases of linear change, non-linear fluxes and saturation. In the phase of a near-linear profile we can provide explicit expres-

sions for the **apparent permeability**, a quantity usually measured in experiments.

These are general results which we used on a showcase system, where the non-linear transport is described by a MICHAELIS-MENTEN profile - a common model of transporter proteins (Mizuarai *et al.* 2004; Sharma *et al.* 2002; Volk & Schneider 2003). The approach presented in this thesis make efflux ratio and time scales accessible. Both *apical* and *basolateral* drug loading can be treated by changing the initial conditions; we furthermore considered the possibilities of *intra*cellular as well as *extra*cellular binding sites. We analysed the importance of each physiological parameter in a wide range of values.

The presented results may contribute to a better understanding of the absorption process and to explain the variability of the observations in identical experimental setups from a more fundamental basis. Knowledge of parameter dependencies, a fundamental analysis of errors (confidence interval) and their consequences becomes possible. This has been left aside for later studies. The most promising experimental setups can furthermore be predicted by treating a newly proposed model in the same way.

A consideration which might be of interest to pharmacology is an efflux $\mathcal{J}$ of Hill type, $\frac{x^\alpha}{k^\alpha + x^\alpha}$, with exponents $\alpha > 1$. This formula is used to describe cooperative binding. Other possible fluxes could be analysed always if assumptions of a closed system with three compartments are fulfilled.

Table 4.4: Experimental parameters drawn from (González-Alvarez *et al.* 2005) used for the calculations.

Parameter	Measured Value
Cl_{AC}	$14.49 \times 10^{-5} cm^3/s$
Cl_{CB}	$3.528 \times 10^{-3} cm^3/s$
V_M	$6.17 \times 10^{-12} mol/(cm^2 s)$
K_M	$0.376 mol/cm^3$
S	$4.2 cm^2$
V_A	$2 cm^3$
V_B	$3 cm^3$
V_C	$0.0738 cm^3$

Table 4.5: Coefficients of solutions (4.14). For equilibrium solution x_{eq}, y_{eq} and coefficients $\tilde{C}_i$ and $\tilde{D}_i$ see text in appendix and table 4.2. The numerical values are calculated for $C_0 = 7500\mu M$ loaded apically.

	INTRA	numerical (μmol)	EXTRA	numerical (μmol)
A_1	$K_M\left(V_C\tilde{C}_1 + V_B\tilde{D}_1\right)$	-8.90	$-K_M V_A\tilde{C}_1$	-5.74
A_2	$K_M\left(V_C\tilde{C}_2 + V_B\tilde{D}_2\right)$	-0.341	$-K_M V_A\tilde{C}_2$	-11.8
A_3	$K_M V_B\tilde{D}_3$	0.348	0	0
Q_A^{eq}	Q_0-			
	$K_M\left(V_C x_{eq} + V_B y_{eq}\right)$	6.1045	$K_M V_A x_{eq}$	6.1057
B_1	$-K_M V_B\tilde{D}_1$	9.11	$-K_M V_B\tilde{D}_1$	5.88
B_2	$-K_M V_B\tilde{D}_2$	-0.0769	$-K_M V_B\tilde{D}_2$	2.82
B_3	$-K_M V_B\tilde{D}_3$	-0.348	$-K_M V_B\tilde{D}_3$	-0.0153
Q_B^{eq}	$K_M V_B\, y_{eq}$	8.6819	$K_M V_B\, y_{eq}$	8.6808
C_1	$-K_M V_C\tilde{C}_1$	-0.204	$K_M\left(V_A\tilde{C}_1 + V_B\tilde{D}_1\right)$	-0.143
C_2	$-K_M V_C\tilde{C}_2$	0.418	$K_M\left(V_A\tilde{C}_2 + V_B\tilde{D}_2\right)$	-14.7
C_3	0	0	$K_M V_B\tilde{D}_3$	0.0153
Q_C^{eq}	$K_M V_C x_{eq}$	0.21358	$Q_0 - K_M\left(V_A x_{eq} + V_B y_{eq}\right)$	0.21355

Chapter 5

Entrainment of coupled circadian oscillators

5.1 Introduction

Circadian rhythms are light-dark dependent cycles of roughly 24 hours present in the biochemical and physiological processes of many living entities (Reppert & Weaver 2002). In mammals the main mediator between the light-dark periodicity and the biological rhythms is formed by two interconnected suprachiasmatic nuclei (SCN), located in the hypothalamus. These nuclei form the so called “circadian pacemaker" and contain about 10.000 neurons each (Moore *et al.* 2002; Reppert & Weaver 2002).

The main property of the SCN is that their activity displays self-sustained oscillations in synchrony with the external forcing imposed by the light-dark cycle. The exact mechanism leading to this behaviour has been the subject of intense research. It has been shown that, when taken individually, neurons produce oscillations

with a constant period ranging from 20 to 28 hours (Honma *et al.* 2004; Welsh *et al.* 1995). The oscillatory behaviour originates in a regulatory circuit with a negative feedback loop. The relevant question is how this individual oscillatory behaviour translates into common, global, oscillations of the SCN activity synchronised with the external light stimulus.

It has been shown that the origin of the oscillatory activity of the circadian pacemaker at the global level resides on the interaction between the SCN neurons. Coupling between cells in the SCN is achieved partly by neurotransmitters (Hastings & Herzog 2004; Honma *et al.* 2004) and it is by means of those neurotransmitters that external forcing by light influences the neuronal synchronisation. For example the vasoactive intestinal polypeptide (VIP) has been shown to be necessary in mediating both the periodicity and the internal synchrony of mammalian clock neurons (Aton *et al.* 2005; Maywood *et al.* 2006; Shen *et al.* 2000). Therefore, a model of coupled and forced neurons appears quite naturally as responsible for the circadian rhythms. Along these lines, an interesting mechanism has been put forward recently by Gonze *et al.* (2005) and by Bernard *et al.* (2007). They proposed that synchronisation to the external forcing is facilitated by the fact that interneuronal coupling transforms SCN into damped oscillators which can then be easily entrained.

In this chapter we show that the presence of some level of heterogeneity or dispersion in the intrinsic periods of the oscillators (Herzog *et al.* 2004; Schaap *et al.* 2003) can improve the response of the coupled neuronal system to the external light-dark forcing. The proposed mechanism for the improvement of the neuronal synchronisation under external periodic forcing bears some similarities with the one proposed in (Bernard *et al.* 2007; Gonze *et al.* 2005) in the sense that the oscillators are brought to a regime of oscillator death (Ermentrout 1990; Mirollo & Strogatz 1990), but in our case this regime is induced by the presence of heterogeneity. Once this regime has been reached, the damped oscillators are more entrainable by the external forcing than the self-oscillating neurons with

different periods, or the synchronised oscillatory state which appears in the strong coupling regime but with a period larger than the individual neuronal periods.

To be more specific, we will assume that the periods of the individual neurons are random variables drawn from a normal distribution. We will then analyse the global response of the system to the light-dark cycle periodicity as a function of the interneuronal coupling strength, external forcing amplitude and neuronal heterogeneity. We show that the presence of the right amount of dispersion in the periods of the neurons can indeed enhance the synchronisation to the external forcing.

Period dispersion arises as a consequence of the cellular heterogeneity at the biochemical level, which is an experimentally well observed fact (Aton & Herzog 2005; Honma *et al.* 2004). It can act in either physiological or pathological conditions. An example of the latter is the diversification of antigenic baggage present in tumor cells that makes them more difficult to be recognised and captured by the defense mechanisms and therefore more prone to migrate and develop metastasis (González-García *et al.* 2002). Our results show that some level of disorder can be of help when synchronising neuronal activity to the external forcing. Although counterintuitive, it has been unambiguously shown that the addition of various forms of disorder can improve the order in the output of a large variety of nonlinear systems. For example, the mechanism of *stochastic resonance* (Gammaitoni *et al.* 1998, 2009) shows that the response of a bistable system to a weak signal can be optimally amplified by the presence of an intermediate level of dynamical noise. Stochastic resonance is not a rare phenomenon; it has been repeatedly shown to be relevant in physical and biological systems described by nonlinear dynamical equations (Gammaitoni *et al.* 1998, 2009). In large systems with many coupled elements, noise is responsible for a large variety of ordering effects, such as pattern formation, phase transitions, phase separation, spatiotemporal stochastic resonance, noise-sustained structures, doubly stochastic resonance, amongst

many others (García-Ojalvo & Sancho 1999). All these examples have in common that some sort of order at the macroscopic level appears only in the presence of the right amount of noise or disorder at the microscopic level. Furthermore, it has been proven that noise may play a constructive role in nonlinear systems, by enhancing coherent (periodic) behaviour near bifurcations and phase transitions (Neiman *et al.* 1997; Pikovsky & Kurths 1997). Here we introduce non-negligible random heterogeneity (so-called quenched noise) into the periods of all neurons. Numerical simulations suggest that the results are valid as well when the quenched noise is introduced into other model parameters. A different approach is the consideration of intracellular stochastic variability due to low molecule numbers (Forger & Peskin 2005) or both variability and heterogeneity.

Close to our work is the study by Ueda *et al.* (2002), where the effect of fluctuations in neuron parameter values is assessed and it is shown that the coupled system is relatively robust to noise. Previous theoretical studies have addressed the effect of noise on genetic oscillators (Becskei *et al.* 2005; Steuer *et al.* 2003; Thattai & van Oudenaarden 2001), and some have proposed an ordering influence of noise on circadian clocks at the single cell level in cases where neither light intensity nor coupling strength by themselves can synchronise the system. Collective phenomena induced by heterogeneity in autonomous, non-forced systems, have also been discussed in the literature. For example de Vries & Sherman (2001) and Cartwright (2000) have shown that collective bursting or firing can appear in excitable systems and a general theory of the role of heterogeneity in those systems has been developed by Tessone *et al.* (2007). We refer to the collective response in systems of non-linear oscillators subjected to the action of an external forcing representing the day-light cycle.

The chapter is organised as follows. In section 5.2 we will describe in detail the model of circadian oscillators and the methods we use. It is a coupled extension of the original Goodwin oscillator (Goodwin

1965) as developed by Gonze *et al.* (2005). In section 5.3 we analyse the system response to the periodic external forcing, as a function of the external forcing amplitude, coupling strength and neuronal diversity or heterogeneity. By simulating numerically the governing differential equations we identify the range of these parameters for which the extended system oscillates in synchrony and entrained to the external light period. We describe the mechanism through which the neuronal heterogeneity favours the synchronisation with the external forcing and analyses the combined influence of the coupling strength, neuronal heterogeneity and light amplitude on the stability of the linearised system of coupled oscillators. We show that a mean variable in this model exhibits a transition from a rhythmic to an arrhythmic dynamics (the so-called oscillator death (Ermentrout 1990; Mirollo & Strogatz 1990)). Concluding remarks are found in section 5.4.

5.2 Model and methods

5.2.1 The circadian pacemaker

As stated in the introduction, our aim is to consider the role that the heterogeneity in the population of neurons plays in the global response of the SCN to an external oscillating stimulus. To this end, we consider an ensemble of coupled neurons subject to a periodic forcing. Each of the neurons, when uncoupled from the others and from the external stimulus, acts as an oscillator with an intrinsic period. Heterogeneity is considered insofar the individual periods are not identical, but show some degree of dispersion around a mean value. For each one of the neurons in the SCN we use a four-variable model proposed by Gonze *et al.* (2005), which is based originally on the Goodwin oscillator (Goodwin 1965), to describe circadian

oscillations in single cells (see as well section 3.3). The variables of the model are as follows: The clock gene *mRNA* (X) produces a clock protein (Y), which activates a transcriptional inhibitor (Z) and this in turn inhibits the transcription of the clock gene, closing a negative feedback loop. The *mRNA* X also excites the production of neurotransmitter V, which in the coupled system will be then the responsible of an additional positive feedback loop. In order to overcome the high Hill coefficients required for self-oscillations, Gonze et al. replaced the linear degradation by nonlinear Michaelis-Menten terms. This leads to the system of equations:

$$\frac{dX}{dt} = \nu_1 \frac{K_1^4}{K_1^4 + Z^4} - \nu_2 \frac{X}{K_2 + X}, \tag{5.1a}$$

$$\frac{dY}{dt} = k_3 X - \nu_4 \frac{Y}{K_4 + Y}, \tag{5.1b}$$

$$\frac{dZ}{dt} = k_5 Y - \nu_6 \frac{Z}{K_6 + Z}, \tag{5.1c}$$

$$\frac{dV}{dt} = k_7 X - \nu_8 \frac{V}{K_8 + V}, \tag{5.1d}$$

which, depending on parameters, might produce oscillations in a stable limit cycle. Using the values $\nu_1 = 0.7$ nM/h, $\nu_2 = \nu_4 = \nu_6 = 0.35$ nM/h, $\nu_8 = 1$ nM/h, $K_1 = K_2 = K_4 = K_6 = K_8 = 1$ nM, $k_3 = k_5 = 0.7$/h, $k_7 = 0.35$/h, the period of the limit cycle oscillations is $T = 23.5$ h.

For the complete model, we take N neuronal oscillators, each one of them described by four variables (X_i, Y_i, Z_i, V_i), $i = 1, \ldots, N$, satisfying the above evolution equations. Heterogeneity in the intrinsic periods is introduced by multiplying the left-hand-side of each one of the equations (5.1) by a scale factor τ_i. Hence, the intrinsic period T_i of the isolated neuron i is $\tau_i T$. The numbers τ_i are independently taken from a normal random distribution of mean 1 and standard deviation σ. Since the periods must be positive, in the numerical simulations we have explicitly checked that, for the values of σ

considered later, τ_i never takes a negative value, which would be unacceptable. The standard deviation σ will be taken as a measure of the diversity. A value of $\sigma = 0.1$ for example corresponds to a standard deviation of 10% in the individual periods of the uncoupled neurons, close to the observed variation of periods in a range between 20 and 28 hours.

Two additional factors influence the dynamics of single cell oscillations: forcing by light and intercellular coupling. Both are assumed to act independently from the negative feedback loop and are added as independent terms in the transcription rate of X (Gonze *et al.* 2005). Light is incorporated through a periodic time-dependent function $L(t)$, which can be realised in various forms. In the majority of the presented results we have used a sinusoidal signal, $L(t) = \frac{L_0}{2}(1 + \sin \omega t)$. In some cases, for comparison and to simulate different day lengths of duration t_{light}, we have used a square wave $L(t) = \begin{cases} L_0, & \text{if } (t \bmod 24h) < t_{light} \\ 0, & \text{otherwise} \end{cases}$. In both ways the signal oscillates between the values $L(t) = 0$ and $L(t) = L_0$ with a period $2\pi/\omega = 24h$.

Coupling between the neurons is assumed to depend on the concentration F of the synchronising factor (the neurotransmitter) in the extracellular medium, which builds-up by contributions from all neurons. Under a fast transmission hypothesis, the extracellular concentration is assumed to equilibrate to the average, mean-field, cellular neurotransmitter concentration, $F = \frac{1}{N}\sum_{i=1}^{N} V_i$. The result-

ing model is:

$$\tau_i \frac{dX_i}{dt} = \nu_1 \frac{K_1^4}{K_1^4 + Z_i^4} - \nu_2 \frac{X_i}{K_2 + X_i} + \nu_c \frac{KF}{K_c + KF} + L(t) \quad (5.2a)$$

$$\tau_i \frac{dY_i}{dt} = k_3 X_i - \nu_4 \frac{Y_i}{K_4 + Y_i}, \quad (5.2b)$$

$$\tau_i \frac{dZ_i}{dt} = k_5 Y_i - \nu_6 \frac{Z_i}{K_6 + Z_i}, \quad (5.2c)$$

$$\tau_i \frac{dV_i}{dt} = k_7 X_i - \nu_8 \frac{V_i}{K_8 + V_i}, \quad (5.2d)$$

$$F = \frac{1}{N} \sum_{i=1}^{N} V_i, \quad (5.2e)$$

with $\nu_c = 0.4$ nM/h, $K_c = 1$ nM.

There is experimental evidence supporting the assumption of a chemical (rather than electrical) mechanism of inter-cell communication among SCN neurons as a synchronisation factor and, in fact, mechanisms other than neurotransmitters or electrical coupling for the SCN communication have been suggested (e.g. by van den Pol & Dudek (1993)). Furthermore, more realistic modelling which takes into account all variables known to participate of the negative feedback loop has been introduced. These models may include up to 10 variables and corresponding equations for each single cell (Bernard *et al.* 2007).

It seems, however, that in order to get understanding of the SCN dynamics, a sufficient tool is the 4 variable model described above. In fact, the synchronisation of damped oscillators is independent from the particular intracellular model used and as discussed by Bernard *et al.* (2007), this system, the model developed by Leloup & Goldbeter (2003), and other simple negative feedback oscillators have similar synchronisation properties. In this chapter we have decided to use the simpler 4-variable model although most of our results would also be valid in the more complex 10-variable model.

A model close to that of Eqs. (5.2) has been used by Ullner *et al.* (2009), where the authors investigate how the interplay between fluctuations of constant light and intercellular coupling affects the dynamics of the collective rhythm in a large ensemble of non-identical, globally coupled oscillators. In their case, however, an inverse dependence of the cell-cell coupling strength on the light intensity was implemented, in such a way that the larger the light intensity the weaker the coupling.

5.2.2 Measures of synchrony and entrainment

Due both to the effect of coupling and of forcing, the neurons might synchronise their oscillations. There are several possible measures of how good this synchronisation is. Here the interneuronal synchronisation will be quantified by the parameter of synchrony ρ, defined as

$$\rho = \sqrt{1 - \left\langle \frac{\sum_{i=1}^{N} [V_i(t) - F(t)]^2}{\sum_{i=1}^{N} V_i(t)^2} \right\rangle} = \sqrt{\left\langle \frac{F(t)^2}{\frac{1}{N}\sum_{i=1}^{N} V_i(t)^2} \right\rangle}, \tag{5.3}$$

where $\langle \dots \rangle$ denotes a time average in the long-time asymptotic state. The parameter ρ varies between a value close to 0 (no synchronisation) and 1 (perfect synchronisation, with all neurons in phase, $V_i(t) = V_j(t), \forall i, j$). It is important to note that even if the neurons synchronise perfectly their oscillations, the period of those oscillations does not necessarily coincide with the mean period T of the individual oscillators or with the period $2\pi/\omega$ of the external forcing. In fact, in the unforced (no light) case, the period of the common oscillations (for the set of parameters given before and a dispersion of $\sigma = 0.05$ and coupling $K = 0.5$) is approximately equal to 26.5 h whereas the period of the forcing is $2\pi/\omega = 24$ h and the mean period of the individual uncoupled oscillators is $T = 23.5$ h (Gonze *et al.* 2005).

Besides the previous measure of synchronisation amongst the oscillators, we are also concerned about the quality of the global response of the neuronal ensemble to the external forcing $L(t)$. A suitable measure of this response can be defined using the average gene concentration,

$$\mathbf{X}(t) = \frac{1}{N}\sum_{i=1}^{N} X_i(t), \tag{5.4}$$

and computing the so-called spectral amplification factor or response order parameter R (see page 27 of chapter 2),

$$R = \frac{4}{L_0^2}\left|\langle e^{-i\omega t}\mathbf{X}(t)\rangle\right|^2. \tag{5.5}$$

R is nothing but the normalised amplitude of the Fourier component at the forcing frequency ω of the time series $\mathbf{X(t)}$. We will show that, under some circumstances, the response R will increase with the intrinsic diversity σ and that the period of the oscillations at the global level coincides with that of the external forcing, these being the main results of this chapter.

5.3 Results

The synchronisation properties of the set of circadian oscillators is influenced by the amplitude of the external forcing L_0, the coupling strength K and the diversity in the individual periods σ. The role of the first two has been studied by Bernard *et al.* (2007), Becker-Weimann *et al.* (2004) and Gonze *et al.* (2005). In this section we focus on the heterogeneity of neuronal periods and analyse the combined influence of L_0, K and σ on the different parameters quantifying interneuronal synchronisation and response to the forcing.

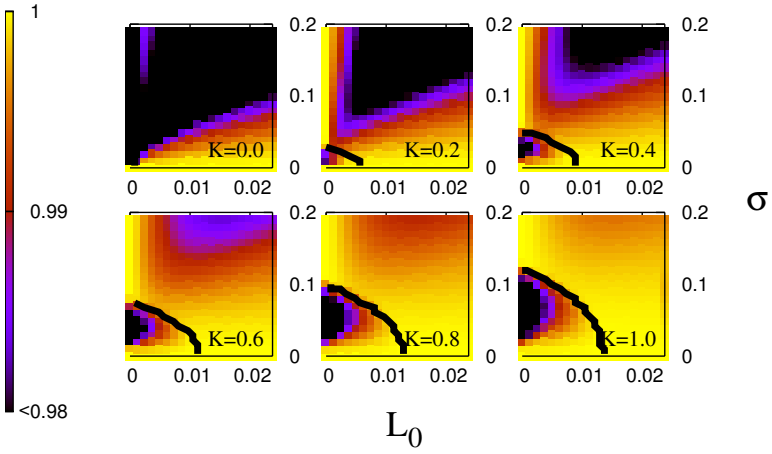

Figure 5.1: Synchrony order parameter ρ (see Eq. (5.3)). Values are coded in colour levels, and displayed as a function of L_0 and σ for several values of K. Data from numerical simulations of $N = 1000$ neurons with dynamics ruled by Eqs. (5.2a–5.2e). Synchrony among the neurons (yellow region) is favored by strong or very weak light intensity L_0, low diversity σ and large coupling K. The thick black line is the linear stability limit discussed in section 5.3.1 (see also Fig. 5.7).

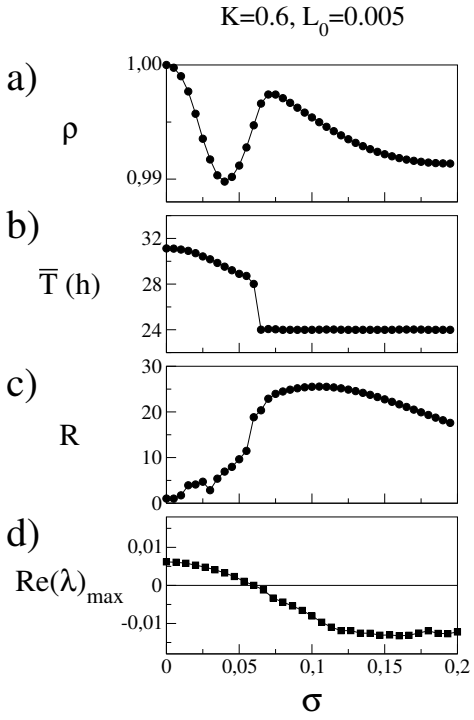

Figure 5.2: Main parameters used for characterising the synchronisation of circadian oscillators as a function of the variance σ. (a) the synchrony parameter ρ; (b) the mean $\bar{T}$ of the individual periods T_i; (c) the response order parameter R; (d) the maximum real part of the eigenvalues of the linearised system.

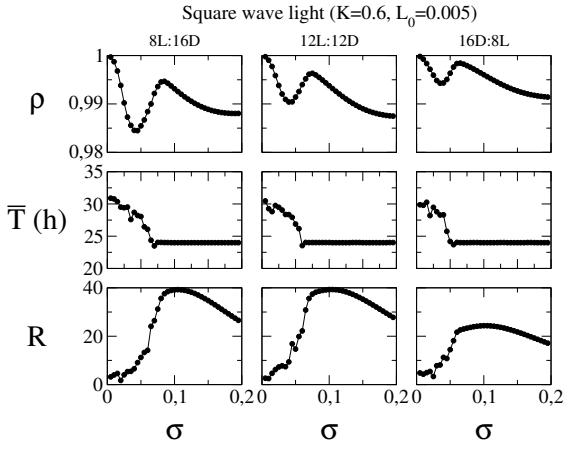

Figure 5.3: Characterisation of synchrony for a light signal of square wave form. The synchrony parameter ρ, the mean $\bar{T}$ of the individual periods T_i and the response order parameter R (from top to bottom) measured for square wave stimuli of various day lengths (t_{light} = 8h, 12h and 16h, from left to right).

Fig. 5.1 shows colour plots of the parameter of synchrony ρ as a function of the diversity σ and the light intensity L_0, for different values of the coupling strength K. High values of the light intensity L_0 favor interneuronal synchrony. Also in agreement with its intuitive disordering role, high neuronal diversity leads to a low synchrony parameter ρ in several parts of the diagrams. However, there is a region of values of $L_0 \in [0, L_{max}]$ for which there is a non-monotonous dependence of the synchrony order parameter with respect to the diversity. This can be seen more clearly in panel (a) of Fig. 5.2 where we plot ρ as a function of diversity σ for fixed values of $K = 0.6$ and $L_0 = 0.005$. ρ first decreases by increasing σ within the interval $0 \leq \sigma \leq 0.05$, but then it develops a maximum. The range of values of L_0 for which this non-monotonous behaviour is observed depends on the coupling constant K: the larger K, the larger L_{max}.

As stated before, the fact that neurons synchronise amongst themselves does not mean that they synchronise to the forcing by light. To study this point, we have computed the individual periods T_i, $i = 1, \ldots, N$, of the oscillators in the ensemble. In those cases in which the concentrations do not oscillate with exact periodicity, we still define the period as the average time between maxima of the dynamical variables. In Fig. 5.4 we plot the mean value $\bar{T} = \frac{1}{N} \sum_{i=1}^{N} T_i$ as a function of σ and L_0 for different values of K. As the dispersion in T_i is small, it turns out that $\bar{T}$ is close to the period of the average variable $\mathbf{X}(t)$.

Although, by construction, individual neurons have periods that fluctuate around $T = 23.5$ h, it turns out that the period of the resulting synchronised oscillations that occur in the unforced but coupled ($L_0 = 0$, $K > 0$) case, increases with increasing coupling K. For example, $\bar{T} \approx 30$ h for $K = 0.6$, mostly independent of the value of σ. As the forcing sets in, at low values of the coupling strength, the mean period is now $\bar{T} = 24$ h for all values of L_0 and σ. As the coupling between neurons increases, larger values of L_0 and/or

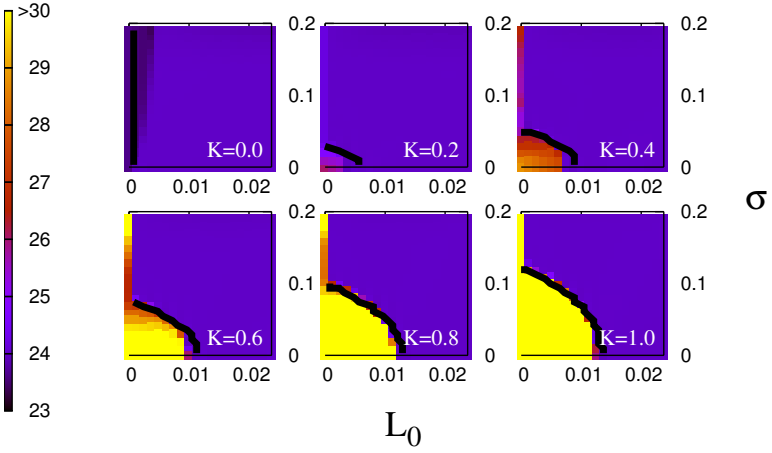

Figure 5.4: Colour level plots of the mean of the individual periods $\bar{T}$ of 1000 neurons under forcing at 24h cycle for the system of Eqs. (5.2a–5.2e). High light intensity L_0 and high diversity σ assures entrainment of oscillations to external frequency (blue region). Increasing coupling enlarges the region (yellow) of oscillations at a period larger than that of the driving force.

σ are needed in order for the mean period to coincide with that of the external forcing. An important feature that emerges from these plots is that for low light intensity it is possible to achieve a mean period of 24 h by increasing the neuronal diversity. For example, in the areas at the left of the different panels of Fig.5.4, or in panel (b) of Fig.5.2 corresponding to the case $K = 0.6$, while identical neurons have periods of $\approx$ 30 h, increasing σ induces an adjustment of the period to 24 h. The transition between $\bar{T} = 24$ h and $\bar{T} \neq 24$ h is rather sharp, specially for large K. This is a clear manifestation that diversity indeed is able to improve the response to the external forcing.

A complementary perspective on this constructive role of diversity is attained looking at spectral amplification factor, R, from Eq. (5.5). This is a normalised measure of the amplitude of the oscillation of the neuronal system at the frequency of the daily forcing. Figures 5.5 and 5.2(c) show that there is a region in parameter space in which the system response to the periodic light forcing displays a maximum value as a function of diversity σ. In fact this maximum is very large as compared with the R value at zero diversity, so that one can say that one of the most noticeable effects of a non-vanishing neuronal diversity is to give the system the capacity to respond efficiently to the 24h forcing in situations of small or no response at this frequency in the absence of diversity (the non-diverse neuronal ensemble could be oscillating at a different frequency, as revealed by high values of ρ). In summary, it is possible to largely improve neuronal synchronisation to the daily-varying light input by taking σ close to an optimal value. Too small or too large diversity will not yield an optimal response at this frequency, although the response is generally larger than for zero diversity.

An external signal of square wave form and with different day lengths lead to similar results. As can be seen in figure 5.3 the response R to the external signal passes through a maximum at a intermediate value of diversity. The mean period and the synchrony parameter behave as in the case with a pure sinusoidal as the driving

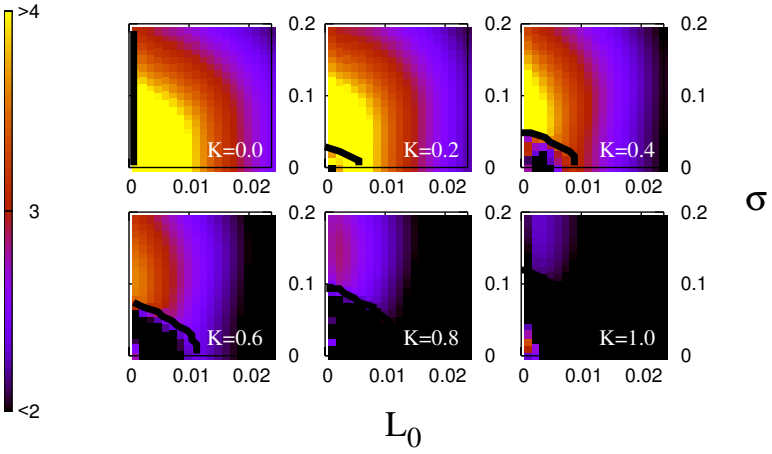

Figure 5.5: Colour plots of the spectral amplification factor R as defined in Eq. (5.5) in logarithmic scale. Too high light intensity L_0 and too much diversity σ lower the response of X to the external frequency. This also happens for low light and low diversity (where the neurons oscillate at a frequency $\neq$ 24 h, see Fig. 5.4). Between both limits R passes a local maximum.

force. Furthermore, the qualitative result is independent of the chosen day length.

5.3.1 Diversity-induced oscillator death

Why does an increase in the diversity of the oscillators lead to an improved response to the external forcing? We argue that the main effect of the increase of the diversity is to take the oscillators into a regime of oscillator death (Ermentrout 1990; Mirollo & Strogatz

1990) in which they can be easily entrained by the varying part of the forcing. To understand this mechanism (in the sinusoidal case) we first split the forcing into a constant (the mean) and a time varying part: $L(t) = \frac{L_0}{2} + \frac{L_0}{2}\sin(\omega t)$. Taking only the constant part, $L(t) = \frac{L_0}{2}$, Figs. 5.6(a)–(c) show that the oscillators go from self-sustained oscillations to oscillator death, i.e. the amplitude of the self-sustained oscillations decreases, as σ increases. Once oscillators are damped, they would respond quasi-linearly to periodic forcing, at least if this forcing is not too large, and linear oscillators always become synchronised to the external forcing, independently of their internal frequency. This is consistent with what is seen in figures 5.6(d)–(f), where the neurons in the case of low heterogeneity oscillate synchronously with each other, but their common period is larger than the one of the light forcing. Only when diversity brings the neurons to oscillator death can all of them be entrained to the period of the forcing signal. The mechanism is related to the one discussed by Gonze *et al.* (2005) and Bernard *et al.* (2007), but here we stress than neuron heterogeneity, as opposed to internal neuron parameters and couplings, is enough to damp the collective neuron oscillations and bring the system to a non-oscillating state where it can be more easily entrained. It is interesting to note that it has been shown experimentally for fruitflies that only a subset of the pacemaker neurons sustain cyclic gene expression after changing the laboratory light conditions to constant darkness, whereas the oscillations of the other pacemaker neurons are damped out (Veleri *et al.* 2003). Although this does not reveal the mechanism by which the oscillations die out it suggests that some of the circadian oscillators do indeed work in the damped regime, at least in *Drosophila*.

An alternative way of checking this mechanism based on *diversity-induced oscillator death* is by analysing the stability of the steady state of the system of Eqs. (5.2a–5.2e) when considering a constant forcing $L(t) = \frac{L_0}{2}$. The numerical calculation of the fixed point of the

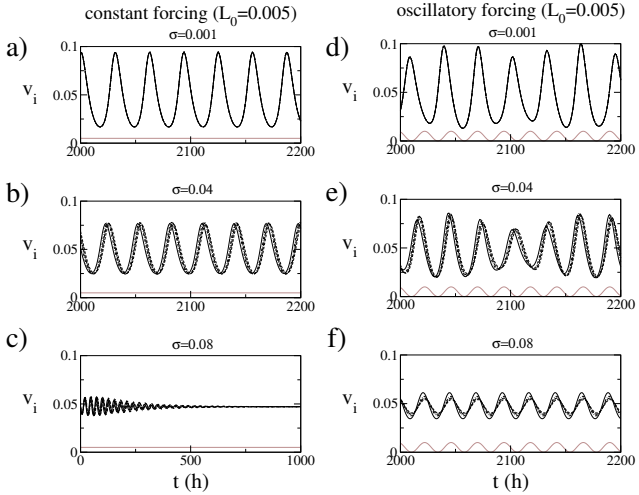

Figure 5.6: Figures (a), (b) and (c) represent the time-dependent amplitude of the V_i variable for a few selected neurons in the presence of constant light and increasing σ, while Figures (d), (e) and (f) represent the amplitude of the same neurons with sinusoidal light and increasing σ. The thin line on the bottom of the graphs is the external light signal. $K = 0.6$.

dynamics is greatly simplified by the fact that the concentrations of the biochemical variables are the same for each one of the N neurons irrespectively of their specific value of τ_i. The system (5.2a–5.2e) is linearised around this steady state and the eigenvalues of the stability matrix computed for several realisations of diversity parameters τ_i. In each case, the positive or negative character of the real part of the eigenvalue with the largest real part indicates the instability or stability, respectively, of the fixed point solution. In Fig. 5.7 we plot the mean of that maximum real part of the eigenvalues averaged over various realisations of the time scales τ_i, for $N = 200$ coupled neurons, as a function of L_0 and σ, and different values of the coupling K (see also panel (d) in Fig.5.2). In every diagram we can see that low diversity or low forcing yield an unstable steady state (yellow region). This is where self-sustained oscillations are observed. A thick black line in the contour plots indicates a zero real part. The relevance of this line separating positive from negative maximum average eigenvalues is more apparent when we note that it also delimits regions of interest in Figs.5.1, 5.4 and 5.5.

In summary, increasing the diversity or the (constant) forcing term decreases (on average) the maximum eigenvalue of the coupled system and thus a Hopf bifurcation (see page 17 of chapter 2) can be crossed backwards, so that self-oscillations disappear. When applying the periodic external forcing on the system formed by self-sustained neurons, coherence with the external frequency is difficult to achieve because there is the competing effect of mutual neuron synchronisation to a different frequency. However, when the periodic external forcing is applied on the system of damped neurons, they all synchronise to the external forcing, and thus with each other since this is the only dynamical regime available to forced damped oscillators (if forcing is not too strong to excite further resonances). Increased coupling strength increases the range of unentrained self-oscillations.

Oscillator death by diversity is not particular to this system. Mirollo & Strogatz (1990) analyse a large system of limit cycle-oscillators

with mean field coupling and randomly distributed frequencies. They proved that when the coupling is sufficiently strong and the distribution of frequencies has a sufficiently large variance, the system undergoes “amplitude death”. In their approach the oscillators pull each other off their limit cycles, which is translated into a stable equilibrium point for the coupled system. Thus, this mechanism suggests that the quenched noise we introduced in the system “pushes apart" the limit cycles of the different neurons, so that their competition enlarges the range of parameters where fixed point behaviour is stable.

A qualitative argument explaining the diversity-induced oscillator death in our system of coupled neurons goes as follows: We know from Gonze *et al.* (2005) that a single oscillator can switch from a limit cycle to a stable steady state by adding a constant mean field (the term containing F in (5.2a) but with time-independent F) of sufficient strength to Eq. (5.1a). A constant light forcing term has the same effect (see the zero coupling case in fig. 5.7). Furthermore we have observed that the amplitude of the oscillations decreases with rising diversity (compare figs. 5.6), but the mean does not change. In a system with low diversity we have large oscillations of F around that mean value. If this value, taken as a constant, determines a stable steady state, then we argue that the large oscillations lead the system into unstable regions, whereas, by increasing σ the amplitude is decreased and the concentrations do not leave neighbourhood of the stable fixed point, thus finding themselves damped all the time. This is a possible mechanism for the *diversity-induced oscillator death* phenomenon.

5.4

Conclusions

In this chapter we have analysed the role of diversity in favoring the entrainment of a system of coupled circadian oscillators. We introduce non-negligible heterogeneity in the periods of all neurons in the form of quenched noise. This is achieved by rescaling the individual neuronal periods by a scaling factor drawn from a normal distribution. The system response to the light-dark cycle periodicity is studied as a function of the interneuronal coupling strength, external forcing amplitude and neuronal heterogeneity.

Most of the cases of order induced by heterogeneity or noise carried out so far (Gammaitoni *et al.* 1998, 2009; Pikovsky & Kurths 1997; Tessone *et al.* 2006, 2007; Toral *et al.* 2009; Ullner *et al.* 2009) emphasise the fact the diversity directly improves oscillator synchronisation. In our case the mechanism is rather different. Diversity does not improve system synchronisation directly. This is achieved indirectly, by a leading first to a diversity-induced stabilisation of the fixed points of the neurons forming the system. Once steady concentrations are asymptotically stable, it is much better entrainable by the external forcing, so that the damped neurons adapt easily to the external forcing (and then, in addition, they appear as synchronised between them). The synchronisation arises therefore not as a result of a direct diversity-induced neuronal synchronisation but indirectly, as a result of the diversity-induced oscillator death. Our results indicate therefore that the right amount of heterogeneity helps the extended system to respond globally in a more coherent way to the external forcing. In addition to the robustness of the results against use of different types of forcing (see figure 5.3) we have checked that resonances in the responses to the external forcing and matching of the circadian period to the external forcing appear in more complex models, such as the 10-variable model of (Bernard *et al.* 2007) with diversity in the time scales τ_i, or the

4-variable model of Gonze *et al.* (2005) with heterogeneity in all the reaction rate parameters v_i. We expect that a similar behaviour will be found in similar models of non-mammalian clocks like those of *Drosophila* (Smolen *et al.* 2004), *Arabidopsis* (Locke *et al.* 2005), *Neurospora* (Heintzen & Liu 2007) or *Cyanobacteria* (Dong & Golden 2008).

Of course, it is an open question whether the observed diversity in the periods of the neurons of the SCN has been tuned by evolution in order to display a maximum response to the 24 h dark-light natural cycle. A detailed experimental check of our predictions would require to be able to vary the amount of diversity. In this sense we suggest the possibility of using chimeric organisms (Low-Zeddies & Takahashi 2001) to introduce diversity in a controlled way.

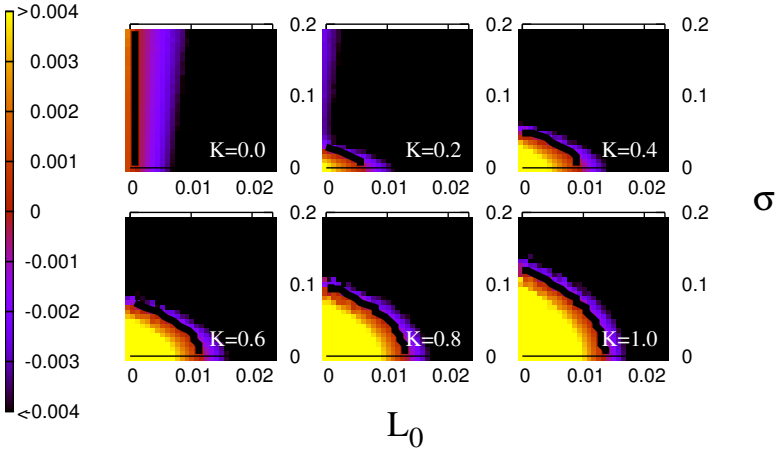

Figure 5.7: Colour plots of the maximum real part of the average eigenvalues of system of Eqs. (5.2a–5.2e), as a function of σ and L_0, at different values of K. Increasing σ or increasing L_0 changes this quantity from positive to negative, i.e. transforms the self-sustained neurons into damped neurons by stabilising their constant concentrations fixed points. Rising the coupling enlarges the region of self-sustained oscillations. Averaged from 10 realisations of heterogeneity in 200 neurons.

Chapter 6

Coherent firing in coupled active rotators

6.1 Introduction

In some cases, a dynamical system with many variables depends on a set of parameters which, although fixed in time, are randomly distributed according to a given probability distribution. The outcome of the system, although deterministic, depends on the actual realization of the set of parameters. The influence of this so–called, depending on the context: quenched noise, static disorder, heterogeneity, variability, diversity, impurities, etc. has been the subject of many investigations. In the last years, some emphasis has been given to identifying those situations in which the presence of the quenched noise induces some sort of macroscopic ordering, such as phase transitions (Buceta *et al.* 2001), patterns (Buceta & Lindenberg 2003); improves the global response to an external forcing (Tessone *et al.* 2006) or enhances synchrony of firing units (Tessone *et al.* 2007).

Due to the complexity of the problem, analytical treatments are usually very difficult to be carried out in full detail and most results rely on extensive numerical simulations. However, a recently introduced technique named "order parameter expansion" (de Monte & d'Ovidio 2002; de Monte *et al.* 2004, 2005, 2003; Komin & Toral 2010; Silva *et al.* 2006) offers a simple approximate way of analyzing the effect of the random quenched terms in the dynamical equations. The approximation scheme allows the reduction of the large number of coupled differential equations for the microscopic variables to just a few effective equations for the relevant macroscopic dynamical variables: the mean values and dispersions from the mean.

It is the purpose of this chapter to apply the order parameter expansion technique to the study of the active rotator model (Acebrón *et al.* 2005; Kuramoto 1975; Strogatz 2000) under the influence of static disorder in the natural frequencies. Previous work (Bulsara & Zador 1996; Shinomoto & Kuramoto 1986; Tessone *et al.* 2007; Toral *et al.* 2007) has shown the somewhat paradoxical result that intermediate levels of disorder at the microscopic level induce macroscopic order which manifests itself in a synchronous, or coherent, firing of the units. Although very sophisticated treatments of this model do exist leading to analytical solutions in some particular cases (Lafuerza *et al.* 2010; Ott & Antonsen 2008, 2009) (and we will refer to them later in the chapter) a particular simple analysis was developed in (Tessone *et al.* 2007), where the authors used an expansion of the dynamical equations of the model up to first order in the deviation of the quenched variables from their mean value and identified a self-consistency equation which had to be solved numerically. The order parameter expansion used in the present article expands consistently this analysis up to terms of second order, thus reaching a higher accuracy. The resulting closed system of three differential equations reproduces the ordering abilities of quenched noise in this system and, furthermore, predicts a sharp transition back into the disordered state where no macroscopic order is observed. In general the study of synchronization between oscillatory systems

is of interest in a variety of research fields, ranging from climatology (Jevrejeva *et al.* 2003) to electronics (Bezruchko *et al.* 2003) and from neurology (Neiman *et al.* 2007) to physiology (Sosnovtseva *et al.* 2002). Existing analytical methods for involved models, like the self-consistent theory, are usually very difficult to carry out. The presented approximate method gives an intuition about a system's dynamics. With its use the change of the nullclines due to diversity in the Fitzhugh-Nagumo model (Pérez *et al.* 2010) and phase transitions induced by diversity (Komin & Toral 2010) have been investigated.

The article is organized as follows. First, in section 6.2, we will define the active rotator model and summarize its main properties. Macroscopic observables that describe the collective behaviour are introduced. Then, in section 6.3, the approximation method is applied and conclusions about steady states are drawn. In section 6.4 we present numerical results that support the previous findings and use the theory of finite–size scaling to determine some of the critical exponents characterizing the transitions. The chapter closes with concluding remarks in section 6.5.

6.2 Model

Let us consider a system of globally-coupled active rotators (Kuramoto 1975), defined by a set of angular variables $\phi_i(t)$, $i = 1, \ldots, N$ which evolve according to the dynamical equations:

$$\dot{\phi}_i(t) = \omega_i - \sin(\phi_i(t)) + \frac{C}{N} \sum_{j=1}^{N} \sin\left(\phi_j(t) - \phi_i(t)\right) . \qquad (6.1)$$

C is the coupling constant. The so-called natural frequencies ω_i are quenched noise, i.e. random variables independently drawn from

a probability distribution $g(\omega)$ with mean $\langle\omega\rangle$. The variance of the distribution, σ^2, is a measure of the dispersion of natural frequencies amongst the oscillators and measures the degree of intrinsic disorder. We will refer to σ as the "diversity".

For uncoupled units, $C = 0$, a value of $|\omega_i| > 1$ results in a rotating behaviour for $\phi_i(t)$. The actual period of rotation is $\frac{2\pi}{\sqrt{\omega_i^2-1}}$ and the direction of rotation depends on the sign of ω_i: clockwise if $\omega_i < 0$ and anti-clockwise otherwise. If $|\omega_i| < 1$, then unit i is in an excitatory regime. In this case there are two fixed points (one stable and the other unstable) located at the two solutions of $\phi_i^* = \arcsin(\omega_i)$. When a perturbation is such that it makes variable ϕ_i to cross over the unstable fixed point, the subsequent dynamics returns to rest again in the stable fixed point through a full turn of ϕ_i on the unit circle (a "spike" or a "pulse"). This is the typical behaviour of an excitable system (Lindner *et al.* 2004).

When the coupling is active, $C > 0$, the dynamics of each unit is influenced by the others which act, effectively, as a perturbation. As a result, individual spikes can be generated. Those spikes can be independent of each other or, alternatively, the units might spike with some degree of synchrony. It is of interest to characterize the global behaviour of the system in order to identify the region of parameter space for which synchronized spiking occurs. To this end one usually defines a complex variable which represents the centre of mass of all rotators (Kuramoto 1984):

$$\rho(t)e^{\imath\Psi(t)} = \frac{1}{N}\sum_{j=1}^{N} e^{\imath\phi_j(t)} \equiv \left\langle e^{\imath\phi_j(t)}\right\rangle. \tag{6.2}$$

Henceforth, $\langle\cdots\rangle$ denotes an average over the N units. The Kuramoto order parameter $\rho = \overline{\rho(t)}$, where the overline denotes an average with respect to time, differentiates between fully synchronized ($\rho = 1$, i.e. $\phi_i(t) = \phi_j(t), \forall i, j$) and desynchronized oscillators ($\rho \approx 0$). When ρ is close to 1, one still needs to distinguish the rest state where

all oscillators are equally constant in time from the coherent firing regime where the units are oscillating synchronously. Amongst other possible measures, one can use the order parameter introduced by Shinomoto & Kuramoto (1986) as $\zeta = \left| \overline{\rho(t) e^{i\Psi(t)}} - \overline{\rho(t) e^{i\Psi(t)}} \right|$, which is different from zero only in the case of synchronous firing. Alternatively, and this is the approach followed here, one can measure the average angular speed of the time evolution of the global phase $\Psi(t)$. In the rest state, $\Psi(t)$ is time independent and the angular speed is zero, whereas in the coherent firing regime, $\Psi(t)$ increases with time and the angular speed adopts a non-zero value.

It has been shown that the system of coupled active rotators displays a disorder-induced transition from the global rest state to synchronized firing (Bulsara & Zador 1996; Shinomoto & Kuramoto 1986; Tessone *et al.* 2007). Higher levels of disorder lead the system again into unsynchronized firing. The disorder can be produced by the existence of diversity amongst the natural frequencies (Toral *et al.* 2007) (as it is the case of interest here), by the presence of noise terms in the dynamical equations, by the existence of competitive interactions, heterogeneity in the network of connectivities (Tessone *et al.* 2008) or any other origin. A general theory to explain this transition has been developed in (Tessone *et al.* 2007), while an exact treatment in the case of disorder in the natural frequencies has been carried out in (Lafuerza *et al.* 2010; Ott & Antonsen 2009). In the next section we present a simplified treatment of this problem in terms of the order parameter expansion. This allows us to derive equations for the macroscopic variables as a perturbative expansion, assuming small fluctuations. This simple approach is able to predict the main features observed in the numerical simulations. Furthermore, it provides an analytic expression for the critical noise intensities in the large coupling limit.

6.3 Method

6.3.1 Derivation of the dynamical equations

As stated in the introduction, our goal is to use the order parameter expansion method to obtain evolution equations for the global phase $\Psi(t)$, defined in Eq.(6.2), and its fluctuations, defined as suitable moments of the variables $\epsilon_i(t) = \phi_i(t) - \Psi(t)$. As it will turn out the dynamics of the global phase at lowest order coincide with the local dynamics. When coupling the units to a mean-field the dynamics of the global phase become coupled to that of the fluctuations $\Omega_2(t) \sim \langle \epsilon_j(t)^2 \rangle$ and the weighted fluctuations $W(t) = \langle \epsilon_j(t)\delta_g \rangle$, where we write $\delta_i = \omega_i - \langle \omega \rangle$ for the deviation of the local natural frequency from the mean. The fluctuations Ω_2 and W have to be taken into account at same order, to obtain a consistent set of equations. The precise derivation of the approximate dynamical system goes as follows.

We first notice that according to the definition of ϵ_i and using Eq. (6.2), a simple calculation leads to

$$\left\langle e^{\imath\phi_j(t)} \right\rangle = e^{\imath\Psi(t)} \left\langle \cos\epsilon_j(t) + \imath \sin\epsilon_j(t) \right\rangle = \rho(t) e^{\imath\Psi(t)} . \tag{6.3}$$

Since $\rho(t)$ has to be a real number we find that $\left\langle \sin\epsilon_j(t) \right\rangle = 0$ and $\rho(t) = \langle \cos\epsilon(t) \rangle$. As a consequence we can rewrite Eq. (6.1) as:

$$\dot{\phi}_i(t) = \omega_i - \sin(\phi_i(t)) - C \left\langle \cos\epsilon_j(t) \right\rangle \sin\epsilon_i(t) . \tag{6.4}$$

If we now take the time derivative of (6.2) one can identify real and imaginary parts and find the identity

$$\dot{\Psi}(t) \left\langle \cos\epsilon_j(t) \right\rangle = \left\langle \dot{\phi}_j(t) \cos\epsilon_j(t) \right\rangle , \tag{6.5}$$

where we substitute $\dot{\phi}_j(t)$ as given by Eq. (6.4) and obtain an equation for $\Psi(t)$ as a function of $\left\langle \cos\epsilon_j \right\rangle$, $\left\langle \cos^2\epsilon_j \right\rangle$, $\left\langle \sin\epsilon_j \cos\epsilon_j \right\rangle$ and $\left\langle \delta_j \cos\epsilon_j \right\rangle$. If we now expand these four terms up to second order around $\epsilon_i = 0$ we are left with:

$$\dot{\Psi} = \langle\omega\rangle - \Omega_2(t)\sin\Psi(t)\,. \tag{6.6}$$

Here we have identified the dynamical variable $\Omega_2(t) = 1 - \dfrac{\left\langle \epsilon_j^2(t) \right\rangle}{2}$. We determine its dynamics by writing $\dot{\Omega}_2(t) = -\left\langle \dot{\epsilon}_j(t)\epsilon_j(t) \right\rangle$, using $\dot{\epsilon}_i(t) = \dot{\phi}_i(t) - \dot{\Psi}(t)$, and replacing $\dot{\phi}_i$ from Eq. (6.4) and $\dot{\Psi}$ from Eq. (6.6). Expanding the resulting expression up to second order around $\epsilon_i = 0$ we arrive at:

$$\dot{\Omega}_2 = -W(t) + 2\left(\cos\Psi(t) + C\right)\left(1 - \Omega_2(t)\right)\,, \tag{6.7}$$

where the third dynamical variable $W(t) = \left\langle \epsilon_j(t)\delta_j \right\rangle$ allows us to close the set of equations. It obeys dynamics given by $\dot{W}(t) = \left\langle \dot{\epsilon}_j(t)\delta_j \right\rangle$ and is found in the same way as above:

$$\dot{W} = \sigma^2 - \left(\cos\Psi(t) + C\right)W(t)\,, \tag{6.8}$$

where we made use of the definition $\left\langle \delta_j^2 \right\rangle = \sigma^2$.

The set of equations (6.6) for the global phase and (6.7-6.8) for the fluctuations, is the result of the order parameter expansion applied to the oscillator ensemble defined by Eqs. (6.1) and is the basis for further analysis. The errors are of the order $O\left(\left\langle \delta_j^n \epsilon_j^m \right\rangle\right)$, $n + m = 3$, or higher. As a consequence, Eq. (6.6) is more accurate than the corresponding equation $\dot{\Psi} = \langle\omega\rangle/\rho - \sin\Psi + O\left(\left\langle \delta_j^2 \right\rangle\right)$ obtained in (Tessone *et al.* 2007). Note that this last equation simply identifies ρ as the threshold for excitability. In our case, the full stability analysis is more involved as $\Omega_2(t)$ is considered to be a variable of time. The Shinomoto-Kuramoto order parameter can be

approximated by carrying out the appropriate time averages of $\zeta \approx \left|\overline{\Omega_2(t)e^{i\Psi(t)}} - \overline{\Omega_2(t)e^{i\Psi(t)}}\right| + \overline{O(\langle\epsilon^4\rangle)e^{i\Psi(t)}}$ but, as stated above, we will use a different order parameter. In the next subsection we will determine the fixed points of the system (6.6-6.8) and their stability.

6.3.2 Phase diagram

The fixed points $(\Psi^*, \Omega_2^*, W^*)$ of the system of equations (6.6-6.8) must satisfy:

$$\langle\omega\rangle = \Omega_2^* \sin\Psi^*, \tag{6.9}$$

$$\Omega_2^* = 1 - \frac{\sigma^2}{2\left(\cos\Psi^* + C\right)^2}, \tag{6.10}$$

$$W^* = \frac{\sigma^2}{\cos\Psi^* + C}. \tag{6.11}$$

Graphically, the coordinates Ψ^* of the fixed points correspond to the intersections of the function $\Omega_2^*(\Psi^*)\sin(\Psi^*)$ with the horizontal line representing $\langle\omega\rangle$. As shown in figure 6.1, it turns out that, for fixed $\langle\omega\rangle$ and C the amplitude of the oscillatory rhs of eq. (6.9) is a function that first decreases continuously with σ until eventually reaching its lowest value to then increase continuously for larger σ (see figure 6.2). Therefore there exist two limiting values of the diversity σ_c and σ_c' such that two solutions are found whenever $\sigma < \sigma_c$ or $\sigma > \sigma_c'$. A linear stability analysis shows that in this case the global phase behaves as an excitable system, with one of the solutions corresponding to a stable and the other to an unstable fixed point. If, otherwise, $\sigma \in (\sigma_c, \sigma_c')$ there will be no fixed points and the global phase will rotate in time, signalling the existence of coherence firing in the global system. The linear stability analysis also shows that the stable and unstable fixed points, found in the low and high noise limits, collide and disappear when the maximum of the right-hand-side of Eq. (6.9) coincides with $\langle\omega\rangle$. This is a so-called

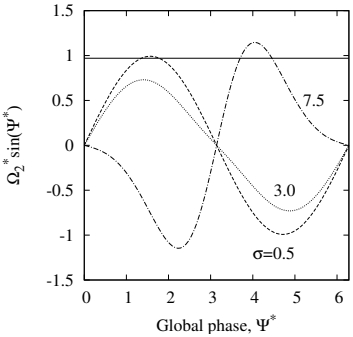

Figure 6.1: Graphical analysis of the solutions of the equation $\langle\omega\rangle = \left(1 - \frac{\sigma^2}{2(\cos\Psi^* + C)^2}\right)\sin(\Psi^*) \equiv \Omega_2^*(\Psi^*)\sin(\Psi^*)$ for $C = 4.0$ and $\sigma = 0.5, 3.0, 7.5$ (dashed, dotted, dash dotted). The horizontal line marks $\langle\omega\rangle = 0.97$. Note that the line corresponding to $\sigma = 3.0$ does not cut the horizontal line, thus no stable steady state exists for this value of σ, whereas two solutions exist for the other values of σ.

SNIC bifurcation (saddle-node on an invariant cycle, see page 15). The steady states in the macroscopic equations (6.6-6.8) at high and at low values of σ are caused by different underlying microscopic dynamics: whereas individual rotators are moving at high levels of noise, they are all at rest in the low noise limit.

The phase diagram identifying regions of synchronized global firing can be obtained from the existence of solutions to equations (6.9-6.11) as discussed above. In general, this has to be performed numerically, but to an arbitrary degree of accuracy. Results for the case that the mean of natural frequencies is $\langle\omega\rangle = 0.97$ are shown in figure 6.3. It can be observed that a minimal coupling intensity is needed to introduce a possible state of coherent firing. In the large coupling limit, $C \gg 1$, it is possible to derive analytical expressions for σ_c and σ_c'. Neglecting $\cos\Psi^*$ in the denominator of the right

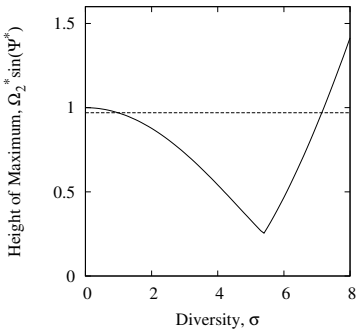

Figure 6.2: Maximum of the rhs of eq. (6.6) for $C = 4.0$ as continuous line and $\langle\omega\rangle$ marked as dashed line. When the curve of the maximum lies above the dashed line a fixed point solution exists. Otherwise not.

hand side of Eq.(6.10), the necessary condition $|\langle\omega\rangle| \leq \Omega_2^*$ leads to

$$\sigma_c = C\sqrt{2}\sqrt{1-\langle\omega\rangle}, \tag{6.12}$$

$$\sigma_c' = C\sqrt{2}\sqrt{1+\langle\omega\rangle}\,. \tag{6.13}$$

In this approximation, the width of the interval (σ_c, σ_c'), where the system fires synchronously, grows linearly with C. This means that an intermediate level of coupling is needed to support a synchronized firing state. The dependence on $\langle\omega\rangle$ of the second transition is rather small for $\langle\omega\rangle \approx 1$. The interval collapses for $\langle\omega\rangle = 0$. The resulting approximate phase diagram for large coupling values is marked with dashed lines in figure 6.3. We conclude that the order parameter expansion correctly identifies the diversity induced transitions that occur at the critical points σ_c and σ_c'. As shown in figure 6.3, it also allows the determination of the value of σ_c with a reasonable accuracy, although σ_c' is grossly overestimated, when compared against the numerical simulations (see section 6.4) or the analytical treatment of (Lafuerza *et al.* 2010) using a Gaussian distribution

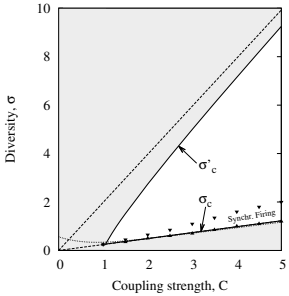

Figure 6.3: Phase diagram: Fixed points of Eqs. (6.9-6.11) (for $\langle\omega\rangle = 0.97$) exist below and above the two continuous lines (gray region). In between no fixed points exist and the global phase rotates, i.e. the individual rotators oscillate in a coherent manner. Approximate values of the critical diversity for $C \gg 1$ according to Eqs. (6.12,6.13) are plotted with dashed lines. Symbols show values taken from numerical simulations of the set of Eqs. (6.1) with a Gaussian distribution. The dotted line marks the approximate solution of the critical diversity given in (Lafuerza *et al.* 2010).

$g(\omega_i)$ for the natural frequencies. As an example, for $\langle\omega\rangle = 0.95$ and coupling $C = 4$, the numerical solution of Eqs. (6.9-6.11) yields a critical noise intensity of $\sigma_c = 1.269$, whereas the approximate solution, Eq, (6.12) yields $\sigma_c = 1.265$. This is to be compared with the value $\sigma_c = 1.272$ obtained from the exact treatment given by Lafuerza *et al.* (2010) based on recent developments by Ott & Antonsen (2008, 2009).

From the microscopic point of view, one could argue that the destruction of coherence at high noise values is due to the coexistence of individual oscillators rotating at opposite directions, as they would certainly be present for many general distributions $g(\omega)$ of natural frequencies. However, the only requirements we have made on the distribution $g(\omega)$ is that its first and second moments are well

defined. Therefore, according to our treatment, the existence of elements rotating in both directions can not be the only responsible for the transitions. To analyze this issue, we have considered that the individual frequencies were drawn from an exponential distribution $g(\omega_i) = e^{-\omega_i/\langle\omega\rangle}/\langle\omega\rangle$, for $\omega_i \geq 0$ such that all natural frequencies ω_i would be positive. In this case the variance σ^2 and the mean $\langle\omega\rangle$ are not independent of each other, as they satisfy $\sigma = \langle\omega\rangle$ and there is only one parameter in the distribution. Replacing $\sigma = \langle\omega\rangle$ in Eqs. (6.12) and (6.13) we obtain

$$\sigma_c = C\left(\sqrt{C^2+2} - C\right) \tag{6.14}$$

$$\sigma_c' = C\left(\sqrt{C^2+2} + C\right), \tag{6.15}$$

as the limits of the zone for which synchronized firing exists. The phase diagram for this exponential distribution has been plotted in figure 6.4. As it is a special case of the general distributions considered above, the qualitative image is the same: an intermediate value for the intensity of the quenched noise is required to induce a state of coherent firing, while a too high intensity destroys it. As in the case of Gaussian distribution of natural frequencies, the qualitative picture agrees with the exact treatment and the numerical simulations. The lower critical point σ_c is also given with a reasonably degree of accuracy, but the upper critical point is overestimated, again compared with the numerical simulations or the analytical treatment of (Lafuerza *et al.* 2010).

To end this section, we note that, for a general distribution $g(\omega)$, a very large diversity satisfying $\sigma > \sigma_c'$ will never induce another SNIC bifurcation into a new state of coherent firing. With this observation one would expect that distributions $g(\omega)$ with infinite variance, as is the case for a Lorentzian distribution, would never show a regime of synchronized firing. This is in agreement with the detailed theory of (Lafuerza *et al.* 2010) only for $\langle\omega\rangle < 1$. In the case $\langle\omega\rangle > 1$, however, the complete theory predicts that oscillators rotate coherently for low diversity and incoherently for high diversity.

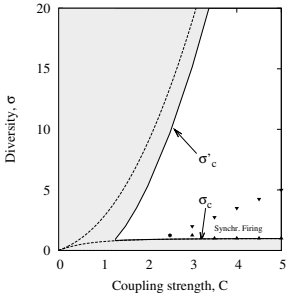

Figure 6.4: Phase diagram for the exponential distribution of natural frequencies which satisfies $\sigma = \langle\omega\rangle$. As in figure 6.3, fixed points of Eqs. (6.9-6.11) exist below and above the two continuous lines (gray region). Approximate values of the critical diversity for $C \gg 1$ according to Eqs. (6.14-6.15) are plotted with dashed lines. Symbols show numerical simulations with exponential distribution.

In summary, and in agreement with more involved treatments of the coupled active rotator model, the order parameter expansion scheme predicts a transition into coherent firing and out of it, induced by the exclusive presence of quenched noise. The only assumptions we made on the frequency distribution to derive the results are the existence of well defined first and second moments. In the following section we present numerical simulations of the full system, Eqs. (6.1).

6.4 Numerical simulations

In the previous section we demonstrated that for very low and very high values of σ the system (6.6-6.8) is in a steady state characterized

by $\dot{\Psi} = \dot{\Omega}_2 = \dot{W} = 0$, whereas for intermediate values the global phase Ψ is not constant. This reproduces, in a simple manner, the prediction of the existence of this intermediate level of disorder for which the system fires synchronously and shows the validity of the order parameter expansion applied to this model. In this section, we will present results of numerical simulations of the full system of coupled equations (6.1). Our goal is to show that the transitions occurring at σ_c and σ_c' show all the features of true phase transitions and can be characterized, besides by the vanishing of the order parameter, by a divergence of the fluctuations. The divergence, as usual, is smeared out by finite size effects and it is possible to carry out an analysis in terms of finite size scaling with the number N of rotators (Cardy 1988). Furthermore we want to compare the macroscopic behaviour of systems with symmetrically distributed natural frequencies and systems with only positive frequencies. Namely, Gaussian distributions are used in the first case and exponential distributions in the second.

As order parameter, m, quantifying the collective firing regime we have chosen the time average of the slope of the global phase $m = \overline{\dot{\Psi}}$. This is expected to vanish for small, $\sigma < \sigma_c$, and large $\sigma > \sigma_c'$ disorder and be non-zero in between. In the figures we plot the ensemble average $\langle\langle m \rangle\rangle$, and the normalized fluctuations $\chi = \frac{N}{\sigma^2}\left[\langle\langle m^2 \rangle\rangle - \langle\langle m \rangle\rangle^2\right]$, where $\langle\langle \cdots \rangle\rangle$ denotes an ensemble average over realizations of the random noise terms and initial conditions. We present separately the results for Gaussian and for exponentially distributed frequencies.

6.4.1 Gaussian distributed frequencies

The natural frequencies ω_i are drawn from a Gaussian distribution of mean $\langle\omega\rangle$ and variance σ^2. In figure 6.5a we present the results for different values of the mean frequency $\langle\omega\rangle$ as a function of the noise

intensity σ. One can see that for small σ the order parameter $\langle\langle m \rangle\rangle$ vanishes or, equivalently, that the global phase is constant indicating that all oscillators are in the rest state. When reaching the critical value σ_c, the global phase $\Psi(t)$ starts to rotate, i.e. $\dot{\Psi}(t) \sim m \neq 0$. This is the regime of synchronized firing where a macroscopic fraction of the oscillators fire in synchrony. Increasing the diversity over the second critical value σ_c', the global phase Ψ is constant again. This is the phase where all units fire in a desynchronized manner. As predicted by Eq. (6.13) the second transition is relatively constant regarding small changes in $\langle\omega\rangle$ when it is close to one.

The precise numerical determination of the location of the transition points σ_c and σ_c' is hindered by the finite size effects. We have found that the location of the maximum of the fluctuations of m can give us a good estimator of the transition points, as it is relatively constant with system size, see figure 6.5b. The results for different values of the coupling strength C are indicated with symbols in the phase diagram, figure 6.3. The first transition is predicted with high accuracy whereas the second transition is highly overestimated by the order parameter expansion. Another feature predicted by the order parameter expansion, namely the existence of a minimal coupling necessary for inducing coherent firing, is indeed observed in the simulations. The discrepancy between the predicted σ_c' and the observation is a consequence of the large diversity as there the omitted higher order terms become relevant. We note that the solution of the fixed point equations (6.9)-(6.11) can be obtained with arbitrary precision and for the calculation of the phase diagram we assured a sufficient convergence of the result.

In the vicinity of both transitions at σ_c or σ_c', the ensemble fluctuations χ of the order parameter diverge with system size. As figure 6.6(a) shows, the maximum value $\chi_{max}(N)$ scales as N^c with $c = 0.65 \pm 0.03$ at the first transition and $c = 0.61 \pm 0.07$ at the second. Interestingly enough, the values of the critical exponent at both transitions seem to be consistent with the value $c = 2/3$ observed in a phase transition induced by quenched noise in a

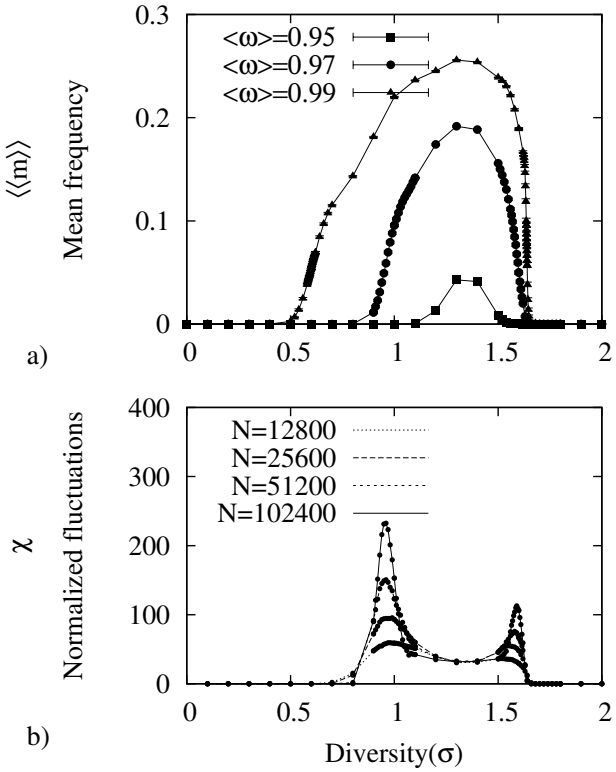

Figure 6.5: Simulation results for Gaussian distributed ω_i's: a) The order parameter $\langle\langle m \rangle\rangle$ for $C = 4.0$ and various values of $\langle\omega\rangle$. The location of the second transition changes little by small variations in $\langle\omega\rangle$ if it is close to one. Simulations were done with $N = 102400$. b) Ensemble fluctuations (performed over 1000 realizations of the quenched noise variables and initial conditions) of the order parameter increase with system size ($\langle\omega\rangle = 0.97$ and $C = 4.0$).

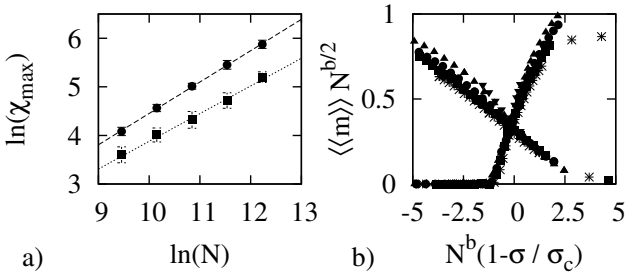

Figure 6.6: Finite size analysis for Gaussian distributed frequencies with $\langle\omega\rangle = 0.97$ and $C = 4$: a) Linear fits of maximal fluctuations yield $\ln(\chi_{max}) \sim c \ln(N)$ with $c = 0.65 \pm 0.07$ for the first transition (circles) and $c = 0.6 \pm 0.1$ for the second (squares). b) Rescaled order parameter $\langle\!\langle m(\sigma, N)\rangle\!\rangle N^{b/2}$ collapses as a function of ϵN^b with exponent $b = 1/3$, ($N = 12800, \ldots, 204800$).

Ginzburg–Landau model (Komin & Toral 2010). It turns out that the full dependence of N and σ at both transitions can be fitted using standard finite-size-scaling theory (Cardy 1988; Deutsch 1992*a*) as $\langle\!\langle m(\sigma, N)\rangle\!\rangle = N^{-b/2} f_m(\epsilon N^b)$ and $\chi(\sigma, N) = N^c f_\chi\left(\epsilon N^b\right)$ with $\epsilon = 1 - \sigma/\sigma_c$ or $\epsilon = 1 - \sigma/\sigma_c'$, and being f_m and f_χ suitable scaling functions different for the two transitions. Our numerical results are not sufficiently precise to allow an accurate determination of the exponent b, but reasonable scaling collapse of the data, see figure 6.6(b), is achieved using $b = 1/3$, as suggested by the analogy with the Ginzburg–Landau model mentioned before.

6.4.2 Exponentially distributed frequencies

The probability distribution function for the natural frequencies is $g(\omega_i) = \mathrm{e}^{-\omega_i/\langle\omega\rangle}/\langle\omega\rangle$ for $\omega_i \geq 0$. As mentioned before, this distribu-

tion has only one parameter as the standard deviation is equal to the mean $\sigma = \langle\omega\rangle$. It is chosen such that all rotators have natural frequencies in the same, anti-clockwise, direction. As shown in figure 6.7 we find the same dynamical regimes as a function of the disorder σ as in the case of an arbitrary distribution. This is in accordance to the theoretical predictions displayed in figure 6.4. the transition into coherent firing is rather constant and happens around $\sigma_c \approx 1$, the interval grows with rising coupling strength and a minimal C is needed to induce coherent firing. Again the second transition is overestimated. As before, we use the maximum of the fluctuations in the order parameter (see figure 6.7b for the case of the transition at σ_c) to estimate values for the critical noise intensities and annotate them in the corresponding phase diagram (figure 6.4).

The first transition, into coherent firing, is marked by diverging fluctuations (for a particular case, $C = 5.0$, see figure 6.7b) which scale in the same way with system size N as we have seen in the Gaussian case (see evidence in figure 6.8). However, in stark contrast to Gaussian distributions, the simulations with exponential distributed frequencies give strong evidence that the transition into asynchronous firing is now of first order. We compare the histograms of steady states for 1000 noise realizations around both transitions in figure 6.9. At the first transition (left column) the distribution broadens at the critical disorder and moves continuously to higher values. On the contrary the equilibria near the second transition are narrowly distributed around zero, or around the nonzero value in the ordered state, typical for a first order transition (right column).

It turns out that the order parameter expansion developed in the previous section predicts that the second transition into asynchronous firing occuring at $\sigma = \sigma_c'$, is of second order for the Gaussian distribution and of first order for the exponential distribution of frequencies. In fact it predicts that any distribution leads to a first order transition out of the ordered state if the mean and variance are set equal (or in any other linear relationship) and varied simultaneously. The

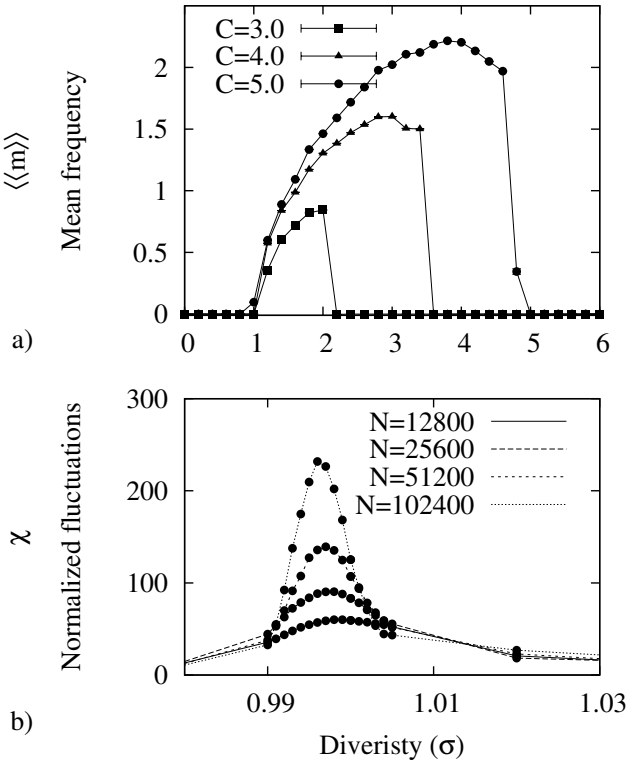

Figure 6.7: Simulation results for exponentially distributed ω_i's: a) The order parameter is non-zero for finite disorder. Fluctuations show that the first transition takes place around $\sigma \approx 1$, as Eq. (6.14) predicts for large C. b) Ensemble fluctuations (for $C = 5.0$) diverge at the first transition for increasing N.

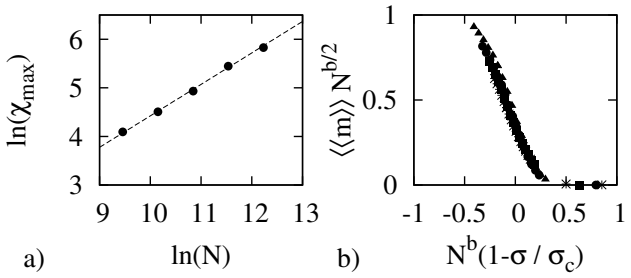

Figure 6.8: Finite size analysis for exponentially distributed frequencies ($C = 5$): a) Linear fit of maximal fluctuations yields $c = 0.65 \pm 0.02$. b) Rescaled order parameter with scaling exponent $b = 1/3$.

results of the numerical integration of the system of equations (6.6-6.8) for selected sets of parameters ($\langle\omega\rangle$, σ, C) for the mean phase velocity $\overline{\Psi}$ are plotted in figures 6.10 (Gaussian) and 6.11 (exponential). It is evident the jump of $\overline{\Psi}$ at the second critical point σ_c' in the case of the exponential distribution whereas it is continuous for the Gaussian distribution. The first transition to synchronized firing at $\sigma = \sigma_c$ is predicted to be continuous independently of the distribution of frequencies.

6.5 Conclusions

We have used the order parameter expansion to approximate the dynamics of the global phase in systems of coupled active rotators under the influence of quenched disorder. The method leads straightforwardly to a system of three differential equations easier

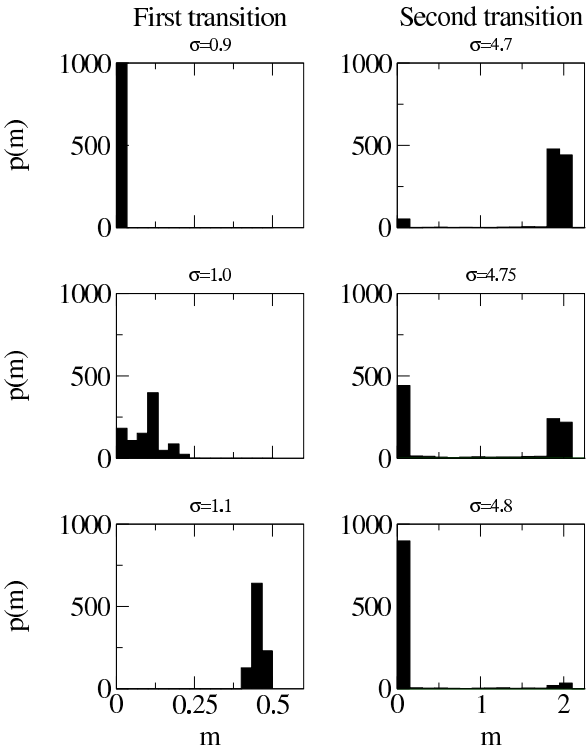

Figure 6.9: Histogram of 1000 steady states from simulations of equations (6.1) with exponentially distributed frequencies. At the transition into coherent firing (left column) the values are distributed around one single value, broadening near the critical disorder. The destruction of the ordered state is a first order transition (right column), the values are distributed narrowly around zero or the non-zero value, $C = 5.0$.

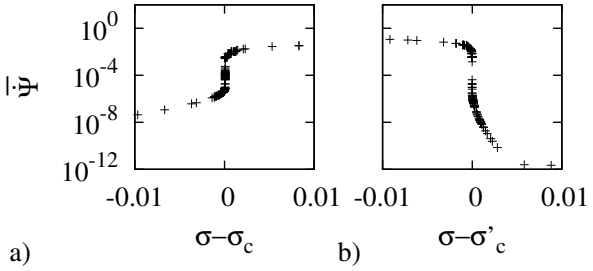

Figure 6.10: Results from the integration of Eqs. (6.6-6.8) in the vicinity of the transition points with $\langle\omega\rangle = 0.97$ and $C = 4.0$. Both transitions, into the ordered state and into asynchronous firing, panel a) and b) respectively, are of second order.

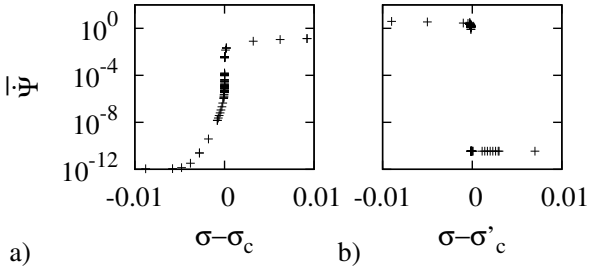

Figure 6.11: Results from the integration of Eqs. (6.6-6.8) in the vicinity of the transition points with $\langle\omega\rangle = \sigma$. Whereas the transition into the ordered state is of second order, panel a), the second transition is discontinuous, panel b).

treatable than the full system and more accurate than other approximations used in previous works. In agreement with exact results for the full system, the global phase of the reduced system can undergo a transition from a rest state into a rotating regime and back into a rest state, when subjected to increasing diversity. In the rest states, $\Psi(t)$ is time independent and the angular speed is zero, whereas in the intermediate regime of coherent firing, $\Psi(t)$ increases with time and the angular speed adopts a non-zero value. Our treatment allows us to give analytic expressions for the critical disorder values in the limit of large coupling. We have seen that the first transition is predicted to a high degree of accuracy whereas the second is highly overestimated.

We have used numerical simulations to show that the ensemble fluctuations of the order parameter diverge at the transition points. The simulations with Gaussian distributed frequencies show continuous transitions, both in and out of the coherent firing state, but if the frequencies are distributed according to an exponential distribution (and therefore the mean and variance are varied simultaneously) then the destruction of the ordered state is achieved through a first order transition. The order parameter expansion scheme predicts this distinction of the transitions. A finite-size scaling analysis of the numerical simulations data indicate that the critical exponents of the transitions are consistent with those found in the athermal Ginzburg-Landau model with additive quenched noise.

Chapter 7

Phase transitions induced by microscopic disorder

7.1 Introduction

The effect of time-dependent noise in extended dynamical systems has been the subject of intensive study in the last years (García-Ojalvo & Sancho 1999). Besides the expected disordering role, it has been found that some kind of order at the macroscopic level can appear by increasing the intensity of the noise. Examples of this paradoxical result include stochastic resonance (Gammaitoni *et al.* 1998, 2009), or enhancement of the effect of an external forcing under the right amount of noise, coherence resonance (Pikovsky & Kurths 1997) (also named as stochastic coherence (Zaikin *et al.* 2003)) where a dynamical system displays optimal periodicity at the right noise value, noise sustained patterns, structures and fronts (Clerc *et al.* 2006; Santagiustina *et al.* 1997), phase transitions where a more

ordered phase appears when increasing the noise intensity (van den Broeck *et al.* 1994*b*, 1997), etc.

In a very general framework, it has been argued that the resonance with an external forcing can also be achieved when the time-dependent noise is replaced by a more general source of disorder. This includes natural diversity or heterogeneity, competitive interactions, disorder in the network of connectivities, etc. and can appear in driven bistable and excitable systems (Tessone *et al.* 2006, 2007; Toral *et al.* 2007), in linear (Toral *et al.* 2009) and chaotic (Chen & Zhang 2008) oscillators and in a variety of other systems (Acebrón *et al.* 2007; Chen *et al.* 2009; Gosak 2009; Perc *et al.* 2008; Postnova *et al.* 2009; Tessone & Toral 2009; Ullner *et al.* 2009; Wu *et al.* 2009; Zanette 2009*a*)). A unifying treatment of the role of noise and diversity for non-forced excitable systems, has been developed in (Tessone *et al.* 2007).

In this work we examine the effect that structural disorder or diversity, in the form of quenched noise, has on some prototypical models of phase transitions which have been studied thoroughly in the presence of noise. From the practical point of view, the models we will be considering bear some similarities with random-field, or impurities, models. As tool of investigation we will refine a previously developed order parameter expansion method of approximating large systems of coupled differential equations (de Monte & d'Ovidio 2002; de Monte *et al.* 2004, 2005, 2003; Silva *et al.* 2006) with diverse parameters. This allows the reduction of the large set of differential equations to just three: one for the global, mean field, value and two which describe the fluctuations around this mean value. Within this approximation (which is valid in the vicinity of the homogeneous state) we will analyse three different models and show its ease to deliver some understanding of the emergent properties of the global behaviour. To find the limits of the order parameter expansion method we will compare the results with the solution of the self-consistency equation which arises from the property of self-averaging.

The chosen models are a set of globally coupled ϕ^4-systems both in the presence of additive and multiplicative quenched noise and the canonical model for noise-induced phase transition (van den Broeck *et al.* 1994*b*, 1997). It will be seen that quenched noise can induce phase transitions (in, out and reentrant) of ordered phases.

The rest of this chapter is organized as follows: In the next section we will describe the analytical methods, self-consistency and order parameter expansion; in section 7.3 we will apply those methods to the showcase models and compare with the results of numerical simulations; the last section closes the chapter with the discussion of the presented results.

7.2 Models and method

The type of models we will be considering in this thesis is defined via differential equations for the dynamics of a set of real variables x_i:

$$\dot{x}_i = f(x_i, \eta_i; X)\,, \qquad i = 1, \ldots, N. \tag{7.1}$$

The time derivative $\dot{x}_i(t) = dx_i(t)/dt$ depends on the constant parameter η_i, a kind of quenched noise. The values $\{\eta_1, \ldots, \eta_N\}$ are independently drawn from a probability distribution $g(\eta)$ of mean H and variance σ^2. Coupling between the different dynamical equations is provided by the presence of the global variable or mean value $X(t) = \langle x_i(t) \rangle \equiv \frac{1}{N}\sum_{i=1}^{N} x_i(t)$ in Eq. (7.1). For a given realization of the η_i's variables the x_i's tend in the limit $t \to \infty$ to some asymptotic, stationary values which, in general, will depend on initial conditions. Some insight can be obtained if we write Eq. (7.1) as a relaxational dynamics (San Miguel & Toral 2000) in a potential

$V(x_i, \eta_i; X) = -\int^{x_i} dx_i' f(x_i', \eta_i; X)$:

$$\dot{x}_i = -\frac{\partial V(x_i, \eta_i; X)}{\partial x_i}. \tag{7.2}$$

If the potential $V(x_i, \eta_i; X)$ is monostable for a particular value of X, then the variable $x_i(t)$ tends during the dynamical evolution towards the single minimum of $V(x_i, \eta_i; X)$. Note that the location of this minimum will change with time as X evolves. If, on the contrary, $V(x_i, \eta_i; X)$ presents several minima, the dynamics will tend towards one of the local minima of the potential.

In the following we will be interested in characterizing the stationary solution by the ensemble average value and fluctuations with respect to realizations of the quenched noise and initial conditions of the global variable X. We first review briefly the self-consistency method and then explain the approximate method based on the order parameter expansion.

7.2.1 Self-consistency

This method uses ideas borrowed from the Weiss molecular field theory (Stanley 1971), which is known to be exact for systems with long-range interaction or, equivalently, in which the interaction occurs through the global variable X, a mean-field scenario, as it is our case. Let us denote the stable stationary solution of Eq. (7.1) by x_i^*. This is nothing but the absolute minimum of the potential $V(x_i, \eta_i; X)$. It will be a function of η_i and the global variable X, i.e. $x_i^* = x^*(\eta_i, X)$. For a given realization of the quenched noise variables η_i's, the value of the global variable must be obtained from the self-consistency relation $X = \frac{1}{N}\sum_{i=1}^{N} x^*(\eta_i, X)$. It is clear that for large N the sum can be replaced by an integral over the distribution $g(\eta)$ of the independent η_i's variables:

$$X = \int d\eta g(\eta) x^*(\eta, X)\,. \tag{7.3}$$

It is then assumed that one can identify the value of X, obtained solving this equation, as the desired ensemble average, i.e. assuming the property of self-averaging (Landau & Binder 2000). In general, the possible solutions X of the self-consistency equation (7.3) have to be found numerically. A possible scenario is that by changing some parameter (e.g. the root mean square σ or the mean H) of the distribution $g(\eta)$, the solutions bifurcate and the system then undergoes a phase transition between the possible solutions. We will present the results of this procedure in the examples below, but will not give any further details about the (in general, very involved) numerical method used to solve Eq. (7.3). Explanations of how to determine the actual value of the critical diversity is given in Appendix B.2.

7.2.2 Order parameter expansion

For the development of this approximate method we assume, as in the previous subsection, that the number of degrees of freedom N is very large and then it is possible to substitute the mean value of the distribution $g(\eta)$ by the system average $H = \langle \eta_i \rangle = \frac{1}{N}\sum_{i=1}^{N} \eta_i$, the variance by $\sigma^2 = \langle (\eta_i - \langle \eta_i \rangle)^2 \rangle = \frac{1}{N}\sum_{i=1}^{N} (\eta_i - \langle \eta_i \rangle)^2$, and similar expressions for other cases.

Our goal is to find an approximate equation describing the dynamics of the mean value variable X. To this end, we will expand the evolution equations in the deviations $\epsilon_i(t) = x_i(t) - X(t)$ of the dynamical variables from the mean value, and in the deviations $\delta_i = \eta_i - H$ of the parameters from their mean value. The Taylor expansion of Eqs. (7.1) around the mean values up to second order

gives:

$$\begin{aligned}\dot{x}_i &= f(X,H;X) + \epsilon_i\, f_x(X,H;X) + \delta_i\, f_\eta(X,H;X) + \\ &\frac{1}{2}\,\epsilon_i^2\, f_{xx}(X,H;X) + \epsilon_i\delta_i\, f_{x\eta}(X,H;X) + \frac{1}{2}\,\delta_i^2\, f_{\eta\eta}(X,H;X) + \end{aligned} \tag{7.4}$$

With the usual notation $f_x(X,H;X) = \left.\frac{\partial f(x,\eta;X)}{\partial x}\right|_{x=X,\eta=H}$, etc. We now take averages and use that $\langle\epsilon_i\rangle = \frac{1}{N}\sum_{i=1}^N \epsilon_i = 0$ and $\langle\delta_i\rangle = \frac{1}{N}\sum_{i=1}^N \delta_i = 0$. Furthermore we have $\langle\delta_i^2\rangle = \sigma^2$ as the parameter distribution's variance. So when we average over Eq. (7.4) we are left with:

$$\begin{aligned}\dot{X} &= f(X,H;X) + \frac{1}{2} f_{xx}(X,H;X)\langle\epsilon_i^2\rangle + f_{x\eta}(X,H;X)\langle\epsilon_i\delta_i\rangle + \\ &\frac{\sigma^2}{2} f_{\eta\eta}(X,H;X) + O(\langle\epsilon_i^3\rangle, \langle\epsilon_i^2\delta_i\rangle, ...)\,. \end{aligned} \tag{7.5}$$

The evolution of X is then coupled to that of the second moment of the *snapshot probability density* $\Omega = \langle\epsilon_i^2\rangle = \frac{1}{N}\sum_{i=1}^N \epsilon_i^2$ and the so-called *shape parameter* (de Monte *et al.* 2005) $W = \langle\epsilon_i\delta_i\rangle = \frac{1}{N}\sum_{i=1}^N \epsilon_i\delta_i$. We will now obtain evolution equations for these two variables. We follow closely the method of (de Monte *et al.* 2003) but keep all terms up to second order in ϵ_i and δ_i. We start by subtracting (7.5) from (7.4) to obtain $\dot{\epsilon}_i = \dot{x}_i - \dot{X}$, which can then be replaced in $\dot{\Omega} = \langle 2\epsilon_i\dot{\epsilon}_i\rangle$, $\dot{W} = \langle\delta_i\dot{\epsilon}_i\rangle$. After some algebra, and neglecting terms of order $O(\langle\epsilon_i^3\rangle, \langle\epsilon_i^2\delta_i\rangle, \dots)$ or higher, we get:

$$\begin{aligned}\dot{X} &= f(X,H;X) + \frac{\Omega}{2} f_{xx}(X.H;X) + f_{x\eta}(X,H;X)\, W + \\ &\frac{\sigma^2}{2} f_{\eta\eta}(X,H;X), \end{aligned} \tag{7.6a}$$

$$\dot{\Omega} = 2\,\Omega\, f_x(X,H;X) + 2\, W\, f_\eta(X,H;X), \tag{7.6b}$$

$$\dot{W} = W\, f_x(X,H;X) + \sigma^2 f_\eta(X,H;X). \tag{7.6c}$$

In summary, within this approximation we have obtained a closed set of three differential equations (7.6a-7.6c). They have the feature

of being coupled only in one direction, i.e. $W(t)$ is independent of the others and $\Omega(t)$ depends only on $W(t)$. These equations are valid to study the global behaviour in the general case, including non-stationary collective states. Steady state conditions $\dot{W} = \dot{\Omega} = \dot{X} = 0$ lead to $W = -\sigma^2 \frac{f_\eta}{f_x}$ and $\Omega = \sigma^2 \frac{f_\eta^2}{f_x^2}$, and the equilibrium of variable X is given by the solution of:

$$0 = f + \frac{\sigma^2}{2}\left[f_{\eta\eta} + f_{xx}\frac{f_\eta^2}{f_x^2} - 2\frac{f_{x\eta}\, f_\eta}{f_x} \right], \tag{7.7}$$

where we have simplified notation $f = f(X, H; X)$, etc. As before, an analysis of the bifurcations of this equation will allow us to find the possible phase transitions of the model.

Our results, Eqs. (7.6), differ slightly from those in the cited sources. The authors de Monte & d'Ovidio (2002) and de Monte *et al.* (2004, 2005) require the parameter to be additive, thus setting $f_\eta = 1$. In other works (de Monte *et al.* 2003; Silva *et al.* 2006) any parameter dependence is allowed, but a coherent regime is required, such that terms of order $O(\langle \epsilon_i^2 \rangle)$ and higher are neglected.

7.3 Examples

After presenting the general development of the order parameter expansion method, we will now apply it to a few models of relevance in the field of phase transitions. Our purpose is to compare the results of our approximation with those coming from the self-consistency equation analysis as well as with numerical simulations of the different models. Solving the self-consistency equation requires in practice a complicated numerical calculation, while our

treatment is simple and predicts the existence of phase transitions with reasonable accuracy in some cases.

7.3.1 Globally coupled Ginzburg-Landau model with additive quenched noise

The Ginzburg-Landau or ϕ^4 scalar-field has been studied thoroughly from the analytical and numerical points of view, as a paradigmatic model undergoing a second-order phase transition (see Amit & Mayor 2005). Here we are interested in this model in the case that the stochastic thermal fluctuations have been replaced by additive quenched noise, as an example of a random-field scalar model (Young 1998). The dynamical equations for the set of real variables $x_i, i = 1, \ldots, N$, are:

$$\dot{x}_i = a\, x_i - x_i^3 + C\,(X - x_i) + \eta_i\,. \tag{7.8}$$

The study of the model using the self-consistency relation Eq. (7.3) can be found in (Toral *et al.* 2007). Here we want to use the order parameter expansion to derive the main properties of this model, in particular the existence of a phase transition as a function of the intensity σ of the fluctuations of the random fields η_i.

Following the steps from section 7.2, we obtain the set of equations for the order parameter X and the fluctuations W, Ω:

$$\dot{X} = (a - 3\,\Omega)\; X - X^3 + H \tag{7.9a}$$

$$\dot{\Omega} = 2\,\Omega\left(a - C - 3\,X^2\right) + 2\,W \tag{7.9b}$$

$$\dot{W} = W\left(a - C - 3\,X^2\right) + \sigma^2\,. \tag{7.9c}$$

The steady state for the order parameter, Eq. (7.7), leads to:

$$0 = \left(a - 3\,\frac{\sigma^2}{\left(3\,X^2 + C - a\right)^2}\right) X - X^3 + H\,. \tag{7.10}$$

We now consider the case of zero average field $H = \langle \eta_i \rangle = 0$. In that case, Eq. (7.10) can have up to five real solutions. The trivial solution $X = 0$, always exists and it is stable (if $C > a$) whenever $\sigma > \sigma_c$, with

$$\sigma_c = \begin{cases} 0 & if a<0, \\ \sqrt{\frac{a}{3}}(C-a) & if a>0. \end{cases} \tag{7.11}$$

It turns out that for $C > 7a > 0$, the set of Eqs. (7.9a-7.9c) contains two additional real stable fixed point solutions $\pm X_0$ for $\sigma \leq \sigma_c$. At $\sigma = \sigma_c$ it is $X_0 = 0$ and hence σ_c identifies a second order, continuous, phase transition (see right panel of Fig. 7.1). If $7a > C > a > 0$ the range of existence and stability of these two additional solutions extends up to $\sigma \leq \sigma_0$, where $\sigma_0 \geq \sigma_c$ is given by:

$$\sigma_0 = \sqrt{\frac{4}{243}(2a + C)^3}, \tag{7.12}$$

Hence, in the range $\sigma \in [\sigma_c, \sigma_0]$ there is bistability between the $X = 0$ and the $\pm X_0$ solutions. Moreover, two additional symmetric unstable solutions $\pm X_1$ appear in this range. Therefore, the point σ_0 signals the appearance of a first order, discontinuous, phase transition (see Fig. 7.1, *left*). In that range, the three stable solutions coexist with the two unstable solutions.

From a microscopic point of view, the phase transition from the $|X| > 0$ to the $X = 0$ states can be explained as follows: for $\sigma = 0$, it is $\eta_i = 0, \forall i$; all variables end up in the same stationary value $x_i = \sqrt{a}$ or $x_i = -\sqrt{a}$ and the average value satisfies $|X| = \sqrt{a} > 0$. As the noise intensity increases, $\sigma > 0$, the average value $|X|$ tends to zero and the chances that individual values η_i are smaller than $-CX$ grow. This changes the minimum's sign in the (individual) potential. As a consequence the distribution of $\{x_i\}$ becomes bimodal and the mean value approaches zero.

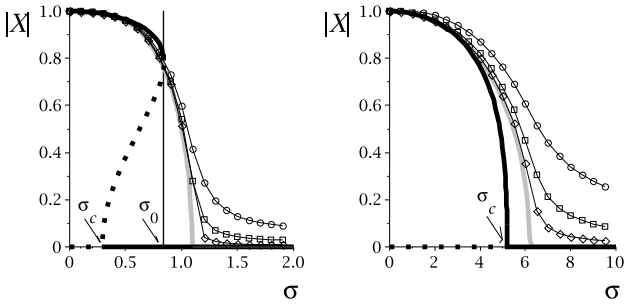

Figure 7.1: Bifurcation diagram of the Ginzburg-Landau model with additive quenched noise. Order parameter expansion (thick black lines) predict a second order transition for $C > a$ (*right*: $C = 10, a = 1$) while bistability (first order phase transition) appears for $C < 7a$ (*left*: $C = 1.5, a = 1$, the unstable solution is plotted as a dotted line). The self-consistency solution (grey line) does not show bistability in any case. Symbols show the results of numerical simulations of the evolution equations averaged over 10^3 realizations of the quenched noise variables η_i and initial conditions. $N = 10^3, 10^4, 10^5$ (circles, squares, diamonds, respectively).

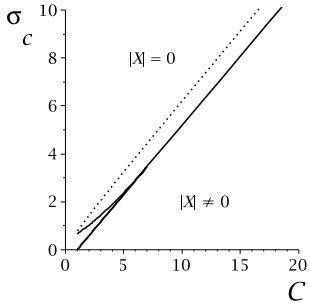

Figure 7.2: Critical intensity of the additive quenched noise for the Ginzburg-Landau model versus coupling strength for $a = 1$. Prediction of order parameter expansion (7.11) as continuous line, exact solution (7.3) as dotted line. The order parameter expansion predicts a bistability region for $C < 7a$.

The existence of a phase transition from order to disorder predicted by the order parameter expansion simple approximation scheme is confirmed by the numerical solution of the self-consistency equation (7.3) (Toral *et al.* 2007). However, the transition appears to be always second-order, so indicating the validity of the prediction of the approximate order parameter expansion in the limit of large coupling. In fact, the critical value σ_c predicted by the order-disorder transition, Eq. (7.11), deviates systematically from the value coming from the numerical integration of the self-consistency equation (7.3) for large coupling constant C, as shown in figure 7.2, although the relative error between the two values decreases as C increases.

We have also compared these predictions versus the results coming from intensive numerical simulations. In the simulations we have integrated the full set of equations (7.8) up to the steady state and, then, we have computed the order parameter $m = \langle\langle |X| \rangle\rangle$ and its fluctuations $\chi = \frac{N}{\sigma^2}\left[\langle\langle X^2\rangle\rangle - \langle\langle |X| \rangle\rangle^2\right]$. Here $X = \frac{1}{N}\sum_{i=1}^{N} x_i$ and $\langle\langle \cdots \rangle\rangle$ denotes an ensemble average with respect to realizations of

the random variables η_i and initial conditions. The simulation results for the order parameter are indicated by symbols in figure 7.1. As usual, the transition from order to disorder is smeared out due to finite-size-effects but the numerical simulations do approach the results of the self-consistency equation as the number N of variables increases. We have analysed our data using standard finite-size-scaling relations (Cardy 1988; Deutsch 1992*a*) and found that the dependence of the order parameter on σ can be well fitted by $m(\sigma, N) = N^{-b/2} f_m(\epsilon N^b)$ with $\epsilon = 1 - \sigma/\sigma_c$, $b \approx 0.33$ and being f_m a scaling function. See evidence in the left panel of figures 7.3 and 7.4 for two different values of the coupling constant. Note that this scaling relation implies that in the thermodynamic limit, the order parameter vanishes as $m(\sigma) \sim (\sigma_c - \sigma)^{1/2}$, the typical mean-field result. Similarly, the fluctuations can be fitted by the form $\chi(\sigma, N) = N^c f_\chi\left(\epsilon N^b\right)$, with $c \approx 0.67$ and f_χ the appropriate scaling function, as demonstrated in the right panels of figures 7.3 and 7.4 again for two different values of the coupling constant. This implies that in the thermodynamic limit, the fluctuations diverge as $\chi(\sigma) \sim |\sigma_c - \sigma|^{-\gamma}$ with $\gamma = c/b \approx 2$.

7.3.2 Globally coupled Ginzburg-Landau model with multiplicative quenched noise

We now consider the case in which the quenched noise couples multiplicatively to the variable x_i:

$$\dot{x}_i = (a + \eta_i)\, x_i - x_i^3 + C\,(X - x_i)\ . \tag{7.13}$$

This model has been studied extensively in the case that the η_i's are independent white noises and it has been found that an increase in the noise intensity leads to a transition from disorder to order (Buceta *et al.* 2001; García-Ojalvo *et al.* 1996; García-Ojalvo & Sancho 1999; van den Broeck *et al.* 1994*a*). We want to compare the predictions of the self-consistency equation with the order parameter expansion

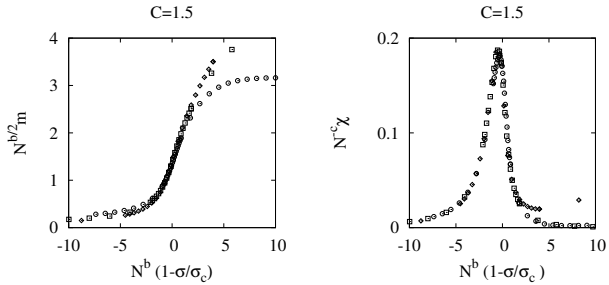

Figure 7.3: Low coupling ($C = 1.5$).

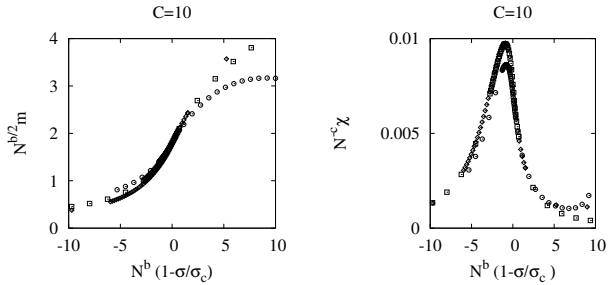

Figure 7.4: Finite-size scaling analysis of the Ginzburg-Landau model with additive quenched noise. Rescaled simulation data for low coupling (*top graphs*, $\sigma_c = 1.094$) and high coupling (*bottom graphs*, $\sigma_c = 6.203$). Ensemble average m (*left*) and fluctuations χ (*right*) as defined in the main text. Exponents: $b = 0.33, c = 0.67$. Ensemble sizes: $N = 10^3, 10^4, 10^5$ (circles, squares, diamonds). In all cases: $a = 1$. Here, σ_c has been determined to a high degree of accuracy by using the numerical solution of Eq. (7.3).

and numerical simulations to check if a similar result holds in the case of quenched noise. Without coupling ($C = 0$) Eq. (7.13) is a prototype of supercritical pitchfork bifurcations (see e.g. the part about bifurcations in section 2.2 on page 13) with two possible sets of solutions: $x_i = 0$ is the stable solution whenever $a + \eta_i \leq 0$, or $x_i = \pm\sqrt{a + \eta_i}$ are stable solutions and $x_i = 0$ is unstable for $a + \eta_i > 0$.

To study the consequences of coupling, $C > 0$, we use the above developed order parameter expansion approximation. After setting $H = \langle \eta_i \rangle = 0$, the equations are:

$$\dot{X} = aX - X^3 - 3X\Omega + W, \tag{7.14a}$$

$$\dot{\Omega} = \left(2a - 6X^2 - 2C\right)\Omega + 2XW, \tag{7.14b}$$

$$\dot{W} = \left(a - 3X^2 - C\right)W + X\sigma^2 . \tag{7.14c}$$

The equilibrium condition (7.7) leads to:

$$0 = a\,X - X^3 - \frac{3X^3\sigma^2}{(C - a + 3\,X^2)^2} + \frac{X\sigma^2}{C - a + 3\,X^2} . \tag{7.15}$$

Similarly to the uncoupled case this equation has two different regimes of solutions: On one hand, if $a \geq 0$ the stable solutions of Eq. (7.14) are $X = \pm\sqrt{a}$ for $\sigma = 0$. As σ increases, $|X|$ monotonically increases as well (see fig. 7.5, *left*). On the other hand, if $a < 0$ then $X = 0$ is a stable solution for small σ. At some value σ_c it becomes unstable and a fork of solutions grows out of zero (see fig. 7.5, *right*). σ_c is determined by Eq. (7.15) and is related to a and C by:

$$\sigma_c^2 = a\,(a - C) . \tag{7.16}$$

σ_c identifies a second-order phase transition from disorder to order (i.e. from $X = 0$ to $X \neq 0$). In this case of $a < 0$, the value σ_c grows monotonously with coupling strength C, a rather counter-intuitive observation, since it means that the coupling hinders the ordering and more structural disorder is needed to induce macroscopic order (fig. 7.6).

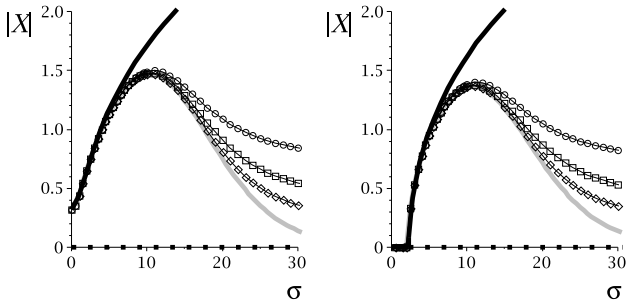

Figure 7.5: Bifurcation diagram of the Ginzburg-Landau model with multiplicative quenched noise. Positive values of a show order without noise (*left:* $a = 0.1$), whereas negative value show order only with a finite value of the noise intensity (*right:* $a = -0.5$). In both panels it is $C = 10$. The order parameter expansion approximation scheme gives a monotonous solution while the exact solution of Eq. (7.3) reaches a maximum and decreases for large σ (grey line). Symbols are the result of direct numerical simulations of Eqs. (7.13) averaged over 10^3 realizations of the quenched noise variables η_i and initial conditions. $N = 10^3, 10^4, 10^5$ (circles, squares, diamonds).

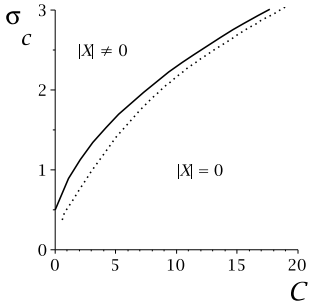

Figure 7.6: Critical noise for bifurcation versus coupling strength for $a = -0.5$ for the Ginzburg-Landau model with multiplicative quenched noise. The prediction by the order parameter expansion is shown as continuous line, the exact solution (7.3) is shown as dotted line.

The numerical solution of the self-consistency equation (7.3) is qualitatively similar to the results of the order parameter expansion approximation, however $|X|$ doesn't increase monotonically with increasing σ. It rather reaches a maximum and decreases after that approaching zero asymptotically. Note that his is not a (reentrant) phase transition since $|X| = 0$ is only reached for $\sigma \to \infty$.

The simulation results for the order parameter are shown as symbols in figure 7.5. At this scale no finite-size-effects can be seen at the phase transition. In a thorough data analysis with finite-size-scaling relations at σ_c, in the way we did in the first example, we found exponents of $b \approx c \approx 0.5$ to fit the order parameter and fluctuations (see fig. 7.7). These scaling relations imply, again in the thermodynamic limit, that the order parameter vanishes and the fluctuations diverge as $m(\sigma) \sim (\sigma_c - \sigma)^{1/2}$ and $\chi(\sigma) \sim |\sigma_c - \sigma|^{-\gamma}$, with $\gamma = c/b \approx 1$ respectively.

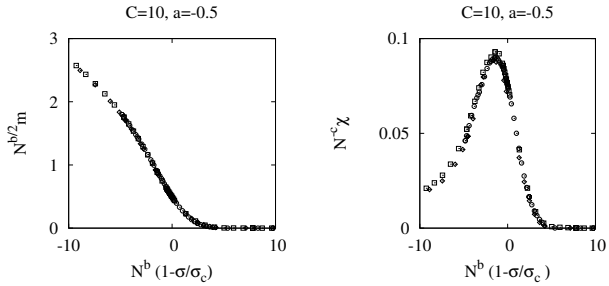

Figure 7.7: Finite-size scaling analysis of the Ginzburg-Landau model with multiplicative noise for $a = -0.5$, $C = 10$. Rescaled ensemble average m (*left*) and fluctuations χ (*right*) of 10^3 numerical simulations with $N = 10^3, 10^4, 10^5$ (circles, squares, diamonds). Critical point, as from Eq. (7.3), is $\sigma_c = 2.169$; exponents: $b = 0.5, c = 0.5$.

7.3.3 Canonical model for noise-induced phase transitions

As the last example we will study a model for which a genuine phase transition induced by multiplicative noise has been shown (van den Broeck *et al.* 1994*b*, 1997) with the feature that the ordered phase is reentrant, it only exists for intermediate noise intensities. The equation for an individual element is:

$$\dot{x}_i = -x_i \left(1 + x_i^2\right)^2 + \left(1 + x_i^2\right) \eta_i + C\,(X - x_i) \tag{7.17}$$

and the reduced system according to section 7.2.2 (again setting $\langle \eta_i \rangle = 0$) reads:

$$\begin{aligned}
\dot{X} &= -X\left(1+X^2\right)^2 + \frac{1}{2}\left[-12\left(1+X^2\right)X - 8X^3\right]\Omega \\
&\quad +2XW \qquad (7.18a)\\
\dot{\Omega} &= 2\Omega\left[-\left(1+X^2\right)^2 - 4X^2\left(1+X^2\right) + C\right] \\
&\quad +2W\left(1+X^2\right) \qquad (7.18b)\\
\dot{W} &= W\left[-\left(1+X^2\right)^2 - 4X^2\left(1+X^2\right) + C\right] \\
&\quad +\sigma^2\left(1+X^2\right). \qquad (7.18c)
\end{aligned}$$

The equilibrium condition (7.7) becomes

$$0 = -X\left(1+X^2\right)^2 + \frac{\left(-\left(6+6X^2\right)X - 4X^3\right)\sigma^2\left(1+X^2\right)^2}{\left(1+6X^2+5X^4+C\right)^2} + \qquad (7.19)$$
$$+2\,\frac{X\sigma^2\left(1+X^2\right)}{1+6X^2+5X^4+C}.$$

Equations (7.18) have the stable solution $X = 0$ for $\sigma < \sigma_c$ or a pair of symmetric solutions $X \neq 0$ for $\sigma > \sigma_c$, when $X = 0$ becomes unstable (see left panel of fig. 7.8). The value of σ_c indicates the location of a second-order phase transition. It follows from analysing the Jacobian of (7.18a-7.18c) and calculates to:

$$\sigma_c = \frac{1+C}{\sqrt{2C-4}}. \qquad (7.20)$$

Accordingly, a minimal coupling $C > 2$ is necessary to induce the phase transition. An analysis of this relation shows that σ_c has a minimum with respect to C. Therefore, see figure 7.9, the transition is predicted to be reentrant with respect to C: the ordered phase only exists in a range of values for C, with the surprising prediction

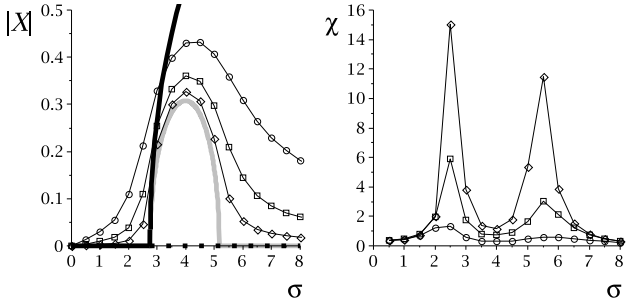

Figure 7.8: Bifurcation diagram of model (7.17) (*left*). Order parameter expansion (thick black line) and exact solution (grey line) together with the ensemble average of 10^3 numerical simulations for $N = 10^3, 10^4, 10^5$ (circles, squares, diamonds). Coupling is $C = 10$. On the *right* the unscaled fluctuations are shown.

that too a large coupling destroys the ordered state. The predictions of the order parameter expansion are in qualitative agreement with those obtained after solving the self-consistency equation. However, whereas the order parameter expansion predicts incorrectly that the order parameter monotonously increases with σ, as shown in figure 7.8, the self-consistency equation instead predicts that the transition is reentrant also with respect to the quenched noise intensity σ, see figure 7.9. Both reentrant behaviours were observed in the case of time-dependent noise (van den Broeck *et al.* 1994*b*, 1997).

Again we have compared the predictions with the numerical integration of the set of equations (7.17). The simulation results are shown as symbols in figure 7.8. Due to finite-size-effects the theoretical results are approached with increasing number N of particles, reentrance and the dependence of σ_c from C are observed. Analysing the data as we have done with the other examples, we

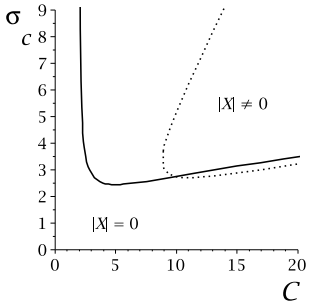

Figure 7.9: Critical noise intensity versus coupling strength for model (7.17). The prediction (7.20) of the order parameter expansion (continuous line) and the exact solution (7.3) as dotted line. Only the latter shows reentrance with respect to σ.

find exponents for the scaling relations of $b \approx 0.33$ and $c \approx 0.67$. As in the first case this implies the relations $m(\sigma) \sim (\sigma_c - \sigma)^{1/2}$ and $\chi(\sigma) \sim |\sigma_c - \sigma|^{-\gamma}, \gamma = c/b \approx 2$ in the thermodynamic limit. Figure 7.10 summarizes the fitted simulation data.

7.4 Conclusions

In this chapter we have constructed an approximate analytical scheme based on the order parameter expansion developed by de Monte & d'Ovidio (2002), de Monte *et al.* (2004, 2005, 2003) and Silva *et al.* (2006), to study the macroscopic behaviour of extended systems which are globally coupled. We have used the method to study in detail the phase diagram of three widely used models of phase transitions in scalar systems: the Ginzburg-Landau scalar model with both additive and multiplicative quenched noise and

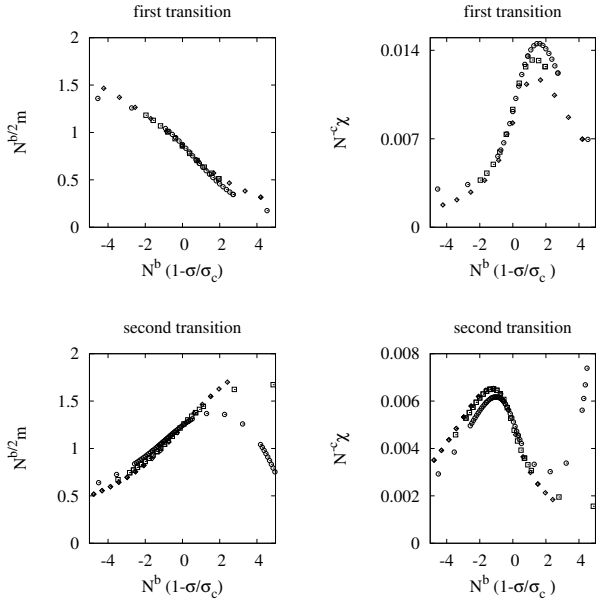

Figure 7.10: Rescaled simulation data for the first (*top*) and the second (*bottom*) phase transition ($C = 10$). Mean value (*left*) and fluctuations (*right*) for ensembles of $N = 10^3, 10^4, 10^5$ (circles, squares, diamonds). Critical points, as from Eq. (7.3), are $\sigma_c = 2.749$ for the first and $\sigma_c = 5.169$ for the second transition. Exponents are: $b = 0.33, c = 0.67$.

a genuine model for noise-induced phase transitions where time-dependent noise has been replaced by quenched, time-independent noise coupled multiplicatively to the dynamical variable (van den Broeck *et al.* 1994*b*).

We have compared the results of our simple approach with those coming from a numerically involved, but in principle exact, treatment based on the self-consistency relation and with extensive numerical simulations of the corresponding dynamical equations for each model. In the case of additive noise, the main result is that macroscopic order is destroyed when increasing the intensity of the quenched noise. In the other two cases, when noise appears multiplicatively, we find that macroscopic order appears for an intermediate value of the intensity of the quenched noise. Since the quenched noise can represent, for instance, diversity or heterogeneity, it appears paradoxically that some amount of structural disorder is needed in order to observe macroscopic order.

Furthermore it has been shown numerically, that all investigated models follow a finite-size scaling law and the exponents have been determined. It suggests a common universality class for the Ginzburg-Landau model with additive quenched noise and the canonical model for noise induced phase transitions, whereas the Ginzburg-Landau model with multiplicative quenched noise yields different exponents. A more detailed analysis of the finite-size relations and their possible dependence with the system parameters will be presented in a chapter further down.

The method of order parameter expansion, which we lead consistently up to terms of second order, is a tool which reduces large systems to only a couple of reduced variables. The advantage is its very easy management. In this chapter we have proven that reliable conclusions can be drawn with that method in some cases. Since it is an expansion around mean values, designed to be applied near the homogeneous state, the method yields good results for low values of the intensity of the quenched noise or for high synchronization

of the subunits. Otherwise, the method might not be reliable. As a consequence the reentrant phase transitions were not predicted in the studied cases for multiplicative noise. It is an open issue how to modify the method in order to predict the reentrant transitions.

Chapter 8

Ginzburg-Landau model: Critical behaviour due to additive quenched noise

8.1

Introduction

In statistical mechanics, models describing the effect of impurities or heterogeneities in the behaviour of magnetic systems are gathered under the label of spin glasses (Young 1998) when the source of heterogeneity affects the local spin interaction (and therefore the interaction term in the Hamiltonian takes into account such disorder). Conversely, the so-called random field models (Young 1998) address those systems where the source of heterogeneity only yields an additive heterogeneous term (perturbation) in the Hamiltonian: in this case the effect of disorder is akin to subject the system to a random external perturbation. In both cases, such sources of heterogeneity typically have slower dynamical evolution than the

spins (or the dynamical variables), and therefore these sources of randomness are said to be quenched. In the last decades a wealth of literature has addressed the phenomenology behind spin glasses and random field models, including phase diagrams, aging and other dynamical behaviour, and comparison with their equilibrium counterparts (see (Calabrese & Gambassi 2005; Crisanti & Ritort 2003; Young 1998) and references therein).

In other branches of science the role of disorder in models characterizing the dynamical behaviour of multicomponent systems has also been addressed in the last years. Noticeable examples include the effect that a certain amount of heterogeneity in the natural frequencies of Kuramoto oscillators can yield on synchronization (Kuramoto 1975, 1984), the paradoxical constructive role that disorder can induce in the formation of ordered structures in a plethora of different contexts (Buceta *et al.* 2001; Chen & Zhang 2008; Gosak 2009; Perc *et al.* 2008; Postnova *et al.* 2009; Tessone & Toral 2009; Tessone *et al.* 2006, 2007; Toral *et al.* 2009, 2007; Ullner *et al.* 2009; Zanette 2009*b*), and the effect that the topology of the underlying network of interactions plays in several types of dynamics (Acebrón *et al.* 2007; Boccaletti *et al.* 2006; Chen *et al.* 2009; Wu *et al.* 2009), to cite some. All these works address similar generic questions, namely study the effect of structural disorder in the dynamics of multicomponent systems.

here, in this chapter we will address a paradigmatic example within equilibrium statistical mechanics, the Ginzburg-Landau, also called ϕ^4, model (Amit & Mayor 2005), in a version subjected to such quenched disorder much in the vein of random field models. Although the expected role of heterogeneity is that of destroying the ordered state, recent works (Tessone *et al.* 2006; Toral *et al.* 2007) have addressed the positive role of the quenched noise in enhancing the response of this model under the presence of an external periodic driving. In (Buceta *et al.* 2001) the authors studied the effects of introducing a quenched multiplicative dichotomous noise, and found that the phase diagram is modified and gives rise to the onset of

reentrant phase transitions not present in the quenched noise free model.

Here we address the mean-field version of the model subjected to quenched additive noise in absence of temperature (Komin & Toral 2010; Toral *et al.* 2007). First, we present an analytical study of the phase diagram by means of a self-consistent theory, both in the non-metastable and metastable regions. The theory predicts an order-disorder transition as a function of the quenched noise intensity σ, with mean field critical exponents equal to those of the thermal equilibrium counterpart. We also perform a detailed numerical study of the system for different sizes N in terms of finite-size-scaling theory and determine the scaling exponents. We show that in the non-metastable region the order parameter fluctuations diverge with an exponent different from the one of the magnetic susceptibility. This indicates a violation of the fluctuation-dissipation relation. In order to justify this finding, we obtain in closed form an expression for the probability density function of the system in terms of an effective Hamiltonian $\mathcal{H}_{\text{eff}}(\mathbf{x})$, and accordingly argue that the fluctuations of the order parameter cannot be straightforwardly related to the linear response of the system. In the region where metastability does take place, results from numerical simulations deviate from the phase diagram found through the self-consistent theory and show a strong dependence on the specific initial conditions. Concretely, we show that for symmetrical initial conditions, the simulations point out the presence of a reentrant phase transition (disorder-order-disorder) with an ordered state whose width varies and eventually disappears in the Ising limit, corresponding to a large valued of a parameter in the Hamiltonian. This counterintuitive phenomenology supports the fact that disorder or heterogeneity can not only induce dynamical disorder but, on the contrary, can have an ordering role. Conversely, for positive-definite initial conditions the phase transition is smoothed in the same limit, and no critical behaviour is found in that case.

The rest of this chapter is organized as follows: in section 8.2 we present the model. In section 8.3 we outline some considerations regarding the presence of metastable states. In section 8.4 we derive the mean-field critical exponents associated to the magnetization and magnetic susceptibility. In section 8.5 we numerically study the order-disorder transition in the range of parameters where the system lacks metastable states. We provide compelling evidence suggesting that the fluctuation-dissipation relation is not satisfied, and we argue that a possible reason is that the influence of the average external field h on the effective Hamiltonian yielding the probability density function of the system cannot be readily stated as $\mathcal{H}_{\text{eff}}(\mathbf{x}) = \mathcal{H}_0(\mathbf{x}) + Nmh$, being m the magnetization, as it happens in equilibrium theory. In section 8.6 we numerically explore the system's behaviour in the presence of metastable states and discuss the role of the initial conditions in the asymptotic stationary state of the system. We also point out the presence of an disorder-order transition induced by diversity in the metastable situation. In section 8.7 we summarize our main results.

8.2 Additive Ginzburg-Landau model: preliminary considerations

We consider a set of N real dynamical variables $x_i(t), i = 1, \ldots, N$ whose evolution is given by a relaxational gradient flow (San Miguel & Toral 2000) in a potential V:

$$\frac{dx_i}{dt} = -\frac{\partial V(\mathbf{x};\eta)}{\partial x_i},$$
$$V = \sum_{i=1}^{N}\left[-\frac{a}{2}x_i^2 + \frac{1}{4}x_i^4 + \frac{1}{4N}\sum_{j=1}^{N}(x_j - x_i)^2 - \eta_i x_i\right], \qquad (8.1)$$

or,

$$\frac{dx_i}{dt} = ax_i - x_i^3 + \frac{1}{N}\sum_{j=1}^{N}(x_j - x_i) + \eta_i\,. \tag{8.2}$$

The Lyapunov potential $V(\mathbf{x};\eta)$ depends, besides on the dynamical variables $\mathbf{x} \equiv (x_1, ..., x_N)$, on a set of variables $\eta \equiv (\eta_1, ..., \eta_N)$. Most commonly these variables represent white noise of amplitude proportional to the temperature and the model defines a class of thermal phase transitions. In this work, however, we take these variables to represent quenched noise and the problem then belongs to a class of zero temperature random field models. Accordingly, $(\eta_1, \ldots, \eta_N)$ are independently drawn from a probability distribution $g(\eta)$ (which typically will be a Gaussian) of mean h and standard deviation σ. The model can be thought as describing a set of globally coupled heterogeneous units, being σ a measure of the amount of diversity or heterogeneity in the system. As we are interested in this work in the effect of the diversity, σ will be taken as a control parameter and we will study the effect that σ has on the collective properties of the system.

This model is indeed a discretization of a mean–field version of the well known Ginzburg-Landau Hamiltonian for a scalar field $x(\vec{r})$ under the presence of a random external field $\eta(\vec{r})$ (Amit & Mayor 2005; Young 1998):

$$\mathcal{H} = \int d\vec{r}\left(-\frac{a}{2}x^2 + \frac{C}{2}|\vec{\nabla}x|^2 + \frac{u}{4}x^4 - \eta x\right), \tag{8.3}$$

where, without loss of generality, we have rescaled variables and time such that $u = 1$, $C = 1/2$. This Hamiltonian provides a coarse-grained description of critical phenomena, and its formulation is based on some phenomenological considerations such as locality and symmetries (rotational and translational); that is to say, this latter expression is not calculated from the microscopic physics, but rather can be understood as a coarse-grained description of the magnetization field x. By using the Boltzmann weight factor $e^{-\mathcal{H}/T}$,

where T is the temperature, this model has been used for instance to describe the paramagnetic-ferromagnetic transition (where the Hamiltonian describes the coarse-grained magnetization field). In the case of a uniform external field, Landau theory elegantly describes a second-order thermal phase transition for this system, with mean-field critical exponents $\beta = 1/2$, $\gamma = 1$ (Amit & Mayor 2005; Young 1998). This Hamiltonian also offers a soft-spin description of the Ising model (Young 1998): as a matter of fact, in the limit $a \to \infty$ one recovers the Ising model (or the Random Field Ising Model (RFIM) in the case of having a random external field). In the last decades the RFIM has been extensively studied (see (Sethna *et al.* 2006; Young 1998) and references therein), where some specific results include the onset of criticality in terms of a second-order phase transition in zero-temperature induced by the disorder of the random field, with mean-field critical exponents (Dahmen & Sethna 1996; Sethna *et al.* 1993) as in the thermal counterpart (Schneider & Pytte 1977). Several other features such as hysteresis, avalanche dynamics, or return point memory effects, to cite a few, have been studied within the RFIM, both in analytical (renormalization-group) and numerical (finite-size scaling) terms (Pérez-Reche & Vives 2004; Sethna *et al.* 2006). The properties of the model have also been studied in the context of domain growth dynamics both in the Ising limitGrant & Gunton (1984, 1987); Grinstein & Fernandez (1984) or using the full Ginzburg-Landau Hamiltonian (Oguz *et al.* 1990) .

8.3 On the presence of metastability

From the dynamical point of view, it has already been said that the evolution is relaxational in the Lyapunov potential V. Hence, the absolute minimum (or ground state) of V located at $\mathbf{x}^* \equiv (x_1^*, \ldots, x_N^*)$ must be considered as the global attractor of the dynamics. It is

obvious that the value of $\mathbf{x}^*$ will depend on the specific realization of the quenched noise variables $(\eta_1, \ldots, \eta_N)$. On the other hand, the solutions of the differential equations (8.2) tend to values $x_i^{st} = \lim_{t\to\infty} x_i(t)$ which might or might not coincide with x_i^*. If the potential V has a single minimum, then the dynamics always leads to $\mathbf{x}^*$, but if there are additional, metastable, minima, then the asymptotic solution $\mathbf{x^{st}}$ depends on the initial condition $\mathbf{x}(t = 0)$ as it might get stuck in one of them. The presence and relevance of these metastable minima depends in general (and besides the particular realization of the quenched-noise variables) on the value of the parameter a and the number of variables N.

In order to find the absolute minimum $\mathbf{x}^*$ one needs to solve the system of N coupled algebraic equations:

$$0 = a{x^*}_i - {x^*}_i^3 + \frac{1}{N}\sum_{j=1}^{N}({x^*}_j - {x^*}_i) + \eta_i. \tag{8.4}$$

The solution is greatly simplified if one introduces the *magnetization* m as

$$m = \frac{1}{N}\sum_{i=1}^{N} {x^*}_i, \tag{8.5}$$

and then writes Eq. (8.4) as:

$$m + \eta_i = (1 - a){x^*}_i + {x^*}_i^3. \tag{8.6}$$

This equation allows one to find x_i^* as a function of m and η_i (in fact as a function of $m + \eta_i$). The explicit solution, $x_i^* = x^*(m + \eta_i)$ can be replaced in the definition of the magnetization to obtain a *self-consistency* equation:

$$m = \frac{1}{N}\sum_{i=1}^{N} x^*(m + \eta_i). \tag{8.7}$$

The problem has been reduced from the simultaneous solution of the N coupled equations (8.4), to the solution of a single one (8.7)

although, in general, all possible solutions $m^{(1)}, m^{(2)}, \ldots$ of this equation have to be obtained numerically. For a given solution $m^{(n)}$ one can then find the respective values of $x^{*(n)}_i$ using the function $x^{*(n)}_i = x^*(m^{(n)} + \eta_i)$. In order to analyze the structure of the possible solutions of Eq. (8.7), it is convenient to split the discussion in the cases $a \leq 1$ and $a > 1$.

8.3.1 Case $a \leq 1$

This is the simplest case. A graphical analysis shows that Eq. (8.6) has a unique real solution $x^*{}_i = x^*(m + \eta_i)$ (see Appendix). Even in this case, it is possible that Eq. (8.7) has more that one solution for m. This is typically the case for small values of N. See an example in Fig. 8.1.

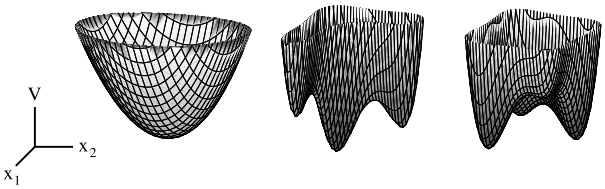

Figure 8.1: Lyapunov potential $V(x_1, x_2)$ as defined in Eq. (8.1) for $N = 2$, $\eta_1 = -0.48, \eta_2 = 0.5$ in the cases $a = -1$ (left), $a = 0.8$ (center) and $a = 2.8$ (right). While the case $a = -1$ displays a single minimum, in the case $a = 0.8$ there are 3 minima (2 metastable) and 2 maxima, whereas for $a = 2.8$ there are 4 minima (3 metastable) and 5 maxima.

However, as N increases the number of metastable solutions decreases greatly. In fact, it is possible to prove that in the thermodynamic limit, $N \to \infty$, Eq. (8.7) can have only either one or three solutions depending on the values of a, h, σ. The proof replaces the sum over N by an integral over the probability distribution of the

quenched-noise variables:

$$m = \int d\eta\, g(\eta) x^*(m+\eta). \tag{8.8}$$

Let us assume that the probability distribution $g(\eta)$ has a generic form $g(\eta) = \frac{1}{\sigma} G\left(\frac{\eta - h}{\sigma}\right)$. Henceforth, all numerical results will use the Gaussian distribution $G(z) = \frac{1}{\sqrt{2\pi}} e^{-z^2/2}$. A change of variables leads to:

$$m = \int d\xi\, G(\xi) x^*(m + h + \sigma\xi) \equiv F_\sigma(m+h). \tag{8.9}$$

As $F_\sigma(z)$ is a monotonously increasing function satisfying $F_\sigma(0) = 0$ and with a sigmoidal shape [*], there will be only one solution for m for all values of h if the derivative satisfies $F'_\sigma(0) \leq 1$. On the other hand, for $F'_\sigma(0) > 1$ there will be either one or three solutions depending on the value of h. This analysis mimics that of the Weiss mean-field theory (Stanley 1971) and allows one to compute the magnetization $m(h; a, \sigma)$ as a function of the mean value of the disorder h and the parameters a, σ. It displays usual critical phenomena and hysteresis. The critical point is defined by the condition $F'_\sigma(0) = 1$ and can be achieved by varying a or σ. It is possible to show that $F'_{\sigma=0}(0) = 1/(1-a)$ and, since $F'_\sigma(0)$ is a decreasing function of σ, the condition $F'_\sigma(0) = 1$ can never be achieved for $a < 0$. This was a priori obvious since in that case the Lyapunov potential in the absence of quenched noise has the global minimum at $x_i = 0, \forall i$, already a disordered state. Some numerical values (for the Gaussian distribution) for the location of the critical diversity σ_c as a function of a are: $(a = 0.1, \sigma_c = 0.19616)$, $(a = 0.5, \sigma_c = 0.50041)$, $(a = 2/3, \sigma_c = 0.595233)$. In the case $a = 1$, the Cardano formula simplifies to $x^* = (m+h)^{1/3}$ and it is possible to perform analytically the integrals (again for a Gaussian distribution for the quenched-noise variables) with the result (Toral *et al.* 2007) $(a = 1, \sigma_c = \left[\frac{\Gamma(1/6)}{2^{1/3} 3\pi^{1/2}}\right]^{3/2} = 0.7573428\ldots)$.

[*] This assertion is certainly true for a Gaussian distribution $g(\eta)$ as well as for other probability distributions, although we have not been able to give a general proof of its validity.

8.3.2 Case $a > 1$

The problem in this case is that the cubic equation (8.6) can have either one or three real solutions depending on whether the discriminant $\Delta_i = 27(m + \eta_i)^2 + 4(1 - a)^3$ is, respectively, positive or negative. Besides, as before, several values of m can satisfy the self-consistency Eq. (8.7). When there are three solutions for x_i^*, ($\Delta_i < 0$, this requires $a > 1$) it is not clear a priori which one to chose in order to substitute in the self-consistency relation (8.7). A possibility is to compute the Lyapunov potential V for each of the possible solutions. However, since the maximum number of solutions can be as large as 3^N, this is not possible to carry out in practice for large N. The answer arises when one realizes that the dynamical equation for $x_i(t)$ can be written also as relaxational in a local potential $v_i(x_i, m)$:

$$\frac{dx_i}{dt} = -\frac{\partial v_i(x_i, m)}{\partial x_i},$$
$$v_i = \frac{1-a}{2}x_i^2 + \frac{1}{4}x_i^4 - (m + \eta_i)x_i + \frac{m^2}{2}. \tag{8.10}$$

The solutions $x^*(m + \eta_i)$ are nothing but the extrema of this local potential. Now we notice that the Lyapunov potential can be written as sum of the local potentials:

$$V(x_1, \ldots, x_N) = \sum_{i=1}^{N} v_i(x_i, m). \tag{8.11}$$

Therefore, the absolute minimum of V is achieved by choosing in each case the solution $x^*(m + \eta_i)$ that minimizes the local potential $v_i(x_i, m)$. Explicit expressions for the function x^* are obtained using Cardano's formula and are given in Appendix B.1.

The process to find the absolute minimum $\mathbf{x}^*$ of the Lyapunov potential proceeds, as before, by finding first m after solving numerically the self-consistency equation (8.7), but using the correct function

$x^*(m+\eta)$. Similarly, the integral equation (8.8) can be used to find the magnetization $m(h;a,\sigma)$ in the thermodynamic limit. The phenomenology of the solutions is similar to what was found in the case $a \leq 1$ and will not be repeated here.

An important difference, however, with the case $a \leq 1$ is that now the Lyapunov potential displays a large number of metastable minima for all values of N and, consequently, also in the thermodynamic limit (a recent study for the metastable states of the zero-temperature RFIM has been carried on in (Rosinberg *et al.* 2008, 2009)). Therefore, starting from arbitrary initial conditions, the asymptotic solution of the evolution equations x_i^{st} will in general differ from the values x_i^* of the absolute minimum. It will be shown that new phase transitions occur when one looks at the magnetization values that derive from the stationary solution.

8.4 Critical behaviour

We have seen that this mean-field model displays a second order phase transition between an ordered state ($|m| > 0$) and a disordered state ($m = 0$) at a critical value of the diversity σ_c. In order to derive the critical exponents of such transition, we consider the self-consistency Eq. (8.9) and expand $F_\sigma(m+h)$ in a Taylor series. Since $x^*(-m-h) = -x^*(m+h)$ (see Appendix) and assuming that the distribution of noises is symmetric with respect to the mean value, $G(-\xi) = G(\xi)$, the function F_σ is antisymmetric $F_\sigma(-m-h) = -F_\sigma(m+h)$ and we get:

$$m = a_1(\sigma)(m+h) + a_3(\sigma)(m+h)^3 + \dots \tag{8.12}$$

with $a_k(\sigma) = F_\sigma^{(k)}(0)/k!$. Hence, the magnetization at $h = 0$ is:

$$|m| = \begin{cases} 0 & \text{for } \sigma > \sigma_c, \\ \sqrt{\frac{1-a_1(\sigma)}{a_3(\sigma)}} & \text{for } \sigma < \sigma_c. \end{cases} \tag{8.13}$$

As $F'_\sigma(0) - 1$ changes sign at $\sigma = \sigma_c$, we can expand $a_1(\sigma) = 1 + \alpha_1(\sigma_c - \sigma) + \dots$. Accordingly, close to the transition the spontaneous magnetization behaves as $|m| \sim (\sigma_c - \sigma)^\beta$, with a critical exponent $\beta = 1/2$, as in Landau's treatment of the thermal phase transition.

To compute the critical behaviour of the susceptibility $\chi_h \equiv \left.\frac{\partial m}{\partial h}\right|_{h=0}$, we take the derivative of both sides of Eq. (8.12) and set $h = 0$. This leads to $\chi_h = \frac{a_1(\sigma) + 3a_3(\sigma)m^2}{1 - a_1(\sigma) - 3a_3(\sigma)m^2}$. Replacing Eq. (8.13) and $a_1(\sigma) = 1 + \alpha_1(\sigma_c - \sigma) + \dots$ we find the critical behaviour:

$$\chi_h = A_\pm \, |\sigma - \sigma_c|^{-1} \tag{8.14}$$

with critical amplitudes $A_- = 1/(2\alpha_1)$ for $\sigma < \sigma_c$ and $A_+ = 1/\alpha_1$ for $\sigma > \sigma_c$. Therefore the susceptibility critical exponent is $\gamma = 1$, the same, not surprisingly, than in Landau's theory.

8.5 Numerical results for $a \leq 1$: violation of the fluctuation-dissipation relation

In this section we present the results coming from the numerical integrations * of the dynamical equations (8.2) in the case $a \leq 1$. The

*The simulations were performed using a fourth-order Runge-Kutta method with a time-step $\delta t = 0.05$ and integrating up to the stationary state checking that the magnetization remains constant up to a precision $\epsilon = 10^{-6}$. The initial condition $\mathbf{x}(t = 0)$ was a uniform random distribution in the interval $[-2.5, 2.5]$.

objective is twofold. First, by comparing with the analytical results valid in the thermodynamic limit, we want to check the importance of the metastable states that appear for finite N. Second, we will use the theory of finite-size scaling in order to determine the exponents of the transition. We will show that there is a violation of the fluctuation-dissipation relation in the sense that the magnetic susceptibility can not be computed as the ensemble fluctuations of the magnetization. By ensemble average $\langle\langle \cdots \rangle\rangle$ we mean an average with respect to realizations of the random quenched-noise variables as well as with respect to the initial conditions $\mathbf{x}(t = 0)$. However, for the range of values of system size N employed in the simulations, $N \geq 10^3$, there was hardly any dependence on the initial condition for a given realization of the random variables. This shows that metastable states either do not exist or it is rare to get trapped in them for this range of values of a and N. In the left panel of Fig. 8.2 we plot the order parameter m_0 as a function of the diversity σ for the value $a = 2/3$. As usual (Landau & Binder 2000), the order parameter is defined as the ensemble average of the absolute value of the magnetization $m_0 = \langle\langle |m| \rangle\rangle$ computed from the stationary values as $m = \frac{1}{N} \sum_{i=1}^{N} x_i^{st}$. As predicted by the self-consistent treatment explained in previous sections, there is a phase transition from an ordered (ferromagnetic-like, $m_0 > 0$) to a disordered (paramagnetic-like, $m_0 = 0$) phase as a function of σ. The transition is smeared out by finite-size effects, but it approaches the solution of the thermodynamic limit and the transition point σ_c as the system size N increases. In the right panel of this figure we plot the normalized fluctuations of the order parameter, defined as $\chi \equiv \frac{N}{\sigma^2} \left[\langle\langle m^2 \rangle\rangle - \langle\langle |m| \rangle\rangle^2 \right]$ as a function of the diversity σ. These fluctuations have a maximum in the neighborhood of σ_c and, as shown in the right panel of Fig. 8.3, they increase with increasing N as $\chi(\sigma_c) \sim N^b$ with $b \approx 2/3$ for different values of the parameter a, and hence diverge in the thermodynamic limit. As shown in the left panel of the same figure, the order parameter at the critical point decreases as $m_0(\sigma_c) \sim N^{-c}$ with $c \approx 1/6$ and tends to zero in the thermodynamic limit.

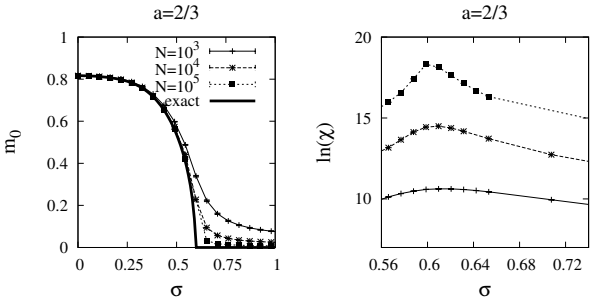

Figure 8.2: *Left panel:* Order parameter m_0 as a function of the diversity σ for $a = 2/3$. The symbols correspond to the numerical integration of the dynamical equations (8.2) for different system sizes N and a Gaussian distribution (zero mean, standard deviation σ) of the quenched noises. The solid line is the magnetization m obtained by solving the self-consistency Eq. (8.9) for $h = 0$. *Right panel:* Order parameter fluctuations, χ, as a function of the diversity σ, for the same system sizes as the left panel (the vertical axis is in logscale for presentation purposes).

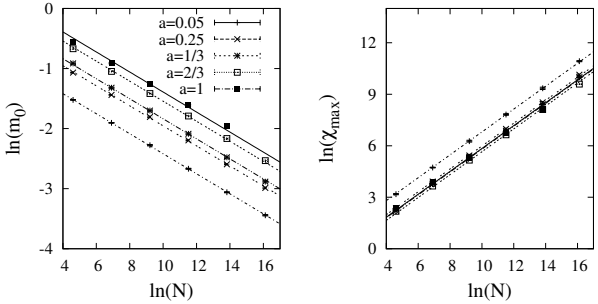

Figure 8.3: Log-log plots of the order parameter m_0 (left panel) and the fluctuations χ (right panel) as a function of system size N for different values of a, at the corresponding critical point $\sigma_c(a)$. In all cases we find a good fit to a power-law behaviour: $m_0 \sim N^{-c}$ and $\chi \sim N^b$ with $c = 0.16 \pm 0.01$ and $b = 0.66 \pm 0.02$.

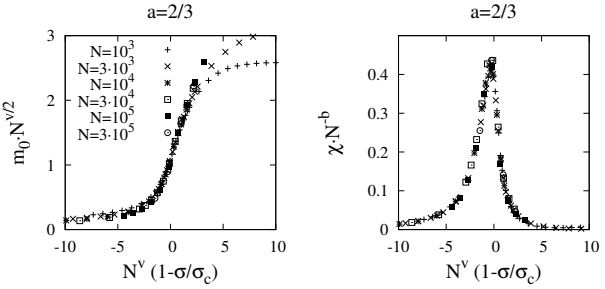

Figure 8.4: Data collapse of the order parameter m_0 (left panel) and the fluctuations χ (right panel) according to the finite-size scaling relations $m_0(\sigma, N) = N^{-v/2} f_m(N^v(1 - \sigma/\sigma_c))$ and $\chi(\sigma, N) = N^b f_\chi(N^v(1 - \sigma/\sigma_c))$ using $v = 1/3$, $b = 2/3$. The goodness of the collapse is an evidence supporting the validity of the scaling relations.

Data for a range of values around the critical region can be collapsed through standard finite-size analysis (Cardy 1988; Deutsch 1992*b*) according to the scaling laws: $m_0(\sigma, N) = N^{-c} f_m(N^v(1 - \sigma/\sigma_c))$ and $\chi(\sigma, N) = N^b f_\chi(N^v(1 - \sigma/\sigma_c))$ with appropriate scaling functions f_m and f_χ. A good fit, see Fig. 8.4, is obtained with $v = 2c \approx 1/3$. Note that this scaling form implies that in the infinite-size limit $m_0(\sigma) \sim |\sigma - \sigma_c|^\beta$ and $\chi(\sigma) \sim |\sigma - \sigma_c|^{-\gamma}$, with critical exponents $\beta = c/v = 1/2$ and $\gamma = b/v = 2$. We have also performed a finite-size scaling of the fluctuations of the stationary value of the energy (global potential) at the critical disorder $\sigma_c(a = 2/3) = 0.595233$, according to which one finds a value for the critical exponent of those fluctuations $\alpha \approx 0$, the same than the (thermal) mean-field result for the specific heat (data not shown).

While the result of the previous section proved that the susceptibility χ_h has a critical exponent $\gamma = 1$, the numerical simulations suggest that the fluctuations χ diverge close to the critical point as a power law with a different exponent $\gamma = 2$. This seems to constitute a violation of the fluctuation-dissipation relation. Since we have restricted this analysis to the range $a \leq 1$, this violation does not seem to be related to typical situations of metastability, absence of time translation symmetry or aging (Calabrese & Gambassi 2005; Crisanti & Ritort 2003; Young 1998). Furthermore, the hyperscaling relation $2\beta + \gamma = d_c v$, that holds in the mean-field regime or for $d \geq d_c$, is satisfied using $\gamma = 2$ as it is known (Imry & Ma 1975) that the upper critical dimension is $d_c = 6$ and $v = 1/2$.

To explain this discrepancy, we note that the fluctuation-dissipation relation is obtained typically for a system in the canonical ensemble at temperature T and whose probability density function (pdf) is $f_{\mathbf{x}} = \mathcal{Z}^{-1} \exp(-\mathcal{H}/T)$, with a partition function $\mathcal{Z} = \int d\mathbf{x} \exp(-\mathcal{H}(\mathbf{x})/T)$, being $\mathcal{H}$ the Hamiltonian of the system. If the Hamiltonian contains a magnetic interaction $\mathcal{H}(\mathbf{x}) = \mathcal{H}_0(\mathbf{x}) + Nmh$, one can prove the fluctuation-dissipation relation between the magnetic susceptibility χ_h and the fluctuations of the magnetization $\langle m \rangle$:

$$\chi_h \equiv \left.\frac{\partial \langle m \rangle}{\partial h}\right|_{h=0} = \frac{N}{T}\left[\langle m^2 \rangle - \langle m \rangle^2\right], \tag{8.15}$$

where $\langle \cdots \rangle$ denotes an average with respect to the probability distribution $f_{\mathbf{x}}(\mathbf{x})$.

In our case, there are two averages: with respect to initial conditions and with respect to realizations of the random variables η. We have already argued that for $a \leq 1$ and large values of N, the results are largely independent of initial conditions, so all that contributes to the ensemble average $\langle\!\langle \cdots \rangle\!\rangle$ are the noise variables. As there is a one to one correspondence between the stationary values $\bar{\mathbf{x}}$ and η we can write the pdf of $\bar{\mathbf{x}}$ in terms of the pdf of η:

$$f_{\mathbf{x}}(x^*{}_1, \cdots, x^*{}_N) = f_\eta(\eta_1, \cdots, \eta_N)\,|J|\,. \tag{8.16}$$

If we take the η_i's to be independently distributed Gaussian variables, we have

$$f_\eta(\eta_1, \cdots, \eta_N) = \prod_{i=1}^{N}\left[\frac{1}{\sigma\sqrt{2\pi}}\exp(-(\eta_i - h)^2/2\sigma^2)\right]. \tag{8.17}$$

As Eq. (8.6) implies

$$\eta_i = (1-a)x^*{}_i + x^{*3}_i - \frac{1}{N}\sum_{j=1}^{N} x^*{}_j, \tag{8.18}$$

it is possible to compute the determinant of the Jacobian matrix $J_{ij} = \frac{\partial \eta_i}{\partial \bar{x}_j}$:

$$|J| = \left(1 - \frac{1}{N}\sum_{j=1}^{N}\frac{1}{3x^{*2}_j + 1 - a}\right)\prod_{i=1}^{N}\left[3x^{*2}_i + 1 - a\right]. \tag{8.19}$$

Replacing Eqs. (8.17-8.19) in Eq. (8.16), one can write the pdf of $\bar{\mathbf{x}}$ as the exponential of an effective Hamiltonian $f_{\bar{\mathbf{x}}}(\bar{\mathbf{x}}) = \mathcal{Z}^{-1}\exp(-\mathcal{H}_{\text{eff}})$,

with:

$$\mathcal{H}_{\text{eff}}(\bar{\mathbf{x}}) = -\ln\left(1-\frac{1}{N}\sum_{j=1}^{N}\frac{1}{3x^{*2}_i+1-a}\right)+ \\ +\sum_{i=1}^{N}\left[\frac{[(1-a)x^*{}_i+x^{*3}_i-m-h]^2}{2\sigma^2}-\ln\left(3x^{*2}_i+1-a\right)\right] \tag{8.20}$$

However, as it can not be split in the form $\mathcal{H}_{\text{eff}} = \mathcal{H}_0 + Nhm$, it is not possible (at least in a trivial manner) to relate the susceptibility to the fluctuations of the order parameter.

8.6 Numerical results for $a > 1$: dependence on the initial conditions

In the case $a > 1$ the presence of metastable states is relevant as the dynamics usually gets trapped in one of them. Therefore, in general, the asymptotic values $\mathbf{x}^{\text{st}}$ depend on initial conditions and the absolute minimum of the potential V might not be reached. Accordingly, deviations from the self-consistent theory are expected to appear. In this section we will study this case and show that a new phenomenology can appear depending on the particular value of a and the distribution of the initial condition $\mathbf{x}(t=0)$. For the sake of concreteness, we have focused on two types of initial conditions: symmetrical and positive-definite.

8.6.1 Symmetrical initial conditions

The initial values $x_i(t=0), i=1,\ldots,N$, are independently drawn from a uniform distribution in the interval $[-\delta,+\delta]$, for a given value

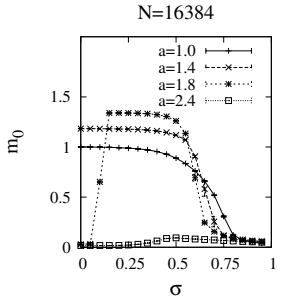

Figure 8.5: Numerical results of the average magnetization as a function of diversity σ, for a system of $N = 16384$ coupled variables for different values of $a \geq 1$ (for the numerical integration of Eq. 8.2, initial conditions are drawn from a symmetrical uniform distribution $U[-\delta, +\delta]$). Note that depending on the specific value of parameter a, three different behaviours take place: (*I*) an order-disorder transition at σ_c for $a = 1, 1.4$, (*II*) a reentrant phase transition formed by a disorder-order transition at σ_c' coupled to an order-disorder one at σ_c for intermediate values of $a = 1.8$, and (*III*) the absence of any transition to an ordered state for the larger value $a = 2.4$.

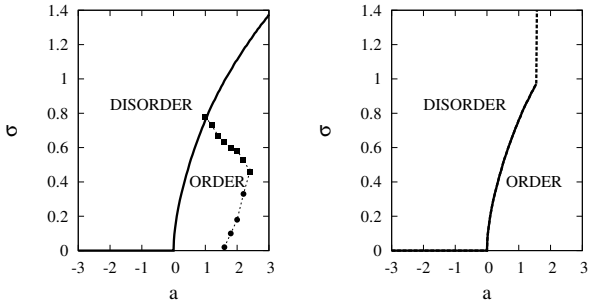

Figure 8.6: *Left panel:* Phase diagram of the system, where the symbols correspond to the values of critical points σ_c (associated to the order-disorder transition) and σ_c' (associated to the disorder-order transition) as a function of a, for a system of $N = 16384$ (derived numerically integrating Eq. 8.2 with initial conditions drawn for a symmetrical uniform distribution $[-\delta, +\delta]$). In the region $a > 0$ the system evidences an order-disorder phase transition at σ_c, the location of this transition increasing with a. The values of σ_c (in the thermodynamic limit) can be derived from the self-consistent theory as those satisfying $F'_{\sigma_c}(0) = 1$, and are represented by the solid line. In the region $a > 1$ the system presents metastable states even in the thermodynamic limit and the solid line refers to the location of phase transition derived from the analysis of the ground state of the Lyapunov potential. At odds with the self-consistent theory, we numerically find for intermediate values of a the coexistence of two phase transitions (reentrant transition), where the location of both critical points converge for increasing values of a until coalescence. At this point the ordered state is completely destroyed for all values of σ. *Right panel:* Same diagram as for the right panel, when the numerical integration of Eq. (8.2) is performed with initial conditions drawn for a uniform distribution in the positive-definite interval $[0, 2\delta]$. In this case, the phase transitions disappear for $a \gtrsim 1.4$ as in this case the order parameter m_0 tends to zero smoothly with σ, see right panel of Fig. 8.8.

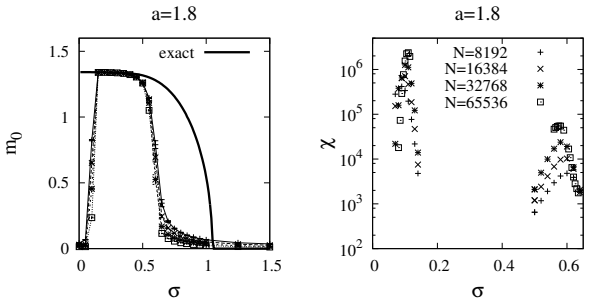

Figure 8.7: *Left panel:* Numerical results of the order parameter as a function of σ, for different system's size and $a = 1.8$, where a reentrant phase transition takes place (for the numerical integration of Eq. (8.2), initial conditions are drawn from a symmetrical uniform distribution $U[-\delta, +\delta]$). Exact results from the self-consistent theory are represented in the solid line. The deviations from the theory are related to the fact that the system does not reach the ground state of the Lyapunov potential as it gets trapped in metastable states. *Right panel:* Fluctuations of the order parameter as a function of σ for the same system as the right panel. Fluctuations have a peaked maximum that scales with system's size close to both transition points.

of δ. In Fig. 8.5 we plot the average magnetization $m_0 = \langle\langle |m| \rangle\rangle$ as a function of diversity σ for different values of a and system size $N = 16384$ for $\delta = 2.5$. The data have been averaged over 10^2 initial conditions for $\mathbf{x}(t = 0)$ and then over 10^2 realizations of the quenched noise variables (10^4 averages in total). At variance with the case $a \leq 1$ (which is also shown in the figure for comparison) we find three possible scenarios: (i) for $a \gtrsim 1$ (weak metastable regime, $a = 1.4$ in the figure) one observes the same phenomenology as for $a \leq 1$: an order-disorder transition at a critical value $\sigma_c(a)$. (ii) For larger values of a, the former transition is still present at σ_c, but a new transition (from a disordered state $m_0 = 0$ to an ordered one $m_0 > 0$ as σ increases) is found at $\sigma_c' < \sigma_c$, see the curve corresponding to $a = 1.8$ in the figure. In this case, we find the counterintuitive result that a certain level of diversity in the quenched noise is needed to induce order at $\sigma = \sigma_c'$, whereas a large level of diversity destroys again the ordered state (reentrant phase transition). (iii) Finally, for increasing a, σ_c' increases and σ_c decreases, eventually coalescing for $a > a_c \approx 2.4$, where the ordered state disappears. Thus, for large values of a, the system does not evidence any transition and the stationary phase is always the disordered one. We point out that in the curve for $a = 2.4$, the magnetization is not exactly zero for intermediate values of the diversity due to a finite-size effect: m_0 decreases and approaches zero for all values of σ as the system size increases, something that does not occur in cases (i) and (ii). All these features are illustrated in the phase diagram plotted in the left panel of Fig. 8.6: (i) For $1 < a \lesssim 1.6$ the usual order-disorder transition appears, although the value of σ_c is smaller that the one derived from the analysis based upon the structure of the global attractor $\bar{\mathbf{x}}$. (ii) For $1.6 \lesssim a \lesssim 2.4$ there is a new transition from a disordered to an ordered state at a value $\sigma_c' < \sigma_c$. (iii) Finally, for $a \gtrsim 2.4$ the only phase encountered is the disordered one.

In order to characterize the transitions that occur in region (ii), we have run extensive simulations for different system sizes in the case $a = 1.8$. The order parameter m_0 is displayed in the left pane of

Fig. 8.7. By looking at the difference with the magnetization curve derived from the theoretical analysis, it is clear from this figure that the system is not able to reach the absolute minimum neither for small or large diversity σ. We observe at both transitions the same qualitative dependence with system size that was discussed in the case $a \leq 1$. As we don't have now a theoretical prediction for σ_c' or σ_c the numerical analysis of the data is much less conclusive. Pseudo-critical points $\sigma_c(N)$ and $\sigma_c'(N)$ can be defined as the location of the maximum of the fluctuations χ of the order parameter, see the right panel of Fig. 8.7. The fluctuations scale roughly as $\chi(\sigma_c'(N)) \sim N^{b'}$ and $\chi(\sigma_c(N)) \sim N^b$ with $b' \approx b \approx 0.9$. However, it is difficult to obtain reasonably good quality fits of the data to the standard finite-size-scaling relations used in the case $a < 1$. Furthermore, the data show a dependence on δ (data not shown) such that σ_c and σ_c' adopt different values for small δ but saturate for $\delta \gtrsim 2.5$.

Summing up: if the initial conditions are distributed in a symmetrical interval, the order region is much reduced with respect to the predictions based upon the structure of the ground state. There is a region in parameter space where the system undergoes what appear to be well defined phase transitions, from disorder to order and back to disorder at σ_c' and σ_c, respectively. The order-disorder transition (σ_c) is related to the one found in the regime $a < 1$, while the disorder-order transition (at $\sigma_c' < \sigma_c$) is a new behaviour whose nature is genuinely metastable. For $a \gtrsim 2.4$ the system is never in the ordered state.

8.6.2 Positive-definite initial conditions

The initial values $x_i(t = 0), i = 1, \ldots, N$, are independently drawn from a uniform distribution in the interval $[0, 2\delta]$, for a given value of δ. Obviously, by symmetry reasons, the same results would be obtained in the initial conditions were drawn from the interval $[-2\delta, 0]$. In Fig. 8.8 we plot the average magnetization $m_0 = \langle\langle |m| \rangle\rangle$

as a function of diversity σ for different values of $a = 1.2$ (left panel) and $a = 1.8$ (right panel), for different system sizes N and values of δ. These two values of a evidence slight different behaviours: for $a = 1.2$, while the sharpening finite-size effect of the magnetization is hardly seen in the plot, the fluctuations still increase with system size close to the transition (data not shown), what suggests the presence of a phase transition in the thermodynamic limit. Note that the dependence on the width of the initial condition δ is very weak and results are basically indistinguishable for $\delta \geq 0.5$. On the other hand, for $a = 1.8$ there is hardly any dependence on the system size both for the magnetization and its fluctuations. The magnetization m_0 tends to zero smoothly with σ and the fluctuations do not increase with system size (data not shown): the transition is smoothed and no critical behaviour is present. Again, there is a dependence with the value of δ for small δ but the curves for $\delta = 2.5$ and $\delta = 5.0$ are indistinguishable from each other. Summing up, for positive-definite initial conditions, the phase transition from order to disorder disappears at a value $a \approx 1.6$ (the actual value depends of the width δ), such that the system shows always some degree of order for $a \gtrsim 1.6$ (see the right panel of Fig. 8.6). In this sense, the ordered region is enhanced with respect to the predictions based upon the structure of the ground state.

8.7 Conclusions

In this chapter we have studied the mean-field version of a Ginzburg-Landau, or ϕ^4, model with additive quenched noise at zero temperature. The model, that has recently been proposed in the framework of collective behaviour induced by diversity (Tessone *et al.* 2006; Toral *et al.* 2007), is a field version of the random field Ising model well studied in the literature. As a function of diversity σ, a self-

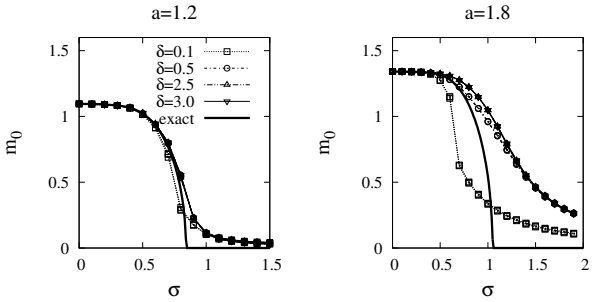

Figure 8.8: Numerical results of the order parameter as a function of σ, for different system's size $N = 4096, 8192, 16384$, and a value $a = 1.2$ (left panel) and $a = 1.8$ (right panel). For the numerical integration of Eq. (8.2), initial conditions are drawn from a positive-definite uniform distribution $U[0, 2\delta]$, with $\delta = 0.1, 0.5, 2.5, 3.0$. The effect of the interval size saturates for approximately $\delta \geq 0.5$ and 2.5 for the left and right panel respectively. While finite size effects in the magnetization are hardly observed for $a = 1.2$, fluctuations still increase with system size close to the transition. On the other hand, for $a = 1.8$ no finite-size effects are observed, neither for the magnetization nor for its fluctuations: the transition is smoothed and no critical behaviour is observed.

consistent theory predicts the presence of an order-disorder transition at a critical value σ_c, with mean field critical exponents that are equal than those of Landau's theory of thermal phase transitions. Numerical integrations of the dynamical equations (8.2) are also performed for comparison. In the range of parameters where the system lacks metastable states ($a \leq 1$), finite-size scaling relations show that the order parameter fluctuations diverge quadratically, rather than with $\gamma = 1$ as in thermal, equilibrium, phase transitions. This suggests a violation of the fluctuation dissipation not associated to metastable effects such as lack of time translational invariance or aging (Calabrese & Gambassi 2005; Crisanti & Ritort 2003; Young 1998). To explain this fact, we compute an effective Hamiltonian and argue that it cannot be readily expressed as $\mathcal{H}_{\text{eff}} = \mathcal{H}_0 + Nhm$: as a consequence, the fluctuations of the order parameter cannot be straightforwardly related to the linear response, as it happens in equilibrium theory. In the range of parameters where metastability is likely to appear ($a > 1$), stationary values typically do not reach the minimum of the Lyapunov potential, and accordingly numerical results deviate from the self-consistent theory, showing a strong dependence in the initial conditions. For a symmetrical distributed initial condition in the interval $[-\delta, +\delta]$, the ordered region is much reduced with respect to the predictions based upon the structure of the ground state of the potential. Furthermore, there is a region of values of a for which a new transition from a disordered to an ordered state takes place at $\sigma_c' < \sigma_c$. In this case, diversity can not only destroy an ordered state but also induce order from a disordered metastable state. This new transition is genuinely metastable, and its location increases for increasing values of a, until coalescing with σ_c, where the ordered phase completely disappears. On the other hand, when the initial condition is distributed in $[0, 2\delta]$, large enough values of a destroy the critical behaviour of the order-disorder transition and some degree of order remains at every value of the diversity σ.

We conclude that structural diversity can induce both the creation and annihilation of order in a nontrivial way, and deeply modify the dynamics of the diversity-free system counterpart. On the other hand, the apparent violation of the fluctuation-dissipation relation should be further investigated; at this point we can conclude that to directly relate the order parameter fluctuations to the linear response of a system can be tricky, even in the absence of metastability. This is particularly relevant in problems involving the estimation of critical exponents in nonequilibrium phase transitions.

Chapter 9

Concluding Remarks

The investigations of this thesis initially were driven by the search for answers to questions that arise in a biological context. They were raised within the BioSim network, a cooperation of scientists from the fields of pharmacology, medicine, mathematics, biology, physics and other disciplines investigating biological, pathological and pharmacological processes underlying the causes and treatments of illnesses. A network of related subjects needs to be entangled and the two first results of this thesis, chapters 4 and 5, are two pieces of the puzzle.

Drug absorption

When a chemical compound is found that might have a beneficial effect on the course of an illness, many steps are needed to find the optimal way of its application and to assure the safety of the drug. In general, a medicine that can be taken up orally like normal food is preferred to other possibilities. To assure that the right amount of substance reaches the desired organ one has to know all properties of the drug very well. The main barrier a substance has to overcome

on its way into the bloodstream is the intestinal wall, a single layer of tight-woven cells. Pharmacologists use a stem of intestinal cells that can be seeded in such a mono layer under laboratory conditions to investigate the properties of a certain drug in experiments. To this end a drug is investigated in experiments with a high number of initial and environmental conditions. With nonlinear fitting techniques to mathematical models for such absorption experiments the pharmacologists estimate the absorption parameters of a substance.

We investigated a widely used model for the absorption from one compartment to another through a third from an analytical perspective. We transformed the model into a form depicting a mass in a potential with a friction force and then approximated the potential by a parabola, an approximation that keeps all relevant features. It allows to calculate the theoretical outcome of an experiment directly which, on one hand, might help to narrow down the range of conditions in which the experiments have to be conducted and, on the other hand, allows to estimate how fluctuations of a parameter would propagate into the measurement.

The physiological conditions as well as external stimuli of habits and social clues are very different between people. The fluctuations resulting from these differences will have to be taken into account to optimise the efficiency of treatments for individual patients. Furthermore the three compartment model can be refined by allowing the cells to be different in size, membrane composition and expression of transporter proteins. Only the assumption of equal cells allows the reduction of the system to the three compartment model. In case of diverse equations for many individual cells (in the order of hundreds of thousands) more sophisticated methods, like the order parameter expansion, would have to be performed.

24 hours - a day is a day

As a drug enters the body, affects it and is cleaned out again the process is all together a dynamical one. As such its interaction with the body (changing hormone and activity levels or body temperature, supply of water and nutritions) is dynamic as well. Doubtlessly, a large part of the dynamical processes in the body is coupled to the daily change between light and darkness. Many processes like the need to sleep or eat interact with periodic hormone levels that are controlled by a kind of master clock in the brain. It receives information directly from the eye and masters hormone levels during the course of a day. It is reported that for example some cancer drugs are more efficient and less toxic when they are applied at the right moment of a day. Also it is known that light stimuli can have a beneficial effect on patients with depression. To learn more about these complex, time-dependent, interactions it seems natural to start by asking how the master clock itself works. It is known that about twenty thousand neurons clumped up in a small part of the brain (the suprachiasmatic nucleus) receive the light stimulus and exhibit protein oscillations. The oscillations have to be shifted when the time zone changes and have to be robust when the duration of darkness changes during the year.

Experiments have shown that isolated cells do oscillate, all with different inherent periods. It was our intention to investigate how the difference of periods affects the way the collective rhythm is maintained in phase with the light stimulus. On one hand we did extensive numerical simulations of the dynamical equations. On the other hand we analysed the system with a constant light term instead of the periodic one. By doing so one can calculate the stability of the fixed point for a given realisation of the random terms and obtain an average stability. It turns out that if the cells were nearly equal in their properties then the overall rhythm is governed by the coupling of the cells – stronger coupling leading to longer day lengths. They show self sustained oscillations. In

the other extreme, when the cells are too diverse, they perform damped oscillations. Thus, an oscillatory forcing maintains the protein oscillations but the cells have poor synchronisation among themselves. The best pronounced and synchronous oscillations occur at intermediate levels of diversity, where the self sustained oscillations due to the coupling die out and give way to a system of neurons that are very susceptible to periodic stimuli from outside.

It is an open question if the results hold for other nonlinear oscillators based on biochemical reactions. Furthermore it seems that the coupling in the suprachiasmatic nucleus is more complex than the assumed mean field coupling. If the diversity can induce oscillator death in a system with hierarchically organised interactions is yet to be proven.

Synchronisation of an excitable system

Models that represent biochemical processes are usually of a large number of variables and furthermore highly nonlinear. In above example of the circadian rhythms we used a four dimensional model with nonlinear terms in all four of the dynamical equations. This makes a complete analytical solution difficult. One can try to find generalities in the synchronization of nonlinear oscillators by analysing a prototypic model with few system parameters. One such model is the one dimensional active rotator model which is the base of our analysis in chapter 6. It is an abstract mathematical model that is controlled by two parameters. One parameter decides if the system actually performs oscillations without any stimulus. If not it rests in a fixed position and a sufficiently high perturbation causes one single oscillation, larger than the original stimulus – an excitation. The length of one oscillation, the period, is governed by the second parameter. It is known that this system in the excitable regime exhibits periodic excitations when it is subjected to small random forces of intermediate strength.

We wanted to know if many rotators together would oscillate in synchrony just by having different inherent periods without the need of random fluctuations. It is indeed so and in fact the onset of synchrony, as well as its offset, show typical properties of phase transitions similar to what is known from thermodynamics and statistical mechanics. Transitions of first and second order were identified. The phase diagram and the order of transition can be predicted by the help of an approximative method that is developed and presented in full detail in chapter 7. Apart from the approximate method we used extensive numerical simulations to investigate the finite size effects of the active rotator model with diverse frequencies. We calculated the size dependence of order parameter and its fluctuations at the phase transition and found critical exponents that are not conform with what is expected from a mean field model as it is the case for our considerations. We decided to have a look at other, non oscillatory models which are known to show synchronisation to an external periodic forcing and phase transitions.

Diversity induced phase transitions

The Ginzburg-Landau model with thermal fluctuations is a scalar model that undergoes second-order phase transitions. Another model we have treated is the paradigmatic model for phase transitions in the presence of multiplicative noise. Our interest was to study how these models behave in the presence of local heterogeneities and without the thermal fluctuations. In a first step to achieve our goal we refined an existing method of approximating coupled diverse differential equation (which we also used in the treatment of the active rotators). It reduces a large number of variables for coupled scalar dynamics to a set of three differential equations for the mean value and the fluctuations. We analysed fixed points and stability of the resulting equations and identified ordered and disordered phases of the collective system for different

values of diversity (width of the distribution of heterogeneities). The critical values obtained from the approximate method have been compared with the numerical evaluation of an exact expression. In one case the method was not reliable as it did not show the reentrant transition into disorder. In the other cases the method reveals analytic formulas for the phase diagram in the limit of strong coupling.

Next, we used numerical techniques to investigate the finite size scaling behaviour and determine critical exponents at the phase transitions. The Ginzburg-Landau model with additive diversity as well as the prototypic model for noise induced phase transitions both exhibit exponents consistent with those found for active rotators, suggesting that they belong to the same universality class. The exponents, however, are different from what is expected in a mean field analysis. We carried out the mean field analysis for the Ginzburg-Landau model with additive heterogeneities in chapter 8. In this case the system can exhibit local metastability: for a given heterogeneity and mean field an element can be in either of the two fixed points. If such is the case the global solution of the coupled system is highly dependent on the initial conditions.

All together we have seen that diversity, i.e. a time independent random element in a collective system, not surprisingly can destroy an ordered phase. But it also can induce the ordered phase. Furthermore, under some circumstances the induced ordered phase is destroyed for even higher diversities, thus a reentrant phase transition is induced. It is the hope, that some results from this thesis deeper the understanding of specific dynamical systems as observed in biochemical processes, others give insights that have a general validity for systems with diversity, not limited to the area of biochemistry.

Part III

Appendices

Appendix A

Related publications

- *"Drug absorption through a cell monolayer: A theoretical work on a non-linear three-compartment model"*, N.K., Raúl Toral, European Journal of Pharmaceutical Sciences **37**, 106-114 (2009)
- *"Synchronization and entrainment of coupled circadian oscillators"*, N.K., Adrian C. Murza, Emilio Hernández-García, Raúl Toral, Journal of the Royal Society Interface Focus, doi:10.1098/rsfs.2010.0327
- *"Order parameter expansion study of synchronous firing induced by quenched noise in the active rotator model"*, N.K., Raúl Toral, Physical Review E **82**, 051127
- *"Phase transitions induced by microscopic disorder: a study based on the order parameter expansion"*, N.K., Raúl Toral, Physica D **239**, 1827-1833 (2010)
- *"Critical behavior of a Ginzburg-Landau model with additive quenched noise"*, N.K., Lucas Lacasa, Raúl Toral, Journal of Statistichal Mechanics: theory and experiment **P12008**

Appendix B

Prototypes of phase transitions induced by diversity

B.1 Solutions of the cubic equation

We give explicit expressions for the function $\bar{x}(m+\eta)$ defined as the convenient real solution of the cubic equation $\alpha x + x^3 = z$, where $\alpha = 1 - a$ and $z = m + \eta$.

In the case $\alpha \geq 0$ there is only one real solution to this equation as given by Cardano's formula

$$\bar{x}(z) = u - \alpha/(3u), \qquad u = \sqrt[3]{\frac{z}{2} + \sqrt{\frac{z^2}{4} + \frac{\alpha^3}{27}}}. \tag{B.1}$$

For $\alpha < 0$, the same formula applies if the discriminant $\Delta \equiv 27z^2 + 4\alpha^3$ is positive $\Delta \geq 0$, i.e. $z \notin \left(-2(-\alpha/3)^{3/2}, +2(-\alpha/3)^{3/2}\right)$. Otherwise, out of the three real solutions, the one that minimizes the local potential $v(x) = \frac{\alpha}{2}x^2 + \frac{1}{4}x^4 - zx$ is obtained using the trigonometric form of Cardano's formula:

$$\bar{x}(z) = 2\,\mathrm{sign}(z)\sqrt{-\frac{\alpha}{3}}\cos\left(\frac{1}{3}\arccos\sqrt{-\frac{27z^2}{4\alpha^3}}\right), \tag{B.2}$$

where the arccos function takes values in the principal branch of $[0, \pi/2]$. Note that, in every case, the function $\bar{x}$ is antisymmetric $\bar{x}(z) = -\bar{x}(-z)$.

B.2 Calculation of critical diversity

The order parameter of the models in chapters 7 and 8 (X and m respectively) was found through the self consistency equation

$$m \equiv X = \int d\eta\, g(\eta) x^*(\eta, m, H) \equiv F(m)\,, \tag{B.3}$$

where $x^*(\eta, m, h)$ is the stable stationary solution of the local dynamics depending on the additive external field h, the local heterogeneity η and the mean value itself. The susceptibility is defined as $\chi_h \equiv \frac{\partial m}{\partial h}\big|_{h=0}$ and therefore we can write:

$$\chi_h(\sigma) = \frac{\partial m}{\partial h} = \int d\eta\, g(\eta)\left(\frac{\partial x^*}{\partial m}\frac{\partial m}{\partial h} + \frac{\partial x^*}{\partial h}\right) \tag{B.4}$$

$$= \frac{\partial m}{\partial h}\int d\eta\, g(\eta)\frac{\partial x^*}{\partial m} + \int d\eta\, g(\eta)\frac{\partial x^*}{\partial h}\,, \tag{B.5}$$

which can be reordered to

$$\chi_h(\sigma) = \frac{\int d\eta\, g(\eta) \frac{\partial x^*(m,\eta,h)}{\partial h}}{1 - \int d\eta\, g(\eta) \frac{\partial x^*(m,\eta,h)}{\partial m}} \,. \tag{B.6}$$

The derivatives are to be taken at $h = 0$. This equation allows us to calculate the critical diversity by finding the singularity where the susceptibility diverges, that is where the denominator is zero.

In chapters 7 and 8 we have calculated the critical diversity for the Ginzburg-Landau model, or Φ^4 model, with an additive random field. In this specific form it is $x^*(m, \eta, h) = x^*(m + \eta, h)$ and the local fixed point solution can be expressed analytically (see Appendix B.1). Function $F(m)$ of equation (B.4) is antisymmetric so one identifies the critical point with the change of slope in the origin where additional, non-zero, solutions arise that characterise the the ordered phase.

To obtain the slope of $F(m)$ in the origin it is convenient to first introduce a new set of variables $\eta = \sigma\xi$, $z = m + \eta$ and $d\xi = dz/\sigma$. Then the probability density of ξ is $g(\xi) = g(\eta/\sigma)$ and $x^*(m + \eta) = x^*(z)$. We can now write Eq. (B.4) in the following way:

$$m = F(m) = \int_{-\infty}^{\infty} d\xi\, g(\xi) x^*(m + \sigma\xi) \tag{B.7}$$

$$= \frac{1}{\sigma} \int_{-\infty}^{\infty} dz\, g\left(\frac{z - m}{\sigma}\right) x^*(z) \,. \tag{B.8}$$

For a Gaussian distribution of the field, now without σ-dependency $g(x) = 1/\sqrt{2\pi} \exp -x^2/2$, the derivative with respect to its argument is $g'(x) = -x\, g(x)$ and then the the derivative of $F(m)$ with respect to

m, $F'(m)$, reads:

$$\begin{aligned} F'(m) &= \frac{1}{\sigma}\int_{-\infty}^{\infty} dz\, \frac{d\left[g\left(\frac{z-m}{\sigma}\right)x^*(z)\right]}{dm} \\ &= \frac{-1}{\sigma^2}\int_{-\infty}^{\infty} dz\, \frac{d\left[g\left(\frac{z-m}{\sigma}\right)\right]}{d\frac{z-m}{\sigma}} x^*(z) \\ &= \frac{1}{\sigma^3}\int_{-\infty}^{\infty} dz\, g\left(\frac{z-m}{\sigma}\right)(z-m)\, x^*(z)\,. \end{aligned}$$

We now set $m = 0$ and reduce the integral to half, as $z\,x^*(z)$ is an even function. We find:

$$F'(0) = \frac{2}{\sigma^3}\int_0^{\infty} dz\, g\left(\frac{z}{\sigma}\right) z\, x^*(z)\,. \tag{B.9}$$

In Appendix B.1 we have seen that for some cases one has to decide for the energetically lowest solution. The system parameter a determines in what regions of the function's argument which formula is valid. In terms of equation (B.9) the integral can be split in two by realising that in case of $|z| < z_c = 2\sqrt{\left(\frac{a-1}{3}\right)^3}$ one has to take formula (B.1) and for $|z| > z_c$ formula (B.2). As a result, to determine the critical diversity one has to determine the solution of

$$1 = F'(0) = \frac{2}{\sigma^3}\left[\int_0^{z_c} dz\, g\left(\frac{z}{\sigma}\right) z x^*_{B.2}(z) + \int_{z_c}^{\infty} dz\, g\left(\frac{z}{\sigma}\right) z x^*_{B.1}(z)\right]. \tag{B.10}$$

List of Figures

References

Acebrón, J. A., Bonilla, L. L., Pérez Vicente, C. J., Ritort, F. & Spigler, R., 2005 The Kuramoto model: A simple paradigm for synchronization phenomena. *Rev. Mod. Phys.* **77**, 137–185.

Acebrón, J. A., Lozano, S. & Arenas, A., 2007 Amplified Signal Response in Scale-Free Networks by Collaborative Signaling. *Physical Review Letters* **99**, 128701.

Acharya, P., Thuy, T. T., Polli, J. W., Ayrton, A., Ellens, H. & Bentz, J., 2006 P-Glycoprotein (P-gp) Expressed in a Confluent Monolayer of hMDR1-MDCKII Cells Has More Than One Efflux Pathway with Cooperative Binding Sites. *Biochemistry* **45**, 15505–15519.

Aidley, D. J. & Stanfield, P. R., 1996 *Ion Channels: Molecules in Action*. Cambridge university press.

Alberts, B., Johnson, A., Lewis, J., Raff, M., Roberts, K. & Walter, P., 2002 *Molecular biology of the cell*. Garland Science, 4th edition.

Amit, D. J. & Mayor, V. M., 2005 *Field Theory, the Renormalization Group and Critical Phenomena*. World Scientific Publishing Co.Pte. Ltd., 3rd edition.

Anishchenko, V. S., Astakhov, V., Neiman, A., Vadivasova, T. & Schimansky-Geier, L., 2007 *Nonlinear Dynamics of Chaotic and Stochastic Systems: Tutorial and Modern Developments (Springer Series in Synergetics)*. Secaucus, NJ, USA: Springer-Verlag New York, Inc.

Artursson, P. & Borchardt, R. T., 1997 Intestinal Drug Absorption and Metabolism in Cell Cultures: Caco-2 and Beyond. *Pharmaceutical Research* **14**, 1655–1658.

Artursson, P., Palm, K. & Luthman, K., 2001 Caco-2 monolayers in experimental and theoretical predictions of drug transport. *Advanced Drug Delivery Reviews* **46**, 27–43.

Aton, S. J., Colwell, C. S., Harmar, A. J., Waschek, J. & Herzog, E. D., 2005 Vasoactive intestinal polypeptide mediates circadian rhythmicity and synchrony in mammalian clock neurons. *Nature Neuroscience* **8**, 476–483.

Aton, S. J. & Herzog, E. D., 2005 Come Together, Right...Now: Synchronization of Rhythms in a Mammalian Circadian Clock. *Neuron* **48**, 531–534.

Balimane, P. V., Chong, S. & Morrison, R. A., 2000 Current methodologies used for evaluation of intestinal permeability and absorption. *Journal of Pharmacological and Toxicological Methods* **44**, 301–312.

Balimane, P. V., Patel, K., Anthony, M. & Chong, S., 2004 Utility of 96 well Caco-2 cell system for increased throughput of P-gp screening in drug discovery. *European Journal of Pharmaceutics and Biopharmaceutics* **58**, 99–105.

Ball, P., 2000 Quinolone generations: natural history or natural selection? *Journal of Antimicrobial Chemotherapy* **46**, 17–24.

Becker-Weimann, S., Wolf, J., Herzel, H. & Kramer, A., 2004 Modeling Feedback Loops of the Mammalian Circadian Oscillator. *Biophysical Journal* **87**, 3023–3034.

Becskei, A., Kaufmann, B. & van Oudenaarden, A., 2005 Contributions of low molecule number and chromosomal positioning to stochastic gene expression. *Nature Genetics* **37**, 937–944.

Benzi, R., Sutera, A. & Vulpiani, A., 1981 The mechanism of stochastic resonance. *Journal of Physics A: Mathematical and General* **14**, L453.

Bermejo, M., Avdeef, A., Ruiz, A., Nalda, R., Ruell, J. A., Tsinman, O., González, I., Fernández, C., Sánchez, G., Garrigues, T. M. & Merino, V., 2004 PAMPA–a drug absorption in vitro model: 7. Comparing rat in situ, Caco-2, and PAMPA permeability of fluoroquinolones. *European Journal of Pharmaceutical Sciences* **21**, 429–441.

Bermejo, M., Merino, V., Garrigues, T. M., Delfina, J. M. P., Mulet, A., Vizet, P., Trouiller, G. & Mercier, C., 1999 Validation of a biophysical drug absorption model by the PATQSAR system. *Journal of Pharmaceutical Sciences* **88**, 398–405.

Bernard, S., Gonze, D., Čajavec, B., Herzel, H. & Kramer, A., 2007 Synchronization-Induced Rhythmicity of Circadian Oscillators in the Suprachiasmatic Nucleus. *PLoS Comput Biol* **3**, e68.

Beuter, A., Glass, L., Mackey, M. C. & Titcombe, M. S., eds., 2003 *Nonlinear Dynamics in Physiology and Medicine*. Springer.

Bezruchko, B., Ponomarenk, V., Rosenblum, M. G. & Pikovsky, A. S., 2003 Characterizing direction of coupling from experimental observations. *Chaos* **13**, 179.

BioSim, 2010 About BioSim, Network of Excellence. [Online; accessed 25-June-2010].

Blake, W. J., KAErn, M., Cantor, C. R. & Collins, J. J., 2003 Noise in eukaryotic gene expression. *Nature* **422**, 633–637.

Boccaletti, S., Latora, V., Moreno, Y., Chavez, M. & Hwang, D.-U., 2006 Complex networks: Structure and dynamics. *Physics Reports* **424**, 175 – 308.

Boyce, W. E. & DiPrima, R. C., 2001 *Elementary Differential Equations and Boundary Value Problems*. John Wiley & Sons, Inc.

Brown, R., 1828 XXVII. A brief account of microscopical observations made in the months of June, July and August 1827, on the

particles contained in the pollen of plants; and on the general existence of active molecules in organic and inorganic bodies. *Philosophical Magazine Series 2* pp. 161–173.

Buceta, J. & Lindenberg, K., 2003 Spatial patterns induced purely by dichotomous disorder. *Phys. Rev. E* **68**, 011103.

Buceta, J., Parrondo, J. & de la Rubia, F., 2001 Random Ginzburg-Landau model revisited: Reentrant phase transition. *Physical Review E* **63**, 031103.

Bulsara, A. & Zador, A., 1996 Threshold detection of wideband signals: A noise-induced maximum in the mutual information. *Phys. Rev. E* **54**, R2185.

Calabrese, P. & Gambassi, A., 2005 Ageing properties of critical systems. *Journal of Physics A: Mathematical and General* **38**, R133.

Cardy, J., 1988 *Finite-Size Scaling*. Elsevier science publishers.

Cartwright, J. H. E., 2000 Emergent global oscillations in heterogeneous excitable media: The example of pancreatic β cells. *Phys. Rev. E* **62**, 1149–1154.

Chen, H., Shen, Y., Hou, Z. & Xin, H., 2009 Resonant response of forced complex networks: The role of topological disorder. *Chaos: An Interdisciplinary Journal of Nonlinear Science* **19**, 033122.

Chen, H. & Zhang, J., 2008 Diversity-induced coherence resonance in spatially extended chaotic systems. *Physical Review E* **77**, 026207.

Clerc, M. G., Falcón, C. & Tirapegui, E., 2006 Front propagation sustained by additive noise. *Phys. Rev. E* **74**, 011303.

Crick, F., 1970 Central Dogma of Molecular Biology. *Nature* **227**, 561–563.

Crisanti, A. & Ritort, F., 2003 Violation of the fluctuationâĂŞdissipation theorem in glassy systems: basic notions and the numerical evidence. *Journal of Physics A: Mathematical and General* **36**, R181.

Cull, P., Flahive, M. E. & Robson, R. O., 2005 *Difference equations: from rabbits to chaos*. Springer Science+Business Media, Inc.

Dahmen, K. & Sethna, J. P., 1996 Hysteresis, avalanches, and disorder-induced critical scaling: A renormalization-group approach. *Phys. Rev. B* **53**, 14872–14905.

Davis, R., Markham, A. & Balfour, J. A., 1996 Ciprofloxacin: An updated review of its pharmacology, therapeutic efficacy and tolerability. *Drugs* **51**, 1019–1074.

de Monte, S. & d'Ovidio, F., 2002 Dynamics of order parameters for globally coupled oscillators. *Europhys. Lett.* **58**, 21–27.

de Monte, S., d'Ovidio, F., Chaté, H. & Mosekilde, E., 2004 Noise-Induced Macroscopic Bifurcations in Globally Coupled chaotic Units. *Phys. Rev. Lett.* **92**.

de Monte, S., d'Ovidio, F., Chaté, H. & Mosekilde, E., 2005 Effects of microscopic disorder on the collective dynamics of globally coupled maps. *Physica D* **205**, 25–40.

de Monte, S., d'Ovidio, F. & Mosekilde, E., 2003 Coherent regimes of globally coupled dynamical systems. *Phys. Rev. Lett* **90**, 054102.

de Vries, G. & Sherman, A., 2001 From spikers to bursters via coupling: Help from heterogeneity. *Bulletin of Mathematical Biology* **63**, 371–391.

Deutsch, H., 1992*a* Optimized analysis of the critical behavior in polymer mixtures from Monte Carlo simulations. *J. Stat. Phys* **67**, 1039.

Deutsch, H., 1992*b* Optimized Analysis of the Critical Behaviour in Polymer Mixtures from Monte Carlo Simulations. *J. Stat. Phys* **67**, 1039.

Devaux, H., 1932 Dünne Lamellen und ihre physikalischen Eigenschaften. *Kolloid-Zeitschrift* **LVIII**.

Dong, G. & Golden, S. S., 2008 How a cyanobacterium tells time. *Current Opinion in Microbiology* **11**, 541 – 546. Growth and Development: Eukaryotes/Prokaryotes.

Ebeling, W., Herzel, H., Richert, W. & Schimansky-Geier, L., 1986 Influence of Noise on Duffing-Van der Pol Oscillators. *Journal of Applied Mathematics and Mechanics / Zeitschrift für Angewandte Mathematik und Mechanik* **66**, 1521–4001.

Eddershaw, P. J., Beresford, A. P. & Bayliss, M. K., 2000 ADME/PK as part of a rational approach to drug discovery. *Drug Discovery Today* **5**.

Elowitz, M. B., Levine, A. J., Siggia, E. D. & Swain, P. S., 2002 Stochastic Gene Expression in a Single Cell. *Science* **297**, 1183–1186.

Ermentrout, G., 1990 Oscillator death in populations of 'all to all' coupled nonlinear oscillators. *Physica D: Nonlinear Phenomena* **41**, 219–231.

Ermentrout, G. B. & Kopell, N., 1986 Parabolic Bursting in an Excitable System Coupled with a Slow Oscillation. *SIAM Journal on Applied Mathematics* **46**, 233–253.

Faassen, F., Vogel, G., Spanings, H. & Vromans, H., 2003 Caco-2 permeability, P-glycoprotein transport ratios and brain penetration of heterocyclic drugs. *International Journal of Pharmaceutics* **263**, 113–122.

Ferdinand, A. E. & Fisher, M. E., 1969 Bounded and Inhomogeneous Ising Models. I. Specific-Heat Anomaly of a Finite Lattice. *Phys. Rev.* **185**, 832–846.

Fick, A., 1855 Ueber Diffusion. *Annalen der Physik* **170**, 59–86.

Fisher, M. E. & Ferdinand, A. E., 1967 Interfacial, Boundary, and Size Effects at Critical Points. *Phys. Rev. Lett.* **19**, 169–172.

Forger, D. B. & Peskin, C. S., 2005 Stochastic simulation of the mammalian circadian clock. *Proceedings of the National Academy of Sciences of the United States of America* **102**, 321–324.

Fricke, H., 1925 The electric capacity of suspensions with special reference to blood. *Journal of General Physiology* **9**, 137–152.

Frye, L. D. & Edidin, M., 1970 The Rapid Intermixing of Cell Surface Antigens After Formation of Mouse-Human Heterokaryons. *J Cell Sci* **7**, 319–335.

Gammaitoni, L., Hänggi, P., Jung, P. & Marchesoni, F., 1998 Stochastic Resonance. *Reviews of Modern Physics* **70**, 223.

Gammaitoni, L., P. Hänggi, P. J. & Marchesoni, F., 2009 Special Issue: Stochastic Resonance. *Eur. Phys. J. B* **69**.

Gang, H., Ditzinger, T., Ning, C. Z. & Haken, H., 1993 Stochastic resonance without external periodic force. *Phys. Rev. Lett.* **71**, 807–810.

García-Ojalvo, J., Parrondo, J., Sancho, J. & van den Broeck, C., 1996 Reentrant transition induced by multiplicative noise in the time-dependent Ginzburg-Landau model. *Phys. Rev. E* **54**, 6918–6921.

García-Ojalvo, J. & Sancho, J. M., 1999 *Noise in Spatially Extended Systems*. New York: Springer–Verlag.

Gardiner, C. W., 1985 *Handbook of Stochastic Methods*. Springer-Verlag.

Goldbeter, A., 1995 A Model for Circadian Oscillations in the Drosophila Period Protein (PER). *Proceedings: Biological Sciences* **261**, 319–324.

Goldbeter, A., Dupont, G. & Berridge, M. J., 1990 Minimal model for signal-induced Ca2+ oscillations and for their frequency encoding through protein phosphorylation. *Proceedings of the National Academy of Sciences of the United States of America* **87**, 1461–1465.

Gonen, T. & Walz, T., 2006 The structure of aquaporins. *Quarterly Reviews of Biophysics* **39**, 361–396.

González-Alvarez, I., Fernandez-Teruel, C., Garrigues, T., Casabo, V., Ruiz-García, A. & Bermejo, M., 2005 Kinetic modelling of passive transport and active efflux of a fluoroquinolone across Caco-2 cells using a compartmental approach in NONMEM. *Xenobiotica* **35**, 1067–1088.

González-García, I., Solé, R. & Costa, J., 2002 Metapopulation dynamics and spatial heterogeneity in cancer. *PNAS* **99**, 13085–13089.

Gonze, D., Bernard, S., Waltermann, C., Kramer, A. & Herzel, H., 2005 Spontaneous Synchronization of Coupled Circadian Oscillators. *Biophys. J.* **89**, 120–129.

Goodwin, B. C., 1965 Oscillatory behavior in enzymatic control processes. *Advances in Enzyme Regulation* **3**, 425–428, IN1–IN2, 429–430, IN3–IN6, 431–437.

Goodwin, B. C., 1966 An Entrainment Model for Timed Enzyme Syntheses in Bacteria. *Nature* **209**, 479–481.

Gorter, E. & Grendel, F., 1925 On bimolecular layers of lipoids on the chromocytes of the blood. *The Journal of Experimental Medicine* **41**, 439–443.

Gosak, M., 2009 Cellular diversity promotes intercellular Ca2+ wave propagation. *Biophysical Chemistry* **139**, 53–56.

Gosh, A. K., Chance, B. & Pye, E. K., 1971 Metabolic Coupling and Synchronization of NADH Oscillations in Yeast Cell populations. *Archives of Biochemistry and Biophysics* **145**, 319–331.

Grant, M. & Gunton, J. D., 1984 Domain growth in the random-field Ising model: The breakdown of self-similar scaling in two dimensions. *Phys. Rev. B* **29**, 6266–6275.

Grant, M. & Gunton, J. D., 1987 Metastable states in the random-field Ising model. *Phys. Rev. B* **35**, 4922–4928.

Griffith, J. S., 1968 Mathematics of Cellular Control Processes. *Journal of Theoretical Biology* **20**, 202–208.

Grinstein, G. & Fernandez, J. F., 1984 Equilibration of random-field Ising systems. *Phys. Rev. B* **29**, 6389–6392.

Hänggi, P., Talkner, P. & Borkovec, M., 1990 Reaction-rate theory: fifty years after Kramers. *Rev. Mod. Phys.* **62**, 251–341.

Hastings, M. & Herzog, E., 2004 Clock Genes, Oscillators, and Cellular Networks in the Suprachiasmatic Nuclei. *Journal of Biological Rhythms* **19**, 400–413.

Heintzen, C. & Liu, Y., 2007 The Neurospora crassa Circadian Clock. *Advances in Genetics* **58**, 25 – 66.

Hennessy, M. & Spiers, J., 2007 A primer on the mechanics of P-glycoprotein the multidrug transporter. *Pharmacological Research* **55**, 1–15.

Herzog, E., Aton, S., Numano, R., Sakaki, Y. & Tei, H., 2004 Temporal precision in the mammalian circadian system: a reliable clock from less reliable neurons. *Journal of Biological Rhythms* **19**, 35–46.

Hill, A. V., 1910 The possible effects of the aggregation of the molecules of haemoglobin on its dissociation curves. *J. Physiol. (Lond.)* .

Holz, M. & Fahr, A., 2001 Compartment modeling. *Advanced Drug Delivery Research* **48**, 249–264.

Honma, S., Nakamura, W., Shirakawa, T. & Honma, K., 2004 Diversity in the circadian periods of single neurons of the rat suprachiasmatic nucleus depends on nuclear structure and intrinsic period. *Neuroscience Letters* **358**, 173–176.

Hooper, D. C., 2001 Emerging Mechanisms of Fluoroquinolone Resistance. *Emerging Infectious Diseases* **7**, 337–341.

Hoppensteadt, F. C., 1982 *Mathematical methods of population biology*. ew York : Cambridge University Press.

Horsthemke, W. & Lefever, R., 1984 *Noise-Induced Transitions*. Springer-Verlag.

Hunter, J. & Hirst, B. H., 1997 Intestinal secretion of drugs. The role of P-glycoprotein and related drug efflux systems in limiting oral drug absorption. *Advanced Drug Delivery Reviews* **25**, 129–157.

Imry, Y. & Ma, S.-k., 1975 Random-Field Instability of the Ordered State of Continuous Symmetry. *Phys. Rev. Lett.* **35**, 1399–1401.

Irvine, J. D., Takashi, L., Lockhart, K., Cheong, J., Tolan, J. W., Selick, H. E. & Grove, J. R., 1999 MDCK (Madin-Darby Canine Kidney) Cells: A Tool for Membrane Permeability Screening. *Journal of Pharmaceutical Sciences* **88**, 28–33.

Izhikevich, E. M., 2007 *Dynamical Systems in Neuroscience: The Geometry of Excitability and Bursting*. The MIT Press.

Jevrejeva, S., Moore, J. C. & Grinsted, A., 2003 Influence of the Arctic Oscillation and El NiÃśo-Southern Oscillation (ENSO) on

ice conditions in the Baltic Sea: The wavelet approach. *Journal of Geophysical Research* **108**, 4677.

Jones, P. & George, A., 2004 The ABC transporter structure and mechanism: perspectives on recent research. *Cellular and Molecular Life Sciences* **61**, 682–699.

Jung, P. & Hänggi, P., 1991 Amplification of small signals via stochastic resonance. *Phys. Rev. A* **44**, 8032–8042.

Kelley, W. G. & Peterson, A. C., 2001 *Difference equations: an introduction with applications*. Academic Press.

Komin, N. & Toral, R., 2009 Drug absorption through a cell monolayer: A theoretical work on a non-linear three-compartment model. *European Journal of Pharmaceutical Sciences* **37**, 106–114.

Komin, N. & Toral, R., 2010 Phase transitions induced by microscopic disorder: A study based on the order parameter expansion. *Physica D: Nonlinear Phenomena* **239**, 1827 – 1833.

Korjamo, T., Kemiläinen, H., Heikkinen, A. T. & Mönkkönen, J., 2007 Decrease in Intracellular Concentration Causes the Shift in *K_m* Value of Efflux Pump Substrates. *Drug Metabolism amd Disposition* **35**, 1574–1579.

Korn, E. D., 1969 Cell Membranes: Structure and Synthesis. *Annual Review of Biochemistry* **38**, 263–288.

Kramer, W. G., Lewis, R. P., Tyson, C. C., Forester Jr., W. F., Visconti, J. F., Wanke, L. A., Boxenbaum, H. G. & Reuning, R. H., 1974 Pharmacokinetics of Digoxin: Comparison of a Two- and a Three-Compartment Model in Man. *Journal of Pharmacokinetics and Biopharmaceutics* **2**, 299–312.

Kramers, H. A., 1940 Brownian motion in a field of force and the diffusion model of chemical reactions. *Physica VII* **4**, 284–304.

Kuramoto, Y., 1975 International Symposium on Mathematical problems in Theoretical Physics. In *Lectures notes in Physics No 30* (ed. H. Araki), p. 420. New York: Springer, first edition.

Kuramoto, Y., 1984 *Chemical Oscillations, Waves and Turbulence.* New York: Springer, first edition.

Lafuerza, L., Colet, P. & Toral, R., 2010 Non-universal results induced by diversity distribution in coupled excitable systems. *http://arxiv.org/abs/1005.0934* .

Landau, D. & Binder, K., 2000 *A guide to Monte Carlo simulations in statistical physics*. Cambridge university press.

Langmuir, I., 1917 The constitution and fundamental properties of solids and liquids. II. Liquids. *Journal of the American Chemical Society* **39**, 1848–1906.

Leloup, J.-C. & Goldbeter, A., 2003 Toward a detailed computational model for the mammalian circadian clock. *Proceedings of the National Academy of Sciences of the United States of America* **100**, 7051–7056.

Lentz, K. A., Polli, J. W., Wring, S. A., Humphreys, J. E. & Polli, J. E., 2000 Influence of Passive Permeability on Apparent P-glycoprotein Kinetics. *Pharmaceutical Research* **17**.

Lindner, B., García-Ojalvo, J., Neiman, A. & Schimansky-Geier, L., 2004 Effects of Noise in Excitable Systems. *Phys. Rep.* **392**, 321.

Locke, J., Millar, A. & Turner, M., 2005 Modelling genetic networks with noisy and varied experimental data: the circadian clock in Arabidopsis thaliana. *Journal of Theoretical Biology* **234**, 383 – 393.

Low-Zeddies, S. S. & Takahashi, J. S., 2001 Chimera Analysis of the Clock Mutation in Mice Shows that Complex Cellular Integration Determines Circadian Behavior. *Cell* **105**, 25–42.

Marban, E., Yamagishi, T. & Tomaselli, G. F., 1998 Structure and function of voltage-gated sodium channels. *The Journal of Physiology* **508**, 647–657.

Marr, A. G. & Ingraham, J. L., 1962 Effect of temperature on the composition of fatty acids in escherichia coli. *J Bacteriol.* **84**, 1260–1267.

Maywood, E. S., Reddy, A. B., Wong, G. K., O'Neill, J. S., O'Brien, J. A., McMahon, D. G., Harmar, A. J., Okamura, H. & Hastings, M. H., 2006 Synchronization and Maintenance of Timekeeping in Suprachiasmatic Circadian Clock Cells by Neuropeptidergic Signaling. *Current Biology* **16**, 599–605.

McNamara, B. & Wiesenfeld, K., 1989 Theory of stochastic resonance. *Phys. Rev. A* **39**, 4854–4869.

Michaelis, L. & Menten, M., 1913 Die Kinetik der Invertinwirkung. *Biochemische Zeitschrift* pp. 333–369.

Mirollo, R. & Strogatz, S., 1990 Synchronization of pulse-coupled biological oscillators. *SIAM J. Appl. Math.* **50**, 1645.

Mitic, L. L. & Anderson, J. M., 1998 Molecular Architecture of Tight Junctions. *Annual Review of Physiology* **60**, 121–142.

Miyazawa, A., Fujiyoshi, Y. & Unwin, N., 2003 Structure and gating mechanism of the acetylcholine receptor pore. *Nature* **423**, 949–955.

Mizuarai, S., Aozasa, N. & Hidehito, K., 2004 Single Nucleotide Polymorphisms Result in Impaired Membrane Localization and Reduced ATPase Activity in Multidrug Transporter ABCG2. *International Journal of Cancer* **109**, 238–246.

Moore, R., Speh, J. & Leak, R., 2002 Suprachiasmatic nucleus organization. *Cell and Tissue Research* **309**, 89–98.

Neiman, A., Saparin, P. I. & Stone, L., 1997 Coherence resonance at noisy precursors of bifurcations in nonlinear dynamical systems. *Phys. Rev. E* **56**, 270–273.

Neiman, A. B., Russell, D. F., Yakusheva, T. A., DiLullo, A. & Tass, P. A., 2007 Response clustering in transient stochastic synchronization and desynchronization of coupled neuronal bursters. *Phys. Rev. E* **76**, 021908.

Nelson, D. L. & Cox, M. M., 2000 *Lehninger Principles of Biochemistry*. Worth Publishers, 3rd edition.

Oguz, E., Chakrabarti, A., Toral, R. & Gunton, J. D., 1990 Domain growth in the two-dimensional time-dependent Ginzburg-Landau model in the presence of a random magnetic field. *Phys. Rev. B* **42**, 704–708.

Okubo, A. & Levin, S. A., 2001 *Diffusion and Ecological Problems: Modern Perspectives*. Springer-Verlag, 2nd edition.

Ott, E. & Antonsen, T. M., 2008 Low dimensional behavior of large systems of globally coupled oscillators. *Chaos: An Interdisciplinary Journal of Nonlinear Science* **18**, 037113.

Ott, E. & Antonsen, T. M., 2009 Long time evolution of phase oscillator systems. *Chaos: An Interdisciplinary Journal of Nonlinear Science* **19**, 023117.

Ozbudak, E. M., Thattai, M., Kurtser, I., Grossman, A. D. & van Oudenaarden, A., 2002 Regulation of noise in the expression of a single gene. *Nature Genetics* **31**, 69 – 73.

Perc, M., Kralj, S. & Gosak, M., 2008 Stochastic resonance in soft matter systems: combined effects of static and dynamic disorder. *Soft Matter* **4**, 1861–1870.

Pérez, T., Mirasso, C. R., Toral, R. & Gunton, J. D., 2010 The constructive role of diversity on the global response of coupled neuron systems. *Philosophical Transactions of the Royal Society A* **in press**.

Pérez-Reche, F. J. & Vives, E., 2004 Spanning avalanches in the three-dimensional Gaussian random-field Ising model with metastable dynamics: Field dependence and geometrical properties. *Phys. Rev. B* **70**, 214422.

Pikovsky, A. & Kurths, J., 1997 Coherence Resonance in a Noise-Driven Excitable System. *Phys. Rev. Lett.* **78**, 775.

Postnova, S., Voigt, K. & Braun, H. A., 2009 A Mathematical Model of Homeostatic Regulation of Sleep-Wake Cycles by Hypocretin/Orexin. *Journal of Biological Rhythms* **24**, 523–535.

Pye, K. & Chance, B., 1966 Sustained sinusoidal oscillations of reduced pyridine nucleotide in a cell-free extract of saccharomyces carlsbergensis. *PNAS* **55**, 888–894.

Rapp, P. E., 1979 An atlas of cellular oscillations. *Journal of Experimantal Biology* **81**, 281–306.

Rappel, W.-J. & Strogatz, S. H., 1994 Stochastic resonance in an autonomous system with a nonuniform limit cycle. *Phys. Rev. E* **50**, 3249–3250.

Raviv, Y., Pollard, H., Bruggemann, E., Pastan, I. & Gottesman, M., 1990 Photosensitized labeling of a functional multidrug transporter in living drug-resistant tumor cells. *Journal of Biological Chemistry* **7**, 3975–3980.

Rayleigh, L., 1890 Measurements of the Amount of Oil Necessary in Order to Check the Motions of Camphor upon Water. *Proceedings of the Royal Society of London* **47**, 364–367.

Rees, D. C., Johnson, E. & Lewinson, O., 2009 ABC transporters: the power to change. *Nature Reviews Molecular Cell Biology* **10**, 218–227.

Reppert, S. & Weaver, D., 2002 Coordination of circadian timing in mammals. *Nature* **418**, 935–941.

Ricard, J. & Cornish-Bowden, A., 1987 Co-operative and allosteric enzymes: 20 years on. *European Journal of Biochemistry* **166**, 255–272.

Risken, H., 1989 *The Fokker-Planck equation*. Springer-Verlag.

Robertson, J. D., 1981 Membrane Structure. *The Journal of Cell Biology* **91**, 189–204.

Rosinberg, M. L., Tarjus, G. & Pérez-Reche, F. J., 2008 Stable, metastable and unstable states in the mean-field random-field Ising model at T = 0. *Journal of Statistical Mechanics: Theory and Experiment* **2008**, P10004.

Rosinberg, M. L., Tarjus, G. & Pérez-Reche, F. J., 2009 The T = 0 random-field Ising model on a Bethe lattice with large coordination number: hysteresis and metastable states. *Journal of Statistical Mechanics: Theory and Experiment* **2009**, P03003.

Ruiz-García, A., Lin, H., Plá-Delfina, J. M. & Hu, M., 2002 Kinetic Characterization of Secretory Transport of a New Ciprofloxacin Derivative (CNV97100) across Caco-2 Cell Monolayers. *Journal of Pharmaceutical Sciences* **91**, 2511–2519.

Sackmann, E., 1994 Membrane bending energy concept of vesicle- and cell-shapes and shape-transitions. *FEBS Letters* **346**, 3 – 16.

San Miguel, M. & Toral, R., 2000 Stochastic effects in physical systems. In *Instabilities and nonequilibrium structures VI* (eds. J. M. E. Tirapegui & R. Tiemann), pp. 35–120. Kluwer academic publishers.

Santagiustina, M., Colet, P., San Miguel, M. & Walgraef, D., 1997 Noise-Sustained Convective Structures in Nonlinear Optics. *Phys. Rev. Lett.* **79**, 3633–3636.

Schaap, J., Albus, H., van der Leest, H. T., Eilers, P. H. C., Détári, L. & Meijer, J. H., 2003 Heterogeneity of rhythmic suprachiasmatic

nucleus neurons: Implications for circadian waveform and photoperiodic encoding. *Proceedings of the National Academy of Sciences of the United States of America* **100**, 15994–15999.

Schlögl, F., 1972 Chemical reaction models for non-equilibrium phase transitions. *Zeitschrift für Physik A Hadrons and Nuclei* **253**, 147–161.

Schneider, T. & Pytte, E., 1977 Random-field instability of the ferromagnetic state. *Phys. Rev. B* **15**, 1519–1522.

Sethna, J., Dahmen, K. & Perkovic, O., 2006 *The Science of Hysteresis*, chapter Random field ising models of hysteresis. Academic Press, New York.

Sethna, J. P., Dahmen, K., Kartha, S., Krumhansl, J. A., Roberts, B. W. & Shore, J. D., 1993 Hysteresis and hierarchies: Dynamics of disorder-driven first-order phase transformations. *Phys. Rev. Lett.* **70**, 3347–3350.

Sharma, K. G., Mason, D. L., Liu, G., Rea, P. A., Bachhawat, A. K. & Michaelis, S., 2002 Localization, Regulation, and Substrate Transport Properties of Bpt1p, a Saccharomyces cerevisiae MRP-Type ABC Transporter. *Eukaryotic Cell* **1**, 391–400.

Shen, S., Spratt, C., Sheward, W. J., Kallo, I., West, K., Morrison, C. F., Coen, C. W., Marston, H. M. & Harmar, A. J., 2000 Overexpression of the human VPAC2 receptor in the suprachiasmatic nucleus alters the circadian phenotype of mice. *Proceedings of the National Academy of Sciences of the United States of America* **97**, 11575–11580.

Shinomoto, S. & Kuramoto, Y., 1986 Phase transitions in active rotator systems. *Prog. Theor. Phys.* **75**, 1105.

Silva, I. G. D., de Monte, S., d'Ovidio, F., Toral, R. & Mirasso, C. R., 2006 Coherent regimes of mutually coupled Chua's circuits. *Physical Review E* **73**.

Singer, S. J. & Nicolson, G. L., 1972 The Fluid Mosaic Model of the Structure of Cell Membranes. *Science* **175**, 720–731.

Skinner, S. M., Clark, R. E., Baker, N. & Shipley, R. A., 1959 Complete solution of the three-compartment model in steady state after single injection of radioactive tracer. *American Journal of Physiology* **196**, 238–244.

Smolen, P., Hardin, P. E., Lo, B. S., Baxter, D. A. & Byrne, J. H., 2004 Simulation of Drosophila Circadian Oscillations, Mutations, and Light Responses by a Model with VRI, PDP-1, and CLK. *Biophysical Journal* **86**, 2786–2802.

Sosnovtseva, O. V., Pavlov, A. N., Mosekilde, E. & Holstein-Rathlou, N.-H., 2002 Bimodal oscillations in nephron autoregulation. *Phys. Rev. E* **66**, 061909.

Stanley, H., 1971 *Introduction to phase transitions and critical phenomena*. Oxford university press.

Steuer, R., Zhou, C. & Kurths, J., 2003 Constructive effects of fluctuations in genetic and biochemical regulatory systems. *Biosystems* **72**, 241–251.

Strogatz, S. H., 1994 *Nonlinear dynamics and chaos: with applications to physics, biology, chemistry and engineering*. Addison-Wesley.

Strogatz, S. H., 2000 From Kuramoto to Crawford: exploring the onset of synchronization in populations of coupled oscillators. *Physica D* **143**, 1–20.

Strogatz, S. H., Mirollo, R. E. & Matthews, P. C., 1992 Coupled nonlinear oscillators below the synchronization threshold: Relaxation by generalized Landau damping. *Phys. Rev. Lett.* **68**, 2730–2733.

Tessone, C. & Toral, R., 2009 Diversity-induced resonance in a model for opinion formation. *European Physical Journal B* **71**, 549.

Tessone, C., Zanette, D. & Toral, R., 2008 Global firing induced by network disorder in ensembles of active rotators. *Eur. Phys. J. B* **62**, 319–326.

Tessone, C. J., 2005 *Synchronisation and collective effects in extended stochastic systems*. Ph.D. thesis, University of Balearic Islands, Palma de Mallorca.

Tessone, C. J., Mirasso, C. R., Toral, R. & Gunton, J. D., 2006 Diversity-Induced Resonance. *Physical Review Letters* **97**, 194101.

Tessone, C. J., Scirè, A., Toral, R. & Colet, P., 2007 Theory of collective firing induced by noise or diversity in excitable media. *Physical Review E* **75**, 016203.

Thattai, M. & van Oudenaarden, A., 2001 Intrinsic noise in gene regulatory networks. *PNAS* **98**, 8614–8619.

Thieffry, D., Huerta, A. M., Pérez-Rueda, E. & Collado-Vides, J., 1998 From specific gene regulation to genomic networks: a global analysis of transcriptional regulation in Escherichia coli. *BioEssays* **20**.

Toral, R., Hernández-Garía, E. & Gunton, J. D., 2009 Diversity-induced resonance in a system of globally coupled linear oscillators. *International Journal of Bifurcation and Chaos* **19**, 3499–3508.

Toral, R., Tessone, C. & Lopes, J., 2007 Collective effects induced by diversity in extended systems. *Eur. Phys. J. Special Topics* **143**, 59–67.

Troutman, M. D. & Thakker, D. R., 2003*a* Efflux Ratio Cannot Assess P-Glycoprotein-Mediated Attenuation of Absorptive Transport: Asymmetric Effect of P-Glycoprotein on Absorptive and Secretory Transport across Caco-2 Cell Monolayers. *Pharmaceutical Research* **20**, 1200–1209.

Troutman, M. D. & Thakker, D. R., 2003*b* Novel Experimental Parameters to Quantify the Modulation of Absorptive and Secretory Transport of Compounds by P-Glycoprotein in Cell Culture Models of Intestinal Epithelium. *Pharmaceutical Research* **20**, 1210–1224.

Tyson, J., 2002 Biochemical Oscillations. In *Computational Cell Biology* (eds. S. S. Antman, J. E. Marsden, L. Sirovich, C. P. Fall, E. S. Marland, J. M. Wagner & J. J. Tyson), volume 20 of *Interdisciplinary Applied Mathematics*, pp. 230–260. Springer New York.

Ueda, H. R., Hirose, K. & Iino, M., 2002 Intercellular Coupling Mechanism for Synchronized and Noise-Resistant Circadian Oscillators. *Journal of Theoretical Biology* **216**, 501–512.

Ullner, E., Buceta, J., Diez-Noguera, A. & García-Ojalvo, J., 2009 Noise-induced Coherence in Multicellular Circadian Clocks. *Biophysical Journal* **96**, 3573.

van den Broeck, C., Parrondo, J., Armero, J. & Hernández-Machado, A., 1994*a* Mean field model for spatially extended systems in the presence of multiplicative noise. *Phys. Rev. E* **49**, 2639–2643.

van den Broeck, C., Parrondo, J. & Toral, R., 1994*b* Noise-Induced Nonequilibrium Phase Transition. *PRL* **73**, 3395.

van den Broeck, C., Parrondo, J., Toral, R. & Kawai, K., 1997 Nonequilibrium phase transitions induced by multiplicative noise. *Phys. Rev. E* **55**, 4084.

van den Pol, A. & Dudek, F., 1993 Cellular communication in the circadian clock, the suprachiasmatic nucleus. *Neuroscience* **56**, 793–811.

van Kampen, N. G., 2007 *Stochastic Processes in Physics and Chemistry*. Elsevier, 3 edition.

Veleri, S., Brandes, C., Helfrich-Förster, C., Hall, J. C. & Stanewsky, R., 2003 A Self-Sustaining, Light-Entrainable Circadian Oscillator in the Drosophila Brain. *Current biology* **13**, 1758–1767.

Volk, E. L. & Schneider, E., 2003 Wild-Type Breast Cancer Resistance Protein (BCRP/ABCG2) is a Methotrexate Polyglutamate Transporter. *Cancer Research* **63**, 5538–5543.

von Nussbaum, F., Brands, M., Hinzen, B., Weigand, S. & Häbich, D., 2006 Antibacterial Natural Products in Medicinal Chemistry - Exodus or Revival? *Angewandte Chemie* **45**, 5072–5129.

Ward, C. W. & Lawrence, M. C., 2009 Ligand-induced activation of the insulin receptor: a multi-step process involving structural changes in both the ligand and the receptor. *BioEssays* **31**, 422–434.

Welsh, D., Logothetis, D., Meister, M. & S.M., R., 1995 Individual neurons dissociated from rat suprachiasmatic nucleus express independently phased circadian firing rhythms. *Neuron* **14**, 697–706.

Wikipedia, 2010*a* Enzymkinetik — Wikipedia, Die freie Enzyklopädie. [Online; accessed 8-August-2010; This work has been released into the public domain by its author, Yikrazul.].

Wikipedia, 2010*b* Enzymkinetik — Wikipedia, Die freie Enzyklopädie. [Online; accessed 8-August-2010; This file is licensed by its author Pro Bug Catcher under the Creative Commons Attribution-Share Alike 2.0 Germany license.].

Wikipedia, 2010*c* Lipid bilayer — Wikipedia, The Free Encyclopedia. [Online; accessed 6-June-2010; This work has been released into the public domain by its author, LadyofHats.].

Wikipedia, 2010*d* Micrographia — Wikipedia, The Free Encyclopedia. [Online; accessed 6-June-2010; This image is in the public domain because its copyright has expired.].

Wikipedia, 2010*e* Zellmembran — Wikipedia, Die freie Enzyklopädie. [Online; accessed 29-July-2010; This work has been released into the public domain by its author, LadyofHats.].

Winterhalter, M., 2000 Black lipid membranes. *Current Opinion in Colloid & Interface Science* **5**, 250 – 255.

Wu, D., Zhu, S. & Luo, X., 2009 Cooperative effects of random time delays and small-world topologies on diversity-induced resonance. *EPL (Europhysics Letters)* **86**, 50002.

Yamashita, S., Furubayashi, T., Kataoka, M., Sakane, T., Sezaki, H. & Tokuda, H., 2000 Optimized conditions for prediction of intestinal drug permeability using Caco-2 cells. *European Journal of Pharmaceutical Sciences* **10**, 195–204.

Young, A., ed., 1998 *Spin Glasses and Random Fields*. World Scientific Publishing Co.Pte. Ltd.

Yu, L. X. & Amidon, G. L., 1999 A compartmental absorption and transit model for estimating oral drug absorption. *International Journal of Pharmaceutics* **186**, 119–125.

Zaikin, A., García-Ojalvo, J., Báscones, R., Ullner, E. & Kurths, J., 2003 Doubly Stochastic Coherence via Noise-Induced Symmetry in Bistable Neural Models. *Phys. Rev. Lett.* **90**, 030601.

Zanette, D., 2009*a* Interplay of noise and coupling in heterogeneous ensembles of phase oscillators. *European Physical Journal B* **69**, 269.

Zanette, D., 2009*b* Interplay of noise and coupling in heterogeneous ensembles of phase oscillators. *European Physical Journal B* **69**, 269.

Zhou, H., 2003 Pharmacokinetic Strategies in Deciphering Atypical Drug Absorption Profiles. *The Journal of Clinical Pharmacology* **43**, 211–227.